

Electronic Thesis and Dissertation Repository

12-2-2021 11:00 AM

Static liquefaction of oil sand tailings: an experimental investigation into the effect of saturation and fines content

Farshad Zehforoosh, *The University of Western Ontario*

Supervisor: Sadrekarimi, Abouzar, *The University of Western Ontario*

A thesis submitted in partial fulfillment of the requirements for the Master of Science degree in Civil and Environmental Engineering

© Farshad Zehforoosh 2021

Follow this and additional works at: <https://ir.lib.uwo.ca/etd>



Part of the [Geotechnical Engineering Commons](#)

Recommended Citation

Zehforoosh, Farshad, "Static liquefaction of oil sand tailings: an experimental investigation into the effect of saturation and fines content" (2021). *Electronic Thesis and Dissertation Repository*. 8258.
<https://ir.lib.uwo.ca/etd/8258>

This Dissertation/Thesis is brought to you for free and open access by Scholarship@Western. It has been accepted for inclusion in Electronic Thesis and Dissertation Repository by an authorized administrator of Scholarship@Western. For more information, please contact wlsadmin@uwo.ca.

Abstract

The main goals of this research are to explore the influence of partial saturation and fines content on the shear response of oil sand tailings, to identify the liquefaction susceptibility under different initial states. Monotonic triaxial compression tests were carried out to understand the mechanical behavior of the saturated oil sand tailings with varying void ratios. Then the effect of fines content on the yield and critical shear strength, critical state line, and instability line were evaluated by increasing the fines content from 0 up to 50%. The experimental results revealed that the shear strength of the oil sand increases with increasing fines content. The effect of degree of saturation (S_r) on liquefaction resistance was examined based on the wave propagation theory and correlating Skempton's B value with S_r . It is found that the reduction in liquefaction susceptibility by decreasing the degree of saturation is due to the increased compressibility of the pore fluid.

Keywords

Critical state, liquefaction, triaxial test, partially saturated, fines content, state parameter.

Summary for Lay Audience

Liquefaction is a phenomenon in which the shear strength of sand or silty sand reduces by monotonic, cyclic, or dynamic loading. Landslides, lateral movement, dam failure, settling and tilting of buildings, and failure of waterfront retaining structures are examples of liquefaction triggered by static or cyclic mechanisms. The substantial economic losses, human fatalities, and environmental subsequences result from the failure related to the liquefaction. These failures range from limited sand boils to devastating flow slides based on the extend of liquefaction. Calaveras dam and Merriespruit gold mine tailings dam failure are examples of liquefaction flow failure cases in California and Virginia. The Calaveras dam failure in 1918 was triggered by the monotonic increasing load by rapid construction and resulted in 200 m travel. Also, the flow slide failure of Merriespruit gold mine tailings dam in 1994 by the over steepening released 600000 m³ of tailings flowed for a distance of 2000 m. Several studies have been done on evaluating the liquefaction susceptibility on the saturated clean sand. However, most natural soil contains some fine particles or is partially saturated based on the liquefaction failure case histories. Triaxial apparatus is the most commonly used device for simulating the soil's natural condition in the laboratory. To evaluate the effect of fine content on the liquefaction potential, the sand with different percentage of fines are prepared and tested. Fines can affect the shear behavior of the sand-silt mixture in various ways since they can separate the coarse grains or locate inside the voids between them. The effect of the level of saturation was examined by preparing samples with varying degrees of saturation. The decreased saturation level leads more compressible soil medium and produces suction forces due to the surface tension.

Co-Authorship Statement

This thesis has been prepared in accordance with the regulations for an Integrated-Article format thesis stipulated by the School of Graduate and Postdoctoral Studies at the University of Western Ontario and has been co-authored as:

Chapter 2: Static Liquefaction Behavior of Oil Sand Tailings

All experimental works for the fulfillment of the concern chapter was conducted by Farshad Zehforoosh under supervision of Dr. Abouzar Sadrekarimi. A paper co-authored by Farshad Zehforoosh and Abouzar Sadrekarimi will be submitted to the journal of Geotechnique.

Chapter 3: Effect of Fines on Instability of Oil Sand Tailings

All experimental works for the fulfillment of the concern chapter was conducted by Farshad Zehforoosh under supervision of Dr. Abouzar Sadrekarimi. A paper co-authored by Farshad Zehforoosh and Abouzar Sadrekarimi will be submitted to the Canadian Geotechnical Journal.

Chapter 4: Effect of Saturation on Instability of Oil sand tailings

All experimental works for the fulfillment of the concern chapter was conducted by Farshad Zehforoosh under supervision of Dr. Abouzar Sadrekarimi. A paper co-authored by Farshad Zehforoosh and Abouzar Sadrekarimi will be submitted to the ASTM Geotechnical Testing Journal.

Acknowledgements

I would like to extend my sincere gratitude and appreciation to all those who made this MEd thesis possible. I want to express my sincere gratitude to my supervisor Dr. Abouzar Sadrekarimi for the continuous support and encouragement during my pursuit to complete my study, for his motivation, and immense knowledge. His guidance helped me in all the time of research and writing of this thesis.

Words cannot express how grateful I am to my Mom and Dad, who formed part of my vision and taught me good things that really matter in life. I must thank them for their endless love and encouraging me in all of my pursuits, and inspiring me to follow my dreams. They are the ultimate role models.

Table of Contents

Abstract.....	ii
Summary for Lay Audience	iii
Co-Authorship Statement.....	iv
Acknowledgements.....	v
Table of Contents.....	vi
List of Tables (where applicable)	ix
List of Figures (where applicable)	x
List of abbreviations and symbols	xv
Chapter 1.....	1
1.1 Statement of the Problem.....	1
1.2 Research Objective	2
1.3 Thesis Outline	3
Chapter 2.....	5
2 « Static Liquefaction Behavior of Oil Sand Tailings».....	5
2.1 Introduction.....	5
2.1.1 Behavior of Sands under Monotonic Loading	9
2.1.2 Yield and post-liquefaction shear strengths	11
2.2 Methodology.....	14
2.2.1 Oil sand tailings physical properties	14
2.2.2 Index properties	17
2.2.3 Triaxial test procedure	17
2.3 Results and Discussions.....	30
2.3.1 Stress paths and stress-strain behaviors of undrained triaxial tests	32
2.3.2 K0-consolidated undrained response	37

2.3.3	Drained shear response	39
2.3.4	Critical state line of oil sand tailings.....	42
2.3.5	Effect of void ratio on yield and post-liquefaction strength ratios	47
2.3.6	Variations of yield and post-liquefaction strength ratios with state parameter.....	51
2.4	Summary and Conclusions	53
	References.....	56
	Chapter 3.....	61
3	Effect of Fines on Instability of Oil Sand Tailings	61
3.1	Introduction.....	61
3.2	Methodology.....	64
3.2.1	Oil sand tailings properties with different fines content.....	64
3.2.2	Triaxial test apparatus	67
3.2.3	Sample preparation and uniformity	68
3.2.4	Sample saturation.....	71
3.2.5	Consolidation Undrained shearing.....	72
3.3	Results and Discussions.....	73
3.3.1	Changes of stress paths and stress-strain behaviors with fines content	75
3.3.2	Effect of FC on critical state line of oil sand tailings	80
3.3.3	Effect of FC on yield and post-liquefaction strength ratios.....	84
3.4	Conclusions.....	86
	References.....	88
	Chapter 4.....	94
4	« Effect of Saturation on Instability of Oil sand tailings »	94
4.1	Introduction.....	94
4.2	Methodology.....	99

4.2.1	Oil sand tailings properties	99
4.2.2	Sample preparation at different saturation ratios	101
4.2.3	Sample partial saturation.....	103
4.2.4	Consolidation	104
4.2.5	Undrained shearing	105
4.2.6	Measurement of saturation ratio	105
4.2.7	Determination of SWCC from pressure plate tests.....	110
4.3	Results and Discussions	112
4.3.1	Soil water characteristic curve for different fines contents	112
4.3.2	Compression wave velocity at different levels of saturation	114
4.3.3	Effect of S_r on stress path and stress-strain response of tailings with different FC.....	117
4.3.4	Comparison of pore pressure generations in saturation and unsaturated samples.....	121
4.4	Conclusions.....	122
	References.....	124
	Chapter 5.....	128
5	Conclusion	128
	Curriculum Vitae	133

List of Tables (where applicable)

Table 2.1: Parameters of the oil sand tailings	17
Table 2.2: Plug samples void ratio.....	21
Table 2.3: Void volume changes during saturation stage	25
Table 2.4: Triaxial testing program on the oil sand tailings	31
Table 2.5: Linear and curved critical state parameters	46
Table 3.1: Parameters of the oil sand tailings with fines	67
Table 3.2: Triaxial testing program on the oil sand tailing with fluid fine tailings	74
Table 4.1: Parameters of the oil sand tailings	101
Table 4.2: SWCC fitting parameters for oil sand tailings with different fines content	113
Table 4.3: Triaxial testing program on the oil sand tailing with different saturation levels.	118

List of Figures (where applicable)

Figure 2.1: Constitutive behavior of both flow failure and cyclic mobility (Kramer 1996)	8
Figure 2.2: Undrained behavior of sand under monotonic loading (a) stress path; (b) stress-strain; (c) pore pressure generation vs. axial strain after Kramer (1996)	10
Figure 2.3: Effective stress path from undrained triaxial compression test (IU-Drc=61%- $P'_c=400\text{kPa}$).....	12
Figure 2.4: Stress-strain response from undrained triaxial compression test (IU-Drc=61%- $P'_c=400\text{kPa}$).....	13
Figure 2.5: Krumbein and Sloss chart to visualize the estimation of sphericity and roundness.	14
Figure 2.6: Particle size distribution of the oil sand tailings.....	15
Figure 2.7: Shape of oil sand particles (SEM images).....	16
Figure 2.8: XRD image of the oil sand tailings	16
Figure 2.9 Schematic diagram of the triaxial testing system (Modified from Omar 2013)....	18
Figure 2.10: Comparison of the void volume change measured by freezing method and inflow/outflow method.....	26
Figure 2.11: Comparison of the void volume change measured by freezing method and inflow/outflow method.....	26
Figure 2.12: Volumetric strain variation with axial strain in a k_0 consolidation stage	28
Figure 2.13: Major and minor effective stress variation in a K_0 consolidation stage	28
Figure 2.14: Void ratio changes during the consolidation stage.....	29
Figure 2.15: K_0 variation with consolidation void ratio.....	29

Figure 2.16: Evaluation of triaxial tests repeatability on specimens with similar initial state	31
Figure 2.17: Effective stress paths of the undrained triaxial tests for samples with confining pressure of $p'_c=400$ kPa and different relative densities.	33
Figure 2.18: Stress-strain response of the undrained triaxial tests for samples with confining pressure of $p'_c=400$ kPa and different relative densities.	34
Figure 2.19: Generated excess for water pressure for the isotropic consolidated undrained triaxial tests with confining pressures of 100, 200, 300, 400 kPa	34
Figure 2.20: Instability line range for the undrained triaxial tests	35
Figure 2.21: Variation of instability line slope with void ratio	36
Figure 2.22: Variation of instability line slope with state parameter	36
Figure 2.23: Comparison of the K_0 values from triaxial tests and Jaky's Eq.	38
Figure 2.24: Stress paths and stress-strain responses of the K_0 -consolidated triaxial tests under undrained loading condition	39
Figure 2.25: Stress-strain response of the oil sand tailings under drained shear condition	40
Figure 2.26: Volumetric strain responses of the oil sand tailings in drained tests	41
Figure 2.27: Effective stress paths for the isotropically consolidated drained triaxial tests	41
Figure 2.28: Initial and final states of the isotropically consolidated samples under undrained loading condition	43
Figure 2.29: Critical state data points obtained from Isotropically-consolidated samples under drained condition	44
Figure 2.30: Initial and final states of the K_0 -consolidated samples under undrained loading condition	45
Figure 2.31: CSL obtained from all triaxial test perform on the oil sand tailing	46

Figure 2.32: Critical state line on the q - p' space obtained from undrained triaxial tests	47
Figure 2.33: Yield shear strength ratio variation with consolidation void ratio for isotropically consolidated and K_0 -consolidated specimens	48
Figure 2.34: Post-liquefaction shear strength ratio variation with consolidation void ratio for isotropically consolidated and K_0 -consolidated specimens	49
Figure 2.35: Yield friction angle variation with consolidation void ratio	50
Figure 2.36: Post-liquefaction friction angle variation with consolidation void ratio	51
Figure 2.37: Schematic definition of the state parameter (Rahemi, 2018)	52
Figure 2.38: Yield shear strength variation with state parameter	52
Figure 2.39: Post-liquefaction shear strength variation with state parameter.....	53
Figure 3.1: Instability stress ratio variation with void ratio (Chu and Leong, 2002)	62
Figure 3.2: Effect of the fines content on the peak shear strength (Abedi and Yasrobi, 2010)	63
Figure 3.3: Shape of oil sand particles (SEM images).....	65
Figure 3.4: Shape of fluid fine tailings (SEM images)	65
Figure 3.5: Soil particle size distribution for oil sand with 0%, 25%, and 50% FFT	66
Figure 3.6: Variation of maximum and minimum void ratio with fines content	66
Figure 3.7: Sample preparation procedure at Western university laboratory	71
Figure 3.8: Normal compression line for sand with 0% and 25%FFT	73
Figure 3.9: Effective stress paths for sand+25%fluid fine tailings at different consolidation stresses	77
Figure 3.10: Comparison of effective stress paths with different fines content	77

Figure 3.11: Comparison of the stress-strain behavior with different fines content.....	78
Figure 3.12: Effect of fines content on effective stress paths at two different consolidation stresses	78
Figure 3.13: Effect of fines content on the effective stress path (Pitman et al, 1994).....	79
Figure 3.14: Effect of fine on stress-strain response (Robertson and Sego (1994)	79
Figure 3.15: Effect of fines content on the friction angle	80
Figure 3.16: Critical state lines of sand-silt mixtures (a) Been and Jefferies (1985); (b) Fear and Robertson (1995).....	82
Figure 3.17: Effect of fines content on the critical state line (Bouckovalas et al, 2003).....	82
Figure 3.18: Critical state line on q-p' space for oil sand with 0% and 25% fines content....	83
Figure 3.19: Critical state lines on e-log p' space for oil sand with 0% and 25% fines content	84
Figure 3.20: Effect of the fines content on shear strength ratios in terms of the void ratio and state parameter	86
Figure 4.1: Schematic interpretation of fully, partially, and unsaturated soil deposits (Tsukamoto et al. 2014).	95
Figure 4.2 Shape of oil sand particles (SEM images).....	100
Figure 4.3: Particle size distribution of the oil sand tailings.....	101
Figure 4.4: Normal compression line for oil sand tailings	104
Figure 4.5: Compression crystals and bender elements installed on triaxial platen	106
Figure 4.6: Sample preparation and pressure plate extractor apparatus	111
Figure 4.7: Soil water characteristic curve for oil sand tailings with different fines contents	113

Figure 4.8: Compressional wave velocities for the oil sand tailings mixture with 0, 10, 25, 50% fines content at different B-values.....	114
Figure 4.9: Effect of poisson's ratio on P-wave velocity.....	115
Figure 4.10: Shear wave velocities of the dense, medium, and loose oil sand tailings at different normalized consolidation stresses (Grytan, 2021).	116
Figure 4.11: Effect of consolidation void ratio on the S_r -B plot.....	116
Figure 4.12: Comparison of the predicted S_r with the measured S_r using the proposed alternative method.....	117
Figure 4.13: Effect of B-value on the stress-strain response and effective stress paths for oil sand with consolidation stress of 400kPa and consolidation void ratio of 0.60 to 0.63	119
Figure 4.14: Effect of B-value on the stress-strain response and effective stress paths for oil sand with consolidation stress of 400 kPa and consolidation void ratio of 0.63 to 0.69	120
Figure 4.15: Effect of B-value on the developed pore water pressure for oil sand tailings..	121

List of abbreviations and symbols

a, n, m	Fitting parameters of SWCC model
B	Skempton's value
C_a	Compressibility of air
C_b	Compressibility of soil skeleton
C_c	Coefficient of curvature
CSL	Critical state line
C_u	Coefficient of uniformity
C_w	Compressibility of water
D_{50}	Median grains size
D_{rc}	Consolidation relative density
Δu	Generated excess pore water pressure
e_0	Initial void ratio
ε_a	Axial strain
e_c	Consolidation void ratio
e_{max}, e_{min}	Maximum and minimum void ratio
η	Slope of the instability line

ε_v	Volumetric strain
FC	Fines content
FFT	Fluid fine tailings
$\phi'(\text{liq})$	Post-liquefaction friction angle
$\phi'(\text{yield})$	Yield friction angle
G	Shear modulus
G _s	Specific gravity
IL	Instability line
K ₀	Coefficient of lateral earth pressure
K _b	Bulk modulus of soil skeleton
K _f	Bulk modulus of fluid
K _w	Bulk modulus of water
n	Porosity
NCL	Normal compression line
P'	Mean effective stress
P _a	Atmospheric pressure
P' _c	consolidation stress
P' _{cs}	Mean effective stress at critical state
PT	Phase transformation
q	Deviator stress

ρ	Density of soil mass
$\sigma'1, \sigma'3$	Major and minor effective stresses
$\Psi_{(cs)}$	State parameter
SEM	Scanning electron microscope image of the tailings
S_r	Degree of saturation
$S_{u(liq)}$	Post-liquefaction shear strength
$S_{u(yield)}$	Yield shear strength
SWCC	Soil water characteristic curve
u_a	Pore air pressure
u_w	Pore water pressure
V_p	Compression wave velocity
V_s	Shear wave velocity
V_v	Void Volume
w	Water content
XRD	X-ray powder diffraction

Chapter 1

1.1 Statement of the Problem

Soil liquefaction is described as a phenomenon in which the shear strength of saturated or partially saturated soil reduces by monotonic, cyclic, or dynamic loading due to excess pore water pressure generation. The substantial economic losses, human fatalities, and environmental subsequences result from the failure related to the liquefaction. Landslides, lateral movement, dam failure, settling and tilting of buildings, and failure of waterfront retaining structures are examples of liquefaction triggered by static or cyclic loading mechanisms. There have been numerous tailings dam failures resulting from monotonically increasing loads worldwide, which lead to high costs, environmental cleanup, and loss of life. Tar Island dike, Calaveras, Merriespruit gold mine, Mount Polley, and Fundao are examples of tailings dam failures. Several studies have been done on evaluating the liquefaction susceptibility of clean sands. However, most natural soil contains some fines, and flow failure commonly occurs in silty sands, based on the liquefaction failure case histories. Obviously, the presence of fine in soil mass significantly affects the stress-strain behavior (Lade & Yamamuro 1997; Thevanayagam 1998; Georgiannou 2006; Rahman 2009; Baki 2011). Some studies demonstrated that with increasing in fines content, the liquefaction resistance increases (Robertson PK et al., 1994; Seed HB, 1987; Georgiannou, 2006). On the other hand, some researchers have arrived at a contrary conclusion and demonstrated that the liquefaction resistance decreases with increasing fines content up to a threshold value $FC_{th} \approx 30\%$ (Ishihara and Verdugo 1997; Lade and Yamamuro 1997; Wang and Sassa 2000; Baziar et al., 2004; Das and Sitharam 2011). So the effect of fines on the stress-strain response of the sand needs to be evaluated.

Examination of the undisturbed samples of frozen tailings sand indicates that the specimens were not fully saturated (Fourier et al., 2001). A few meters below the phreatic

surface, the air bubbles were determined by compression wave velocity measurement, which indicates the partially saturated condition. Soils that contain a large amount of dissolved gas are termed gassy soils (Sobkowcz, 1984). Gassy soil is in the same category as partially-saturated soils in which gas in its free form or solution in the pore water is found. Świdziński and Mierczyński (2017) performed some triaxial monotonic tests on cohesiveless partially-saturated samples. They concluded that liquefaction susceptibility decreased with a reduction in saturation degree. Wheeler (1988) examined the behavior of sea marine deposits. The results show that the undrained shear strength of gassy clays could be higher or lower than that of similar but saturated clays. He Jia (2013) indicated that the occluded gas bubbles in the sand could either strengthen or weaken the liquefaction susceptibility under monotonic loading. So, the effect of partial saturation on the oil sand tailings needs to be investigated.

1.2 Research Objective

The main objectives of this study are to investigate the effect of the degree of saturation and fines content on the shear behavior of the oil sand tailings. In the first part of the study, the influence of fines content is examined; in the second part, the stress-strain behavior of the partially saturated oil sand is assessed. The specific objectives are to answer the following questions:

- What is the effect of the fines content on the shear strengths, position of the critical state line, slope of the instability line for oil sand tailings mixture with fine tailings?
- How would the changes in the level of saturation affect the liquefaction susceptibility of oil sand tailings?

- How do the yield and post-liquefaction shear strength ratios vary with the fines content and the degree of saturation?
- What is the threshold degree of saturation value to circumvent static liquefaction in oil sand tailings?

1.3 Thesis Outline

This thesis has been prepared in "Integrated-Article" format. It comprises five chapters and a brief summary of the oncoming chapters is as follow:

Chapter 2: presents the shear behavior of the oil sand tailings under drained and undrained conditions. Undrained triaxial tests are often used to evaluate the liquefaction susceptibility of the soil sample due to the pore water pressure generation mechanism. One of the major sources of errors that could significantly affect the triaxial test results is sample volume changes during the saturation stage. In this chapter, different methods were employed and compared to have an accurate estimation of sample volume change during the backpressure saturation stage. The critical state concept is used to interpret the experimental results. The yield and critical shear strength of the oil sand were determined, which provided a valuable basis for analyzing the flow failure criteria.

Chapter 3: investigates the effect of fines content (Fluid fine tailings) on the shear behavior of the oil sand tailings. This chapter contains the characteristics of oil sand tailings, fluid fine tailings (FFT), and their mixture. The undrained triaxial test results on the influence of the fine particles on the shear behavior of oil sands are presented and interpreted. The effect of the fines content on the position of the CSL and the shear strength ratios are described.

Chapter 4: evaluates the effect of saturation on the shear response of the oil sand tailings. The required modifications on the triaxial setup that enabled us to have a precise estimation of the saturation level are explained. The procedure adopted based on the theory of wave propagation is discussed in this chapter. Soil water characteristic curves for oil sand tailings with different fines content, measured by pressure plate extractor, are discussed in this chapter. Finally, the yield and post-liquefaction shear strength variation with the degree of saturation (S_r) and the threshold S_r to circumvent static liquefaction in oil sand tailings are presented.

Chapter 2

2 « Static Liquefaction Behavior of Oil Sand Tailings »

2.1 Introduction

Liquefaction is a phenomenon wherein a saturated or partially saturated cohesionless soil loses a great percentage of shear strength due to excess pore water pressure generation (Castro 1969; Casagrande 1976; Poulos 1981; Terzaghi et al. 1996). Dramatic instability and large shear deformation in a relatively short duration have made this phenomenon one of the loose soils' most catastrophic failure mechanisms. In the past decades, considerable efforts have been made to better understand liquefaction susceptibility and stress-strain properties of saturated granular soils using experimental and numerical studies. Hazen (1918); Casagrande (1936); Roscoe et al. (1958); Castro (1969); Castro & Poulos (1977); Casagrande (1975); Ishihara et al. (1975); Poulos (1981); Castro et al. (1982); Been & Jefferies (1985); Sladen et al. (1985); Ishihara (1993); Robertson (1992); Lade (1993); Thevanayagam (1998); Chu & Leong (2002); Cubrinovski & Ishihara (2000); Ni et al. (2004); Yang et al. (2006a); Rahman (2009); Belkhatir et al. (2010a); Lade & Yamamuro (2011); Bayat et al. (2013); Sze & Yang (2014) presented valuable experimental results with respect to the evaluation of liquefaction phenomena. The substantial economic losses, human fatalities, and environmental subsequences result from the failure related to the liquefaction. These failures range from limited sand boils to devastating flow slides based on the extend of liquefaction.

Tar Island dike is an example of oil sand liquefaction flow failure in northern Alberta. Following extraction of bitumen, the waste tailings were placed in ponds. The dike constructed using the upstream method experienced four liquefaction-induced flow slides between 1972 and 1974 in submerged beach sands. The rapid fill placement caused an increase in pore water pressure in loose sand below the starter dike mat. The step over settled 5 m, and the slope of the beach changed for a distance of 240 m to 275 m from the mat. Mittal and Hardy (1977) indicated that a layer of sand about 4.5 m under mat

liquefied and flowed into the pond, whereas the rigid mat settled and broke into several blocks. Calaveras dam and Merriespruit gold mine tailings dam failure are other examples of liquefaction flow failure cases in California and Virginia. The Calaveras dam failure in 1918 was triggered by a monotonically increasing load during rapid construction and resulted in a flowslide with a travel distance of 200 m (Hazen, 1918). Also, the flow slide failure of Merriespruit gold mine tailings dam in 1994 by the over steepening released 600,000 m³ of tailings which flowed for a distance of 2,000 m (Fourie et al., 2001). Barahona Tailings Dam, Chile; Kamenari Landslide, Montenegro; Spitak Embankment, Armenia; Okuli Landslide, Tajikistan; Sullivan Tailings Dam, Canada, are other case histories of the flow failure liquefaction (Muhammad, 2012).

The oil sand deposits in Canada are concentrated mainly in Alberta, Athabasca, Cold Lake, and Peace River. The Athabasca oil sands are the largest and most accessible reserves of bitumen, spanning an area of about 75,000 km². The main resources of mineable oil sands are located north of Fort McMurray, which can be found very close to the surface. The Cold Lake basin extends for about 22,000 km² in the east-central of Alberta. The oil sands deposit is located 985 to 1970 meters below ground surface, making mining economically unprofitable. The composition of the oil sands may vary significantly even in the same geological formation. A typical oil sands deposit contains about 10% bitumen, 5% water, and 85% solids with mostly quartz silica sand. However, the bitumen content can be as high as 20% in some areas. Deposits with higher fines content consist of lower bitumen content. The water content can also vary greatly, from almost zero to as much as 9%.

Qiu and Segoo (2001) compared the undrained response of the oil sand with gold and copper tailings. They indicated that the oil sand shows unusual behavior due to the bitumen and clay minerals. The gold and copper tailings undergo strain-softening behavior while the oil sand shows strain hardening behavior at a similar initial state. Also, Fourie et al. (2001) examined the undisturbed oil sand samples obtained below the phreatic surface using the freezing method. Gas chromatography, cryogenic scanning electron microscopy, and confocal laser scanning microscopy are the methods they employed to investigate the presence of occluded air bubbles. They indicated that a very

small percentage of air bubbles considerably affect the oil sand deposit's undrained response and liquefaction potential.

Depending on the loading condition, several failure mechanisms may occur in a given soil (Kramer 1996). Flow liquefaction can result in substantial slope displacement, landslides, and failure in a dam embankment. Flow liquefaction is associated with undrained strain-softening behavior of a contractive, saturated soil (Baki, 2011) and destroyed static equilibrium in a soil deposit with low shear strength. Static and dynamic undrained loads can trigger flow liquefaction. Rising water levels and rapid fill placement are examples of static loading. Also, earthquakes and blasting are examples of dynamic loading. Harmonic loading produces cyclic stresses and concurrent excess pore water pressure in both contractive and dilative soils. Cyclic instability conditions result from the accumulation of pore pressure during cyclic loading. Excess pore water pressure generation results in deterioration of shear strength, and soil mass may undergo large movements. Shear stress direction changes due to the compressional and extensional loading. The constitutive behavior of sand is affected by various parameters, including void ratio, stress condition, degree of saturation, soil gradation, fines content, and sample preparation method. To understand the shear behavior of soils, the most commonly used devices in the laboratory are triaxial, direct shear, and ring shear devices. The accuracy of these tests in measuring the shear strength parameters depends on the required principles that should be accounted for in each method.

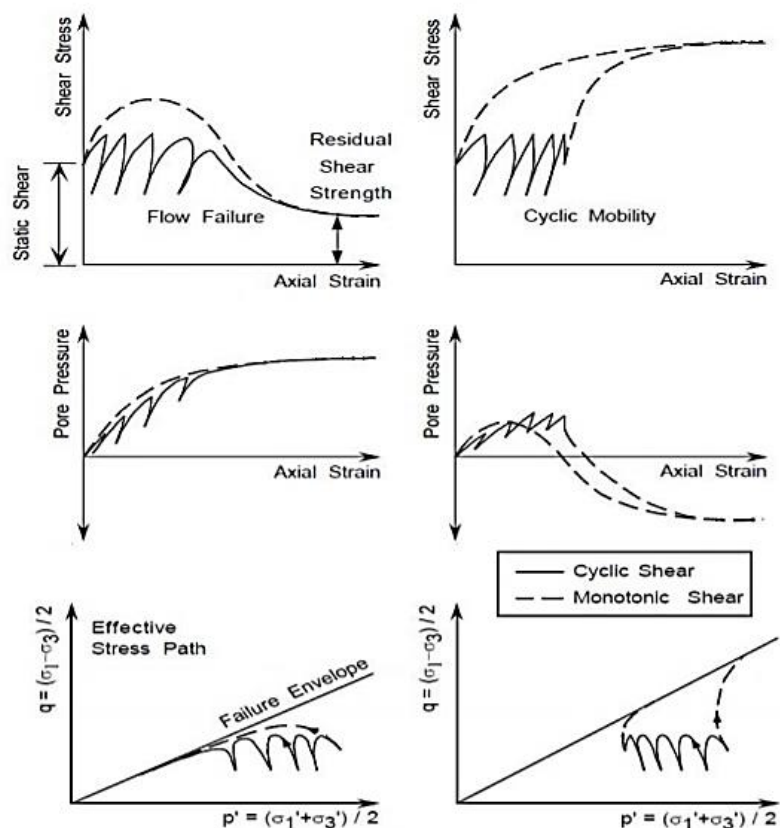


Figure 2.1: Constitutive behavior of both flow failure and cyclic mobility (Kramer 1996)

Undrained triaxial tests are often used to evaluate the liquefaction susceptibility of the soil samples associated with pore water pressure generation mechanism. Regarding triaxial testing, which is used in this study for understanding the shear response of oil sand tailings, the principles and limitations have been discussed by Bishop and Henkel 1962; Lade 1977; Baldi and Nova 1984; Seed 1987; Kramer and Sivaneswaran 1989; Zhang 1997; Finno et al. 1996. The most important factors that could significantly affect test results include:

- Sample volume change during back-pressure saturation

- Variation of specimen cross-section area during loading
- Membrane penetration effect due to confining pressure (Zhu and Anderson 1998)
- Non-uniform deformation at large strain

2.1.1 Behavior of Sands under Monotonic Loading

Evaluating the flow potential of the soil sample and the required triggering mechanism enables us to determine the liquefaction susceptibility of a soil mass. This chapter studies the volumetric response and undrained shear behavior of clean sand under monotonic compression load. Three different types of stress-strain behavior of soil samples based on the initial state of the specimen are illustrated in Figure 2.2.

The loose soil samples show high contractive behavior at initial high mean effective stress (see curve number 3 in Figure 2.2). However, this decrease in volume is inhibited under undrained conditions and offset by an equally opposite pore water pressure generation (Jefferies and Been, 2006). Pore water pressure generation causes a reduction in the effective confining pressure without any tendency for dilation. The stress path under monotonic shear load gradually approaches the peak undrained shear strength, $S_u(\text{yield})$, or instability line at small shear strains where static liquefaction is triggered in a saturated loose sample (Lade, 1992). By further monotonically increasing the shear load after initiation of liquefaction, strain-softening continues until a reduced post-liquefaction strength at large shear strain, $S_u(\text{critical})$, which is also called critical state (Terzaghi et al., 1996) is developed. Steady state, unstable state, flow deformation, instability state are the terminology used in the literature for this stage (Yamamuro & Lade 1997, Guzman et al. 1988, Rahman 2009). When a soil mass is at critical state, it deforms continuously at constant shear stress, constant volume, and constant effective stress (Ishihara 1993, Jefferies and Been 2006, Sadrekarimi and Olson 2009).

Under a monotonic loading condition, a dense soil sample shows contractive tendency at small strains, followed by dilative behavior at higher strains (see curve number 1 in Figure 2.2). Therefore, dense specimens are characterized by strain hardening behavior.

When a medium-dense soil is sheared, initially, its volume tends to decrease, which then changes to dilative behavior at the intermediate strain level. Inhibited volume change during undrained loading condition is offset by an opposite elastic volumetric strain and pore water pressure generation (Jefferies and Been, 2006). Therefore, the soil specimen initially shows a strain-softening behavior which is followed by strain hardening tendency. The point that soil behavior reverses from contractive to dilative is called the phase transformation point (Ishihara et al., 1975).

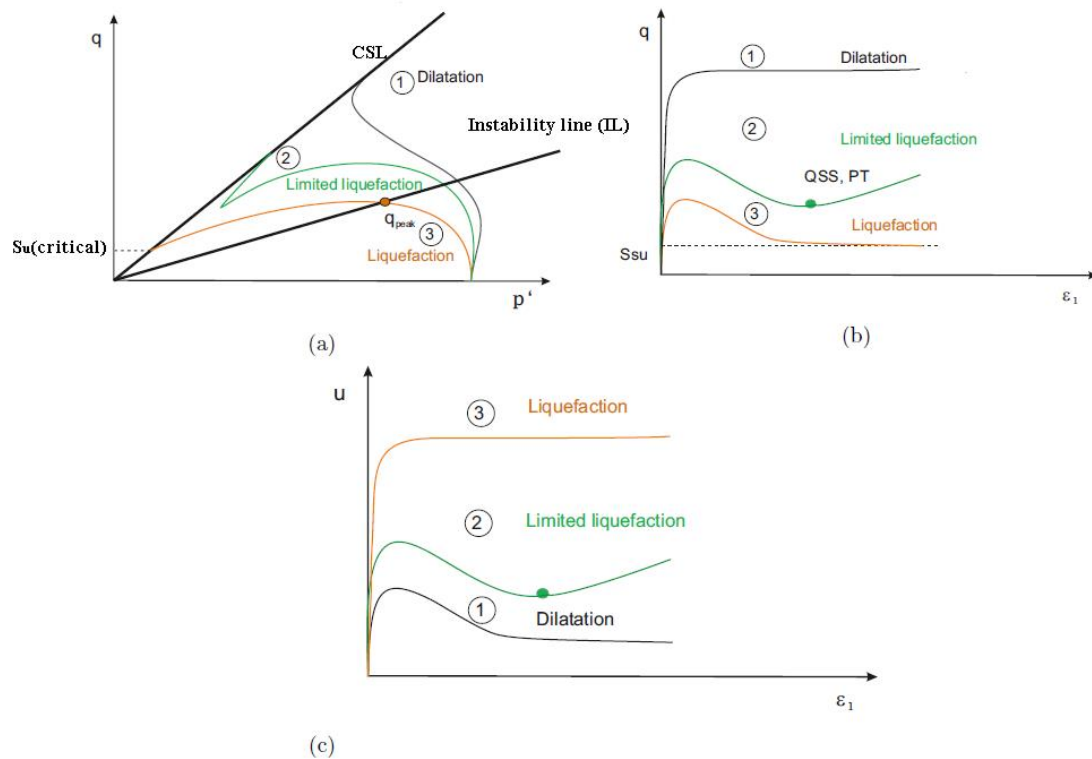


Figure 2.2: Undrained behavior of sand under monotonic loading (a) stress path; (b) stress-strain; (c) pore pressure generation vs. axial strain after Kramer (1996)

Olson (2001) stated three steps for analyzing the liquefaction: (1) Liquefaction susceptibility; (2) Liquefaction triggering mechanism; (3) Post-liquefaction stability. Liquefaction susceptibility includes recognizing the contractive or dilative behavior of soil under shear loading. The soil's strain hardening or strain-softening response depends on its initial state, i.e., the combination of relative density and effective confining pressure.

2.1.2 Yield and post-liquefaction shear strengths

The stress path of an undrained triaxial test performed on a saturated, contractive specimen is illustrated in Figure 2.3. When a contractive or dilative soil is sheared, its volume tends to change, which is inhibited during undrained loading condition. Excess pore water pressure generation compensates this tendency to contraction or dilation. As illustrated in Figure 2.3, the stress path moves toward the peak shear strength at point B, termed yield shear strength ($S_u(\text{Yield})$). Olson and Stark (2003) defined the yield shear strength as a triggering condition or point for static liquefaction. When the stress state in the soil exceeds the yield strength, excess pore water pressure increases, and strain softening occurs. Flow failure continues until the stress path approaches constant shear stress at point C, in which soil deforms at constant effective stress, shear stress, and constant volume (Casagrande 1936). The post-liquefaction shear strength at the critical state is termed post-liquefaction shear strength ($S_u(\text{liq})$) by Olson and Stark (2002). Many researchers recommended post liquefaction shear strength as a proper parameter in evaluating liquefaction susceptibility in practice (Poulos et al. 1985, Seed and Harder 1990, Ishihara 1993, Olson 2006).

The yield and post-liquefaction strengths are normalized by consolidation stress to account for the soil shear strength variation throughout the soil depth ($S_{u(yield)} / \sigma'_v$, $S_{u(liq)} / \sigma'_v$). Many researchers have studied yield and post-liquefaction shear strengths ratios measured in the laboratory, and have found that both increase with reduction in consolidation void ratio (Bjerrum et al. (1961), Hanzawa (1980), Been and Jefferies (1985), Vaid and Sivathayalan (1996)).

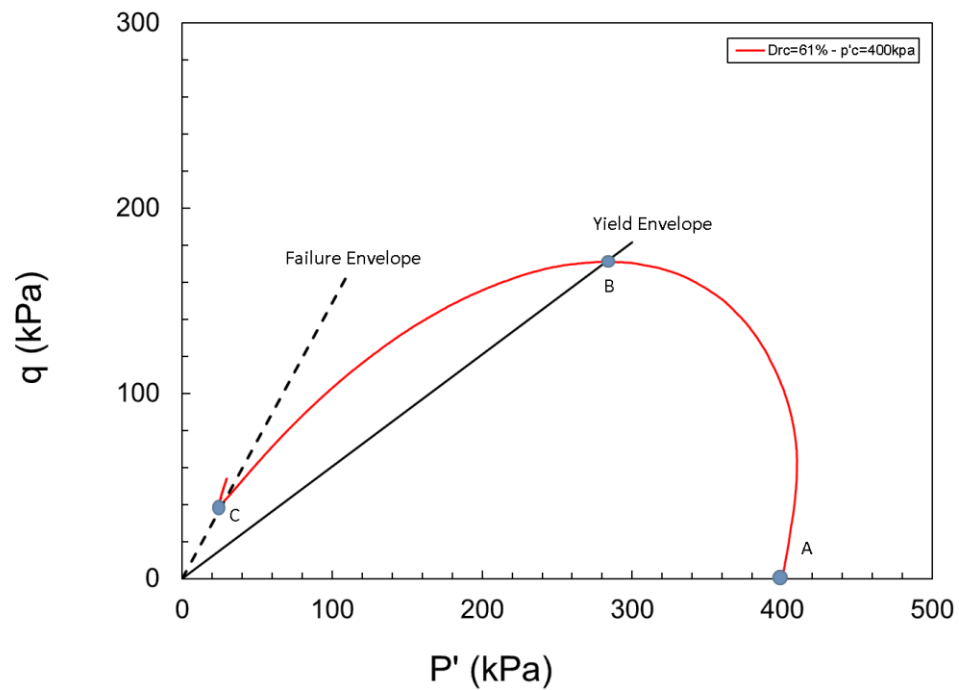
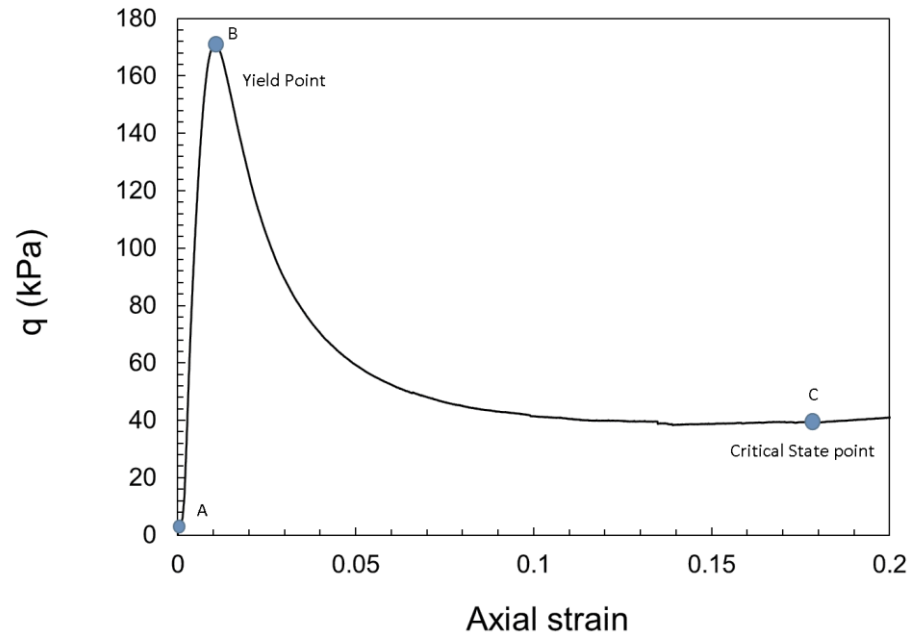


Figure 2.3: Effective stress path from undrained triaxial compression test (IU-Drc=61%-P'c=400kPa)



**Figure 2.4: Stress-strain response from undrained triaxial compression test (IU-
Drc=61%-P'c=400kPa)**

This chapter presents the results of the monotonic triaxial tests performed on the oil sand tailings with different initial states. These results include stress paths and stress-strain behaviors, critical state line, as well as yield and post-liquefaction strength ratios of the oil sand tailings. The critical state framework is used to evaluate the liquefaction potential of oil sand tailings samples and interpret the results.

2.2 Methodology

2.2.1 Oil sand tailings physical properties

In this study, oil sand tailings from a particular mine site in Alberta are adopted as host soil. Oil sand tailings are the material left over after the bitumen extraction, including water, sand, fine particles, residual bitumen, or other hydrocarbons. The oil sand samples were obtained from a particular mine site. The amount of the bitumen was determined as 1.26% using the ignition method. The physical properties of these sands are presented in the following section. The particle size distribution was determined by sieve and hydrometer analysis and presented in Figure 2.6. The grain sizes range from 0.003 mm to 2 mm. Distribution of the soil particles shows a poorly graded material with most particles in the fine-sand size range and 5.45% passing the No.200 sieve (<0.075mm). The sand is classified as SP based on the unified soil classification system as per the ASTM D2487 standard procedure. The sphericity and roundness of the oil sand particles were estimated by Krumbein and Sloss's (1963) chart.

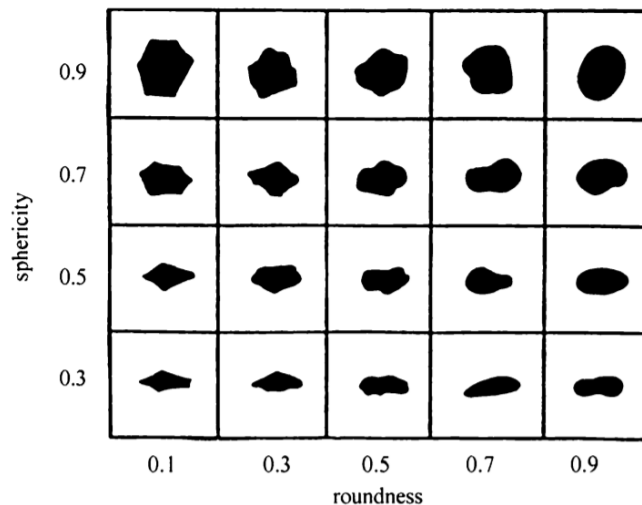


Figure 2.5: Krumbein and Sloss chart to visualize the estimation of sphericity and roundness.

According to the SEM images presented in Figure 2.7, the oil sand particles' sphericity is relatively high, and elongated particles are rare. Also, the roundness varies widely, from angular to well-rounded, with subangular shapes being the most common. XRD analysis reports the presence of quartz (SiO_2) and bitumen in the oil sand tailings.

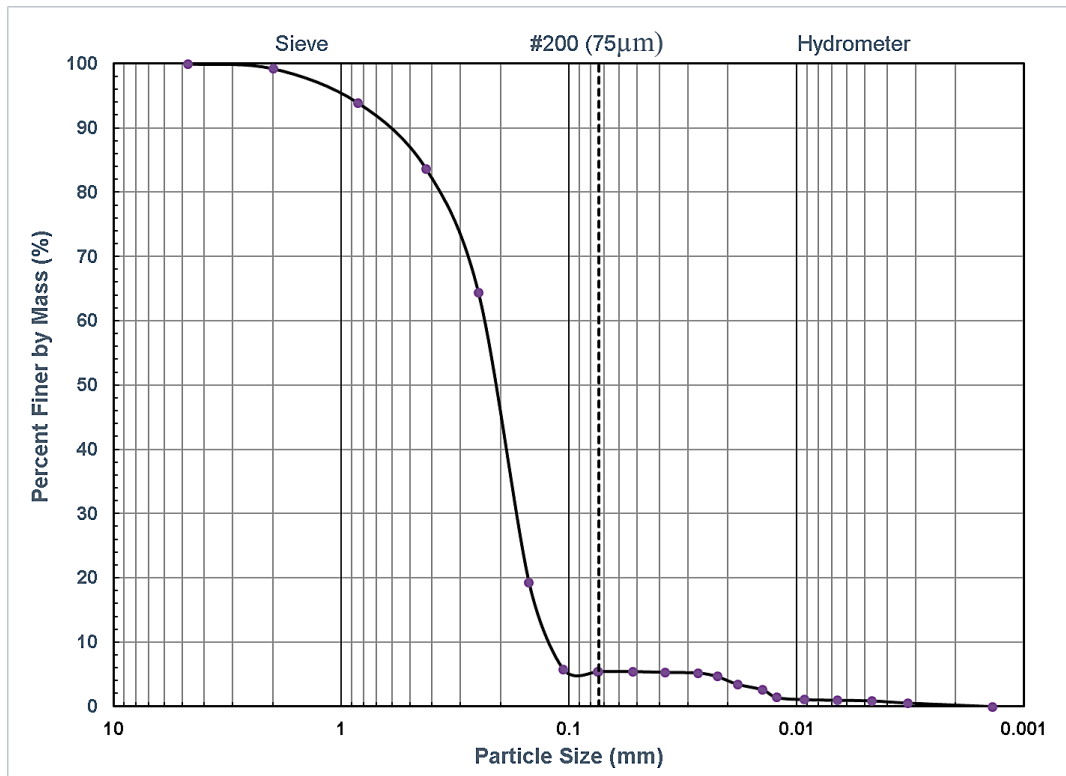


Figure 2.6: Particle size distribution of the oil sand tailings

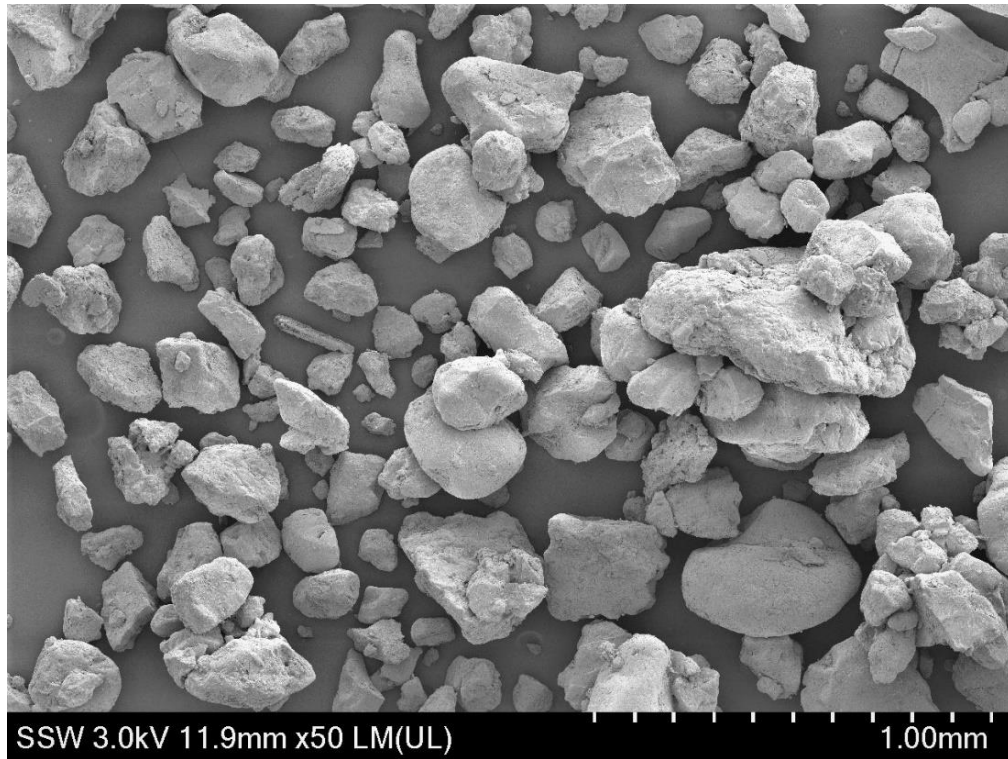


Figure 2.7: Shape of oil sand particles (SEM images)

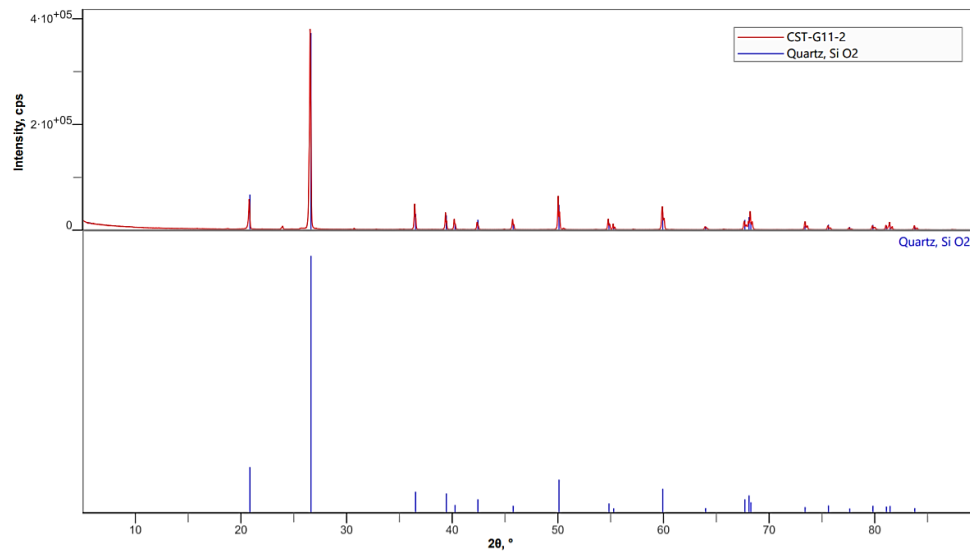


Figure 2.8: XRD image of the oil sand tailings

2.2.2 Index properties

Standard index tests were carried out, and Table 2.1 presents a summary of index properties for the samples. The mean grain size (D_{50}) was determined as 0.218 mm, and the measured coefficient of uniformity (C_u) and the coefficient of curvature (C_c) are 2.01 and 1.05, respectively. The Values of maximum and minimum void ratios were determined according to ASTM D4253 and D4254 standard methods. The specific gravity of the sand particles was about 2.624, following the ASTM-D854 standard procedure.

Table 2.1: Parameters of the oil sand tailings

D_{50} (mm)	G_s	e_{max}	e_{min}	C_u	C_c
0.218	2.624	0.93	0.503	2.01	1.05

2.2.3 Triaxial test procedure

Triaxial test device, sample preparation, sample saturation, and consolidation, and the required measures to minimize the errors during the triaxial compression tests are discussed in detail in the following sections.

2.2.3.1 Triaxial test apparatus

The triaxial test system used for measuring the intermediate and large strain properties in this research is an automated stress path triaxial system (SIGMA-1TM 5K model) manufactured by GeoTac Company. The loading frame, including an external load cell, is used to apply the axial load in displacement control conditions at a rate of 5% per hour.

An internal load cell which has a maximum loading capacity of 2225 N is directly connected to the loading rod. The internal load cell is used to measure the applied axial load to the soil sample accurately. Cell and pore pressure pumps control the pressure and volume of the cell fluid and specimen's pore water. Also, an external pore pressure transducer with a maximum capacity of 1400 kPa is connected to the bottom of the sample to measure the pore water pressure while the pore pump drainage valves are closed. The triaxial cell in the loading frame is presented in Figure 2.9.

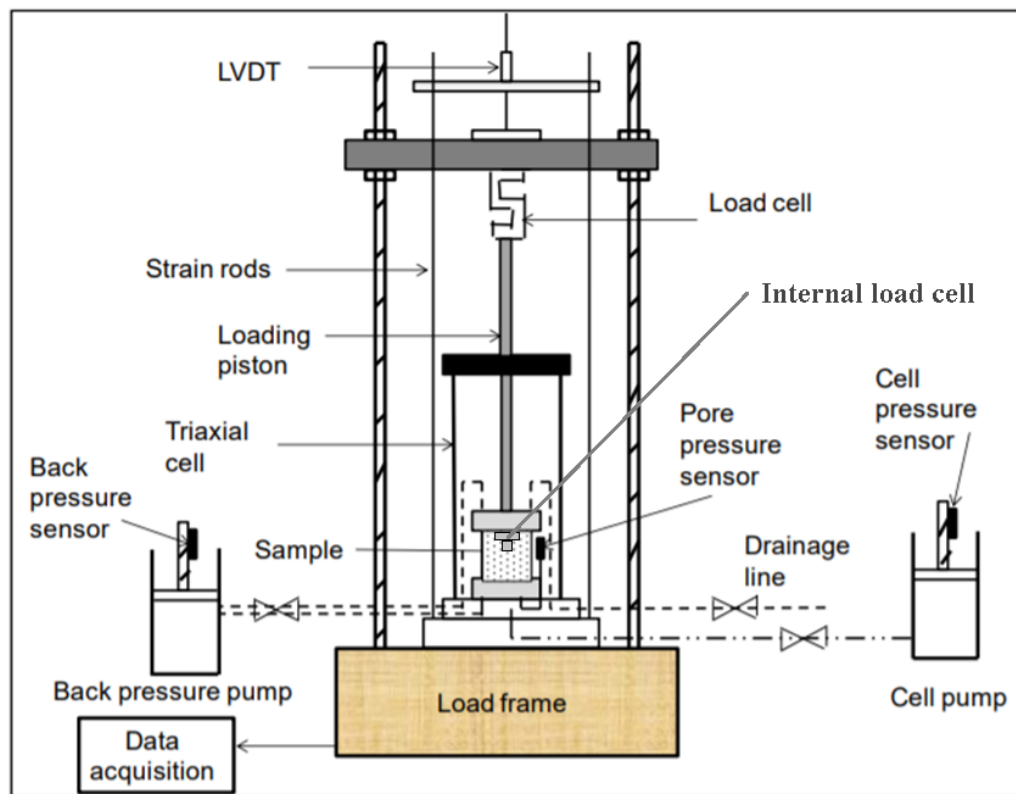


Figure 2.9 Schematic diagram of the triaxial testing system (Modified from Omar 2013)

2.2.3.2 Sample preparation

The arrangement of the soil particles and pore spaces in a given soil sample during deposition is known as the initial fabric (Mitchell & Soga, 2005). The sample preparation method affects the soil specimen's engineering characteristics due to the different soil fabrics (Goudarzy, 2015). There are several methods for preparing sand specimens in the laboratory, including moist tamping, air pluviation, and slurry deposition. Therefore, the reconstituted soil sample preparation method must meet the following criteria (Kuerbis, 1985):

- Uniformity of void ratio throughout the sample
- Fully saturation of the sample

The air pluviation method involves pluviating dry sand through a funnel from a constant height. By changing the fall height, different densities are achievable. This method is not suitable for higher fines content due to particle segregation. The moist tamping method is a more common method to prepare loose samples. In this method reconstituted soil sample is prepared by compacting the mixture of soil with specific water content in layers (Lambe 1951). Due to the water tension forces, the generated suction allows us to prepare samples with higher void ratios (Kuerbis, 1985). Also, the homogeneity of the sample would be high enough (Fourie and Papageorgiou 2001). Employing the traditional method of moist tamping technic results in a non-uniform void ratio distribution within the specimen since compaction of overlying layers increases the density of underlying layers slightly (Sadrekarimi and Olson 2012). Ladd (1978) suggested the under-compaction method to account for this issue. In the under-compaction manner, the preparation density of the underlying layers is lower than the global density, and the density of the overlying layers is higher than the global density of the sample, leading to a uniform soil specimen. The difference in density of the successive layers is called the “under-compaction ratio” (Ladd 1978).

In this study, the under-compaction method is employed to prepare specimens of 70 mm in diameter and a height-to-diameter ratio of one. The step by step procedure used to prepare the specimens is described briefly in the following:

- 1- Porous stone is boiled for 15 minutes to eliminate all the entrapped air inside the porous stone voids.
- 2- Top and bottom acrylic platens were greased to prevent any water leakage inside the sample.
- 3- The latex membrane was installed around the bottom platen and secured with three O-rings to seal it properly.
- 4- The split mold was installed around the bottom platen and rubber membrane. A specific amount of suction was applied through the mold to eliminate all the air between the membrane and the mold. A disk-shaped membrane impregnated with oil is placed on the bottom platen to reduce the friction between the soil particles and the platen surface (enlarged platens).
- 5- A predetermined amount of soil using the under-compaction method was calculated and mixed with water. The prepared mixture was poured into the mold and tamped in 4 layers. Each layer being 1.75 cm thickness.
- 6- Another disk-shaped membrane impregnated with oil similar to the one used for the bottom of the specimen was placed on the top of the soil before placing the upper platen.
- 7- The latex membrane was folded around the upper platen and sealed with three O-rings.
- 8- Once the specimen is prepared, a small amount of suction was applied by the pore pressure pump inside the sample to maintain the stability of the sample while taking apart the mold.

9- The cylindrical triaxial cell was assembled and placed on a load frame, filled with de-aired water, and the vacuum pressure was replaced by an external cell pressure of 10 kPa.

To confirm the uniformity of the specimens, a plug sample test was carried out. In this regard, three aluminum cups were placed through the height of the sample at a constant distance from each other. Once the sample preparation had been completed, the aluminum cups are gently removed from the sample. The weight of the dried soil inside the cups was measured. Also, the volume of each cup was measured by filling them with water and measuring the weight of water. Then the void ratio for each plug sample was calculated. The uniformity test result provided in Table 2.2 shows that void ratios obtained from different heights are very close, and the specimen is uniform.

Table 2.2: Plug samples void ratio

<i>Sample#</i>	W_{cup}	$W_{cup} + W_{drysoil}$	V_{cup}	e
1	1.31	57.77	50.46	0.862
2	1.31	58.4	51.48	0.883
3	1.30	59.6	51.80	0.873

2.2.3.3 Sample saturation

The saturation of the sample consists of three steps: (1) Carbon dioxide percolation, (2) Water flushing, (3) Backpressure saturation. Before sample preparation, boiling the porous stones is necessary to eliminate all the entrapped air inside the porous stone voids. After applying 10 kPa cell pressure in 15 minutes, as seating pressure, the saturation stage begins with carbon dioxide percolation to maintain the specimen fabric. Carbon

dioxide's higher solubility in water than air allows us to reach a fully saturated level in specimen with reduced time and backpressure (Mulilis et al. 1978). The CO₂ percolation through the sample from bottom to top drain lines takes about 60 minutes. And the flow rate was kept to three bubbles in a second to ensure minimal disturbance to the specimen.

The second step of the specimen saturation is de-aired water flushing from the bottom of the sample to the drainage line connected to the top of the sample. In this step, the amount of water that stays inside the sample was measured to calculate the void volume changes of the sample during saturation as the second method for determination of the sample volume change during saturation which is explained in detail at next paragraph. In this regard, the inflow and outflow water volumes were calculated by measuring the weight of the input and output containers connected to the bottom and top drainage lines, respectively, during saturation. The water flow rate was adjusted by the height of the input container from the bottom of the specimen, which should be kept low to prevent fine particles from washing out during water percolation.

The third step of the saturation procedure is backpressure saturation, as Black and Lee (1973) recommended. In this phase, 200 kPa – 400 kPa backpressure was applied via a pore pump to dissolve the remaining carbon dioxide into water. This was done by applying a specific increment of cell pressure while maintaining an effective stress of 10 kPa. Skempton's pore water pressure parameter was used to measure the specimen's level of saturation. The Skempton's pore water pressure B was calculated as the rise in the specimen's pore water pressure divided by the increased cell pressure in each increment. All the saturated specimens in this chapter had a B -value higher than 0.98.

2.2.3.4 Determination of the volume change during saturation

One of the major sources of errors that could significantly affect triaxial test results was sample volume changes during the sample saturation stage. The measured sample volume

change can highly influence specimens void ratio and subsequently the position of the critical state line. The sample freezing method at the end of the test is used in this study as an accurate method to estimate the sample volume change. Sladen and Oswell (1989) employed the specimen freezing technique for Syncrude tailings sand to measured void ratio changes due to saturation. By measuring the final void ratio of the sample using the freezing method, the sample void ratio change during saturation can be calculated using the following equation:

$$\Delta e_{sat} = \Delta e_{total} - \Delta e_{consolidation} \quad \mathbf{2-1)}$$

Where Δe_{total} is difference of the final void ratio (measured by freezing method) and the initial void ratio (sample preparation void ratio), and $\Delta e_{consolidation}$ is the void ratio changes during consolidation which is recorded by the pore pump.

Additional to the freezing method, two other techniques were employed to validate the sample volume change results: (1) measuring the amount of water that remains inside the sample during water flushing and (2) determining the sample volume change by measuring the cell fluid volume changes.

In the first technique, the inflow and outflow water volumes were calculated by measuring the weight of the input and output containers connected to the bottom and top drainage lines, respectively, during saturation. The water flow rate was adjusted by the height of the input container from the bottom of the specimen, which should be kept low to prevent fine particles from washing out during water percolation. The results of the measured void volume changes are presented in Table 2.3. In the second technique, the cell fluid volume change was recorded by the cell pump. And the ratio of the cell volume changes and the sample pore volume change during the consolidation stage was calculated. This ratio was employed to calculate the pore volume change during saturation. The calculated void volume changes are presented in Table 2.3. Figure 2.10 and Figure 2.11 compare the void volume changes measured by the freezing method with

the two other methods proposed above. By comparing these two methods with the freezing method, it is observed that the void volume changes obtained by measuring the amount of water remaining inside the sample (first method) is close to the volume change obtained by the freezing method. Therefore, the first method can be used as an alternative method to the freezing technique to determine the precise sample volume change in triaxial testing. On the other hand, the second method leads to unreliable results and the reported values are far from the values obtained from the freezing method. The lines and cell wall are not rigid and tend to reshape under higher cell pressures during consolidation which causes incorrect cell to pore volume ratio.

Table 2.3: Void volume changes during saturation stage

<i>Test ID</i>	<i>Consolidation relative density</i>	<i>Consolidation void ratio</i>	ΔV_v <i>(Freezing)</i>	ΔV_v <i>(inflow/outflow)</i>	ΔV_v <i>(cell volume ratio)</i>
<i>Test type</i>	<i>Drc (%)</i>	<i>e_c</i>	ΔV_v (ml)	ΔV_v (ml)	ΔV_v (ml)
<i>IU-TXC</i>	44.33	0.7407	-10.244	N/A	-3.86
<i>IU-TXC</i>	59.48	0.676	-1.474	-1.443	1.819
<i>IU-TXC</i>	61.24	0.6685	-11.689	-12.046	-2.072
<i>IU-TXC</i>	52.53	0.7057	-12.74	-12.16	-5.488
<i>IU-TXC</i>	46.51	0.7314	-22.945	-23.394	-5.82
<i>ID-TXC</i>	55.49	0.693	-21.745	-19.623	-9.421
<i>ID-TXC</i>	51.96	0.708	-17.99	-17.032	-8.247
<i>ID-TXC</i>	52.15	0.707	-8.34	-7.713	-6.346
<i>ID-TXC</i>	51.36	0.711	-5.08	-12	-9.05
<i>ID-TXC</i>	58.22	0.681	-3.717	-2.822	-2.648
<i>ID-TXC</i>	71.84	0.623	-2.145	-1.404	-0.266
<i>ID-TXC</i>	82.99	0.576	-1.138	-0.823	-1.238
<i>K₀U-TXC</i>	64	0.657	-23.58	-20.294	-6.618
<i>K₀U-TXC</i>	58	0.682	-21.69	-18.33	-2.495
<i>K₀U-TXC</i>	66	0.65	-8.817	-4.577	-2.852
<i>K₀U-TXC</i>	63	0.66	-1.349	-2.403	-2.776
<i>K₀U-TXC</i>	52	0.71	-15.154	-15.292	-6.303
<i>K₀U-TXC</i>	63	0.663	-18.436	-14.004	-4.78
<i>K₀U-TXC</i>	60	0.675	-0.723	-0.362	-2.01

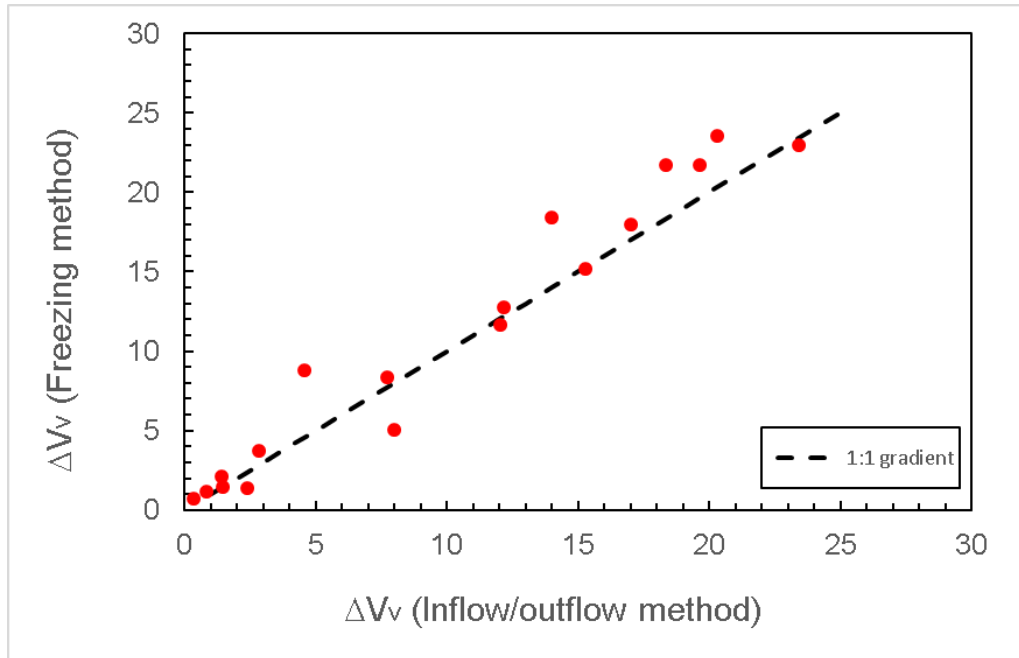


Figure 2.10: Comparison of the void volume change measured by freezing method and inflow/outflow method

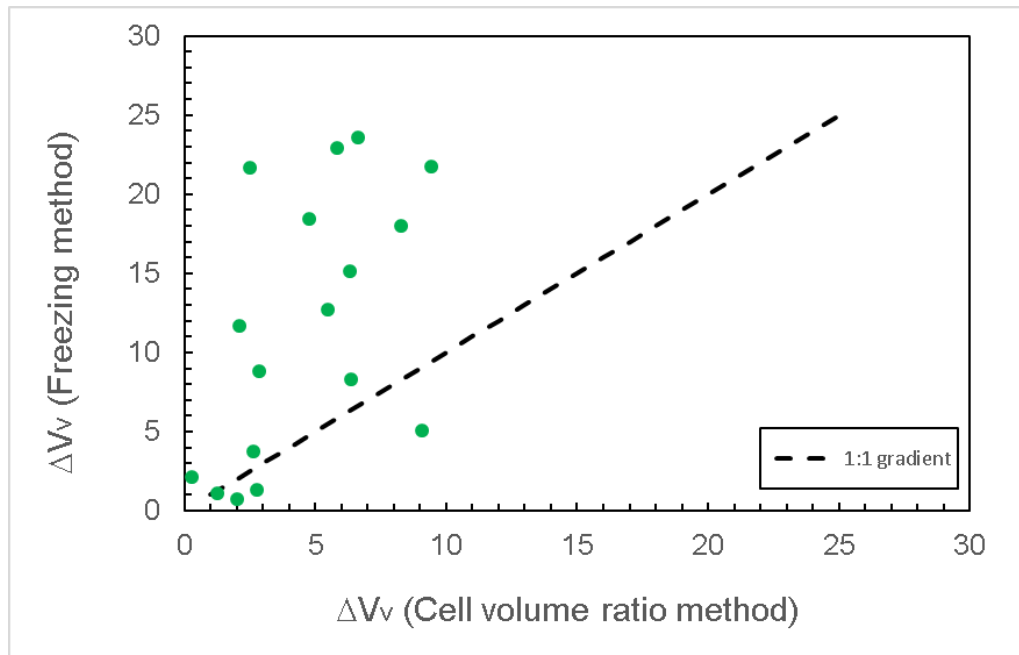


Figure 2.11: Comparison of the void volume change measured by freezing method and inflow/outflow method

2.2.3.5 Consolidated Undrained shearing

All the specimens were consolidated under isotropic or K0 stress states after the completion of sample saturation. Isotropically consolidating the soil samples consisted of maintaining a constant cell pressure while gradually decreasing the pore pressure to a target value. Specimens were allowed to consolidate for about one hour until the pore water volume remained unchanged. The K0 consolidation stress state was performed by adjusting the cell pressure and vertical stress simultaneously to prevent radial deformations of the soil sample. The primary purpose of the K0 consolidated tests was to simulate the field stress state in the laboratory test and understand the naturally deposited soil behavior. During the K0 consolidation, the horizontal strain is kept zero at a constant cross-section area, leading to equal volumetric (ϵ_v) and axial strains (ϵ_a). Figure 2.12 shows an example of volumetric strain changes with axial strain during K0 consolidation. A linear trend with a gradient of 1:1 confirms the K0 condition during the consolidation. The K0 value is determined by calculating the slope of Figure 2.13, which shows the variation of effective horizontal pressure with effective vertical pressure, which is constant during consolidation.

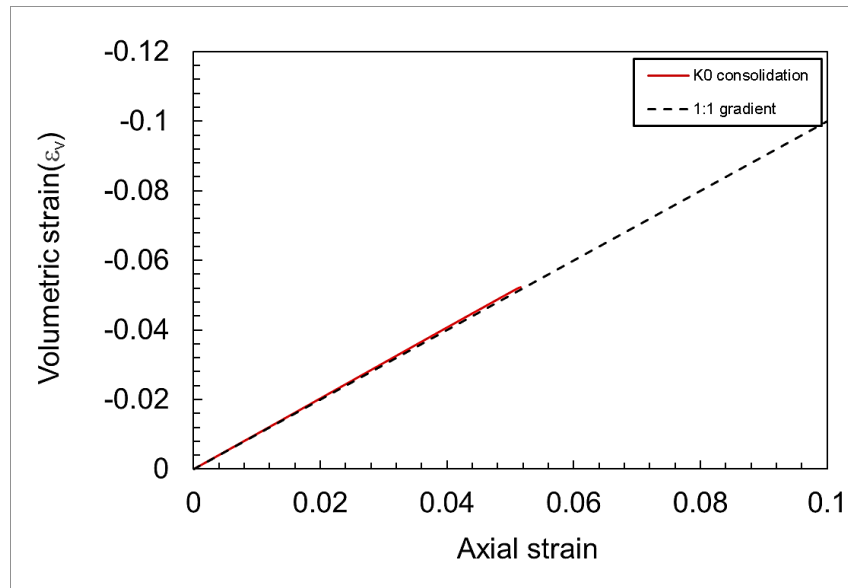


Figure 2.12: Volumetric strain variation with axial strain in a k0 consolidation stage

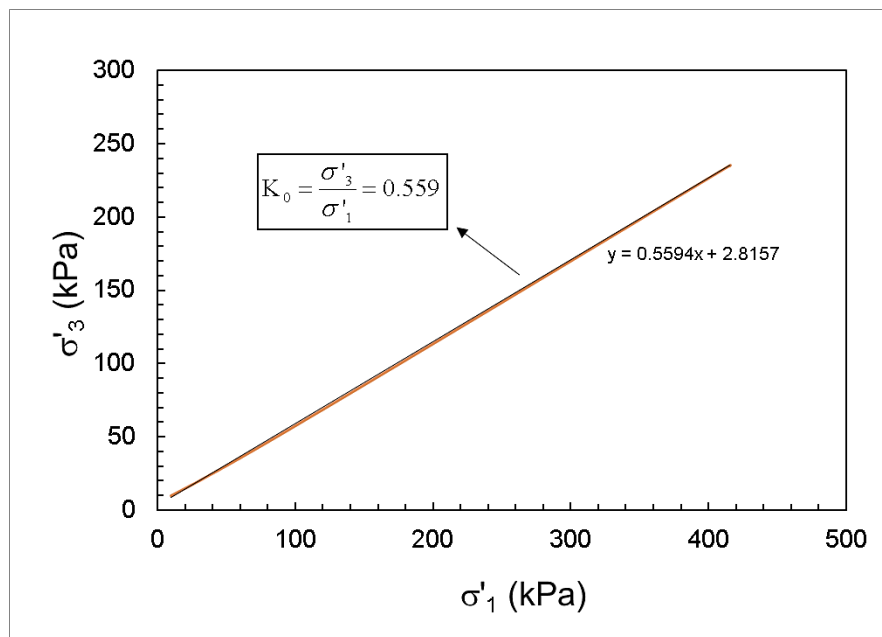


Figure 2.13: Major and minor effective stress variation in a K0 consolidation stage

The specimen void volume change during consolidation is very important, as it was used to indicate the density state of a soil specimen. The pore pump can determine the void ratio change in this phase, which records any water volume change inside the sample during consolidation (Figure 2.14).

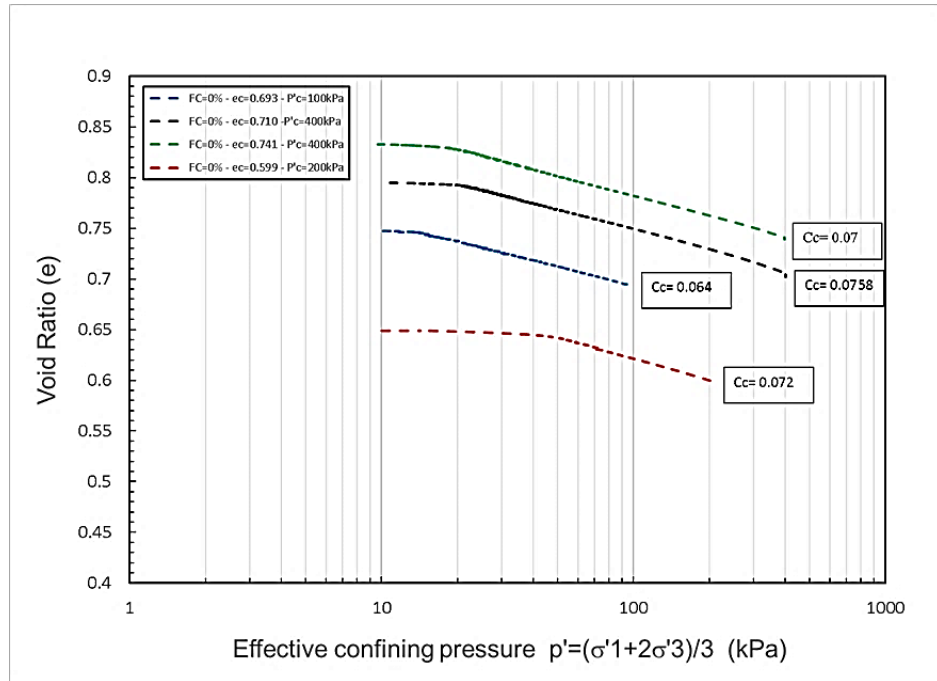


Figure 2.14: Void ratio changes during the consolidation stage

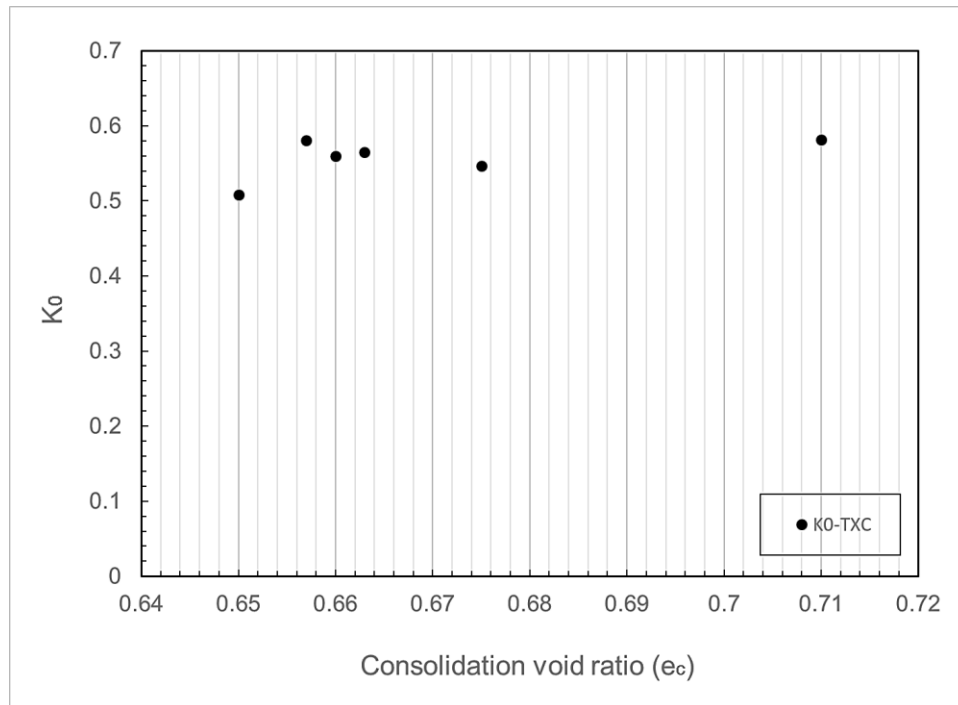


Figure 2.15: K0 variation with consolidation void ratio

2.2.3.6 Monotonic loading system

Once the sample was completely consolidated, and the pore pump volume stabilized, the specimen was sheared. The axial load was applied in strain-controlled mode. The cell pressure was kept constant, and pore pressure was measured with a pressure transducer in the undrained tests, while the backpressure pump recorded volume change during drained shearing. The applied axial deformation rate was chosen based on the ASTM guideline for the drained and undrained shearing condition as below:

$$\left\{ \begin{array}{l} \dot{\varepsilon} = \frac{4\%}{10t_{50}} \Rightarrow CIU \\ \dot{\varepsilon} = \frac{4\%}{16t_{90}} \Rightarrow CID \end{array} \right\} \quad (2-2)$$

Where t_{50} and t_{90} are the times corresponding to the 50% and 90% level of consolidation, respectively. t_{50} and t_{90} values for the undrained and drained triaxial test performed in this research were 1916 s and 3446 s, respectively. The axial deformation rate was chosen to ensure complete pore pressure dissipation in drained loading and equalization of pore water pressure during undrained shearing. The target axial deformation to reach critical states was 30% axial strain.

2.3 Results and Discussions

The results of static triaxial tests carried out on oil sand tailings with the different initial states are presented below. These results include the stress-strain behavior of the oil sand tailings with different relative densities (void ratio) for drained and undrained shearing. The repeatability of the triaxial tests was examined by two undrained triaxial test results

with different initial void ratios but almost similar consolidation void ratios. Both specimens were isotropically consolidated to the 400 kPa. As illustrated in Figure 2.16, the specimens with a similar initial state show similar undrained responses and stress-strain behavior.

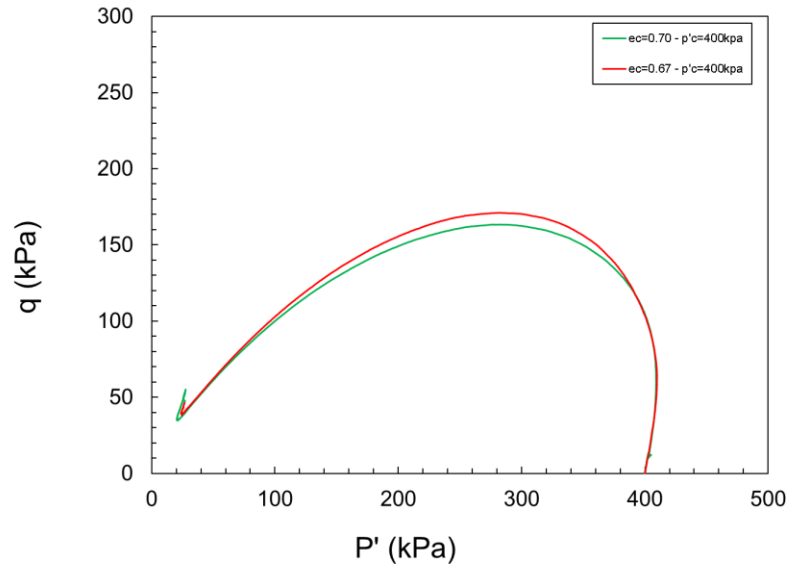


Figure 2.16: Evaluation of triaxial tests repeatability on specimens with similar initial state

Table 2.4: Triaxial testing program on the oil sand tailings

<i>Test ID</i>	<i>Consolidation relative density</i>	<i>Consolidation void ratio</i>	<i>Critical state void ratio</i>	<i>Consolidation stress</i>		<i>CS confining pressure</i>
<i>Test type</i>	<i>Drc (%)</i>	<i>e_c</i>	<i>e(cs)</i>	<i>σ'₁ (kPa)</i>	<i>σ'₃ (kPa)</i>	<i>P'(cs) (kPa)</i>
<i>IU-TXC</i>	44.33	0.7407	0.7407	400	400	11.803
<i>IU-TXC</i>	59.48	0.676	0.676	400	400	69.45
<i>IU-TXC</i>	61.24	0.6685	0.6685	400	400	23.77
<i>IU-TXC</i>	52.53	0.7057	0.7057	400	400	19.9
<i>IU-TXC</i>	46.51	0.7314	0.7314	400	400	13.69
<i>IU-TXC</i>	53.63	0.701	0.701	300	300	11.1

<i>IU-TXC</i>	47.57	0.722	0.722	200	200	13.46
<i>IU-TXC</i>	58.55	0.680	0.680	100	100	27.9
<i>ID-TXC</i>	55.49	0.693	0.6111	100	100	176.76
<i>ID-TXC</i>	51.96	0.708	0.62546	100	100	185.5
<i>ID-TXC</i>	52.15	0.707	0.6211	400	400	693.83
<i>ID-TXC</i>	51.36	0.711	0.625	400	400	692.65
<i>ID-TXC</i>	58.22	0.681	0.632	100	100	178.6
<i>ID-TXC</i>	64.69	0.654	0.595	400	400	638.52
<i>ID-TXC</i>	71.84	0.623	0.6295	100	100	182.2
<i>ID-TXC</i>	82.99	0.576	0.588	400	400	728.45
<i>K₀U-TXC</i>	64	0.657	0.657	300	179	25.28
<i>K₀U-TXC</i>	58	0.682	0.682	330	175	24.74
<i>K₀U-TXC</i>	66	0.65	0.65	320	164	37.28
<i>K₀U-TXC</i>	63	0.66	0.66	310	177	25.1
<i>K₀U-TXC</i>	52	0.71	0.71	410	240	20.09
<i>K₀U-TXC</i>	63	0.663	0.663	415	235	24.84
<i>K₀U-TXC</i>	60	0.675	0.675	400	220	54.54

2.3.1 Stress paths and stress-strain behaviors of undrained triaxial tests

Several studies have been carried out on the effect of the initial state on the undrained monotonic response of soils. For the present study, stress-strain relationships, deviatoric stress variation, and effective stress paths were investigated. Test results for the achieved density ranges are presented in Table 2.4.

The stress-strain curve obtained from the triaxial compression tests on different consolidation relative densities are demonstrated in Figure 2.18. The relative density of

the specimens used for the undrained triaxial tests ranges from 44% to 61% at a confining pressure of $p'_c = 400$ kPa.

All specimens exhibited strain-softening behavior since the deviator stress decreased sharply after a peak value. Both mobilized deviator stress, which corresponds to the peak shear strength, and critical shear strength increase as the specimen becomes denser. The axial strain (ϵ_a) corresponding to the peak deviator stress increases with relative density. The excess pore water pressure generated (Δu) along with the undrained shear for two specimens with relative densities of 44% and 53% consolidated to the same p'_c are illustrated in Figure 2.19. A more-or-less equal pore water pressure is generated at the initial steps. However, the developed pore water pressure at axial strain higher than 1.5% for the looser specimen is higher than the denser samples.

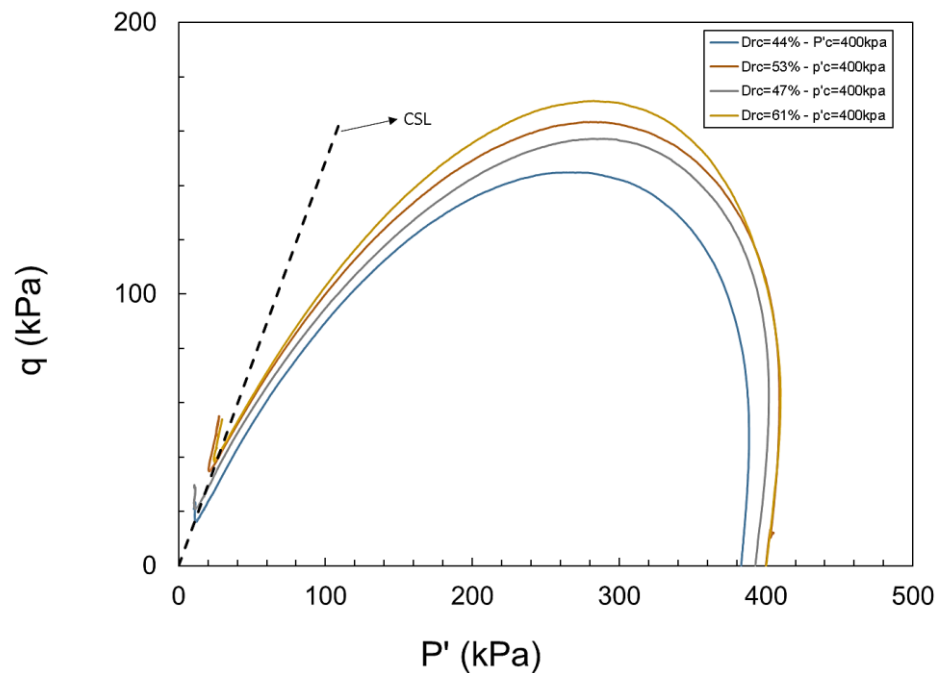


Figure 2.17: Effective stress paths of the undrained triaxial tests for samples with confining pressure of $p'_c=400$ kPa and different relative densities.

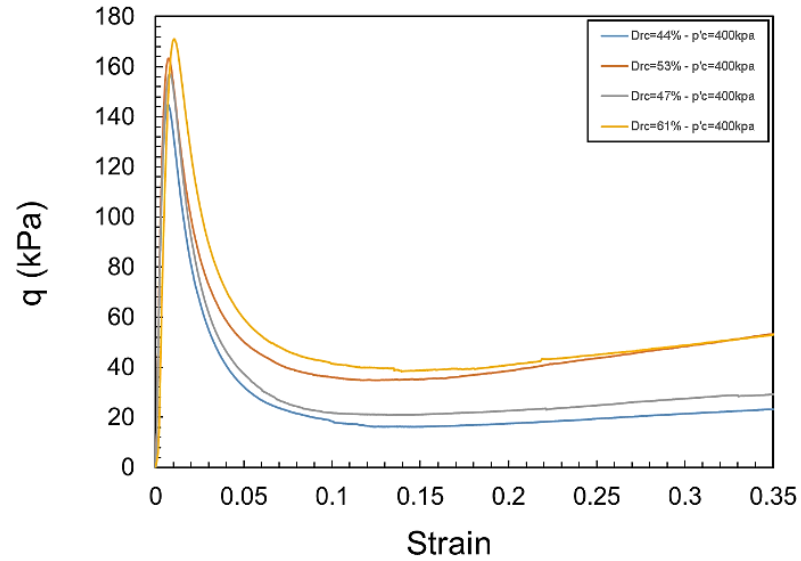


Figure 2.18: Stress-strain response of the undrained triaxial tests for samples with confining pressure of $p'_c=400$ kPa and different relative densities.

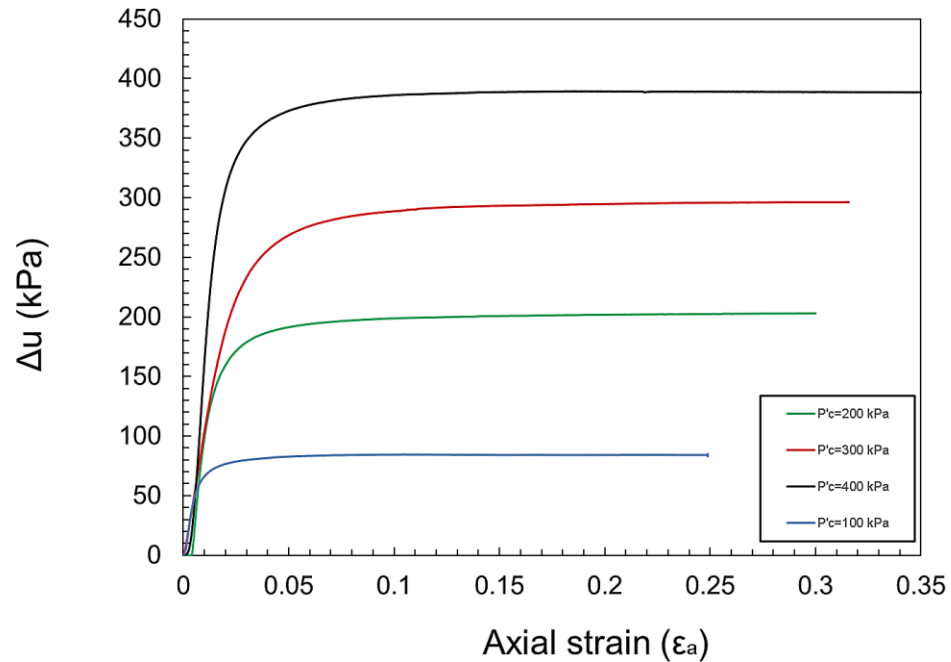


Figure 2.19: Generated excess for water pressure for the isotropic consolidated undrained triaxial tests with confining pressures of 100, 200, 300, 400 kPa

The effective stress paths obtained from undrained shear of the specimens with the consolidation relative densities of 44%, 47%, 53% and 61% are illustrated in Figure 2.17. The undrained response of all samples reaches an instability line as the soil specimen is sheared. The instability line is defined for the stress paths showing flow liquefaction. The instability line crosses the origin of the q - p' plane and the peak point of the stress path. Also, it is known as the initiation of the strain-softening behavior. Lade (1992) defined the instability line as the lower bound of all possible unstable conditions. The instability line is not unique for a soil mass. Chu and Leong (2002) illustrated different instability lines for the specimens with the different void ratios. The stress path inside the instability region tends to move toward the critical state line (CSL). The peak point of the stress path is of paramount importance since it is known as the initiation of static instability (Murthy et al., 2007; Lade & Yamamuro, 2011; Baki, 2011). The slope of the instability line is known as the instability stress ratio ($\eta = q_{peak} / p'_{corresponding\ to\ q(peak)}$). As illustrated in Figure 2.20, the instability stress ratio for the undrained triaxial tests ranges from $\eta = 0.54$ to $\eta = 0.7$. The slope of the instability line increases as the void ratio of the specimen decreases.

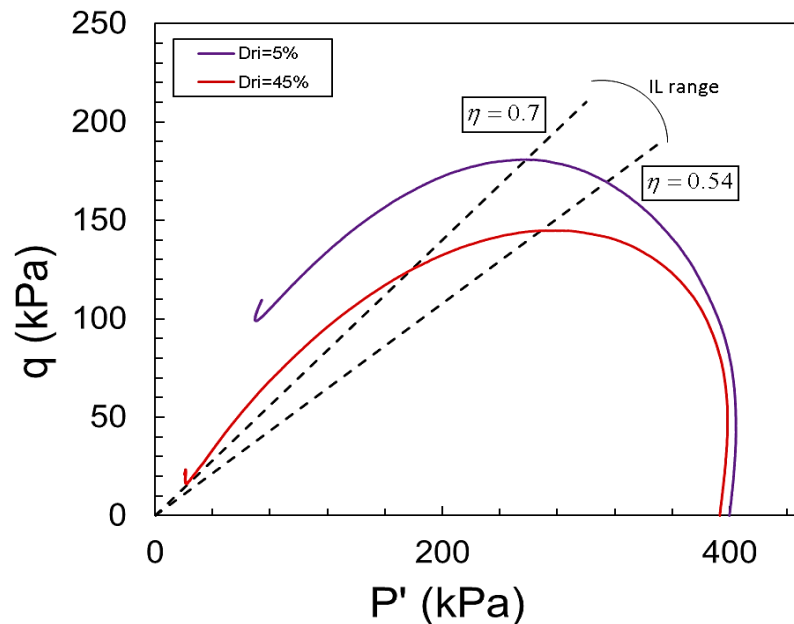


Figure 2.20: Instability line range for the undrained triaxial tests

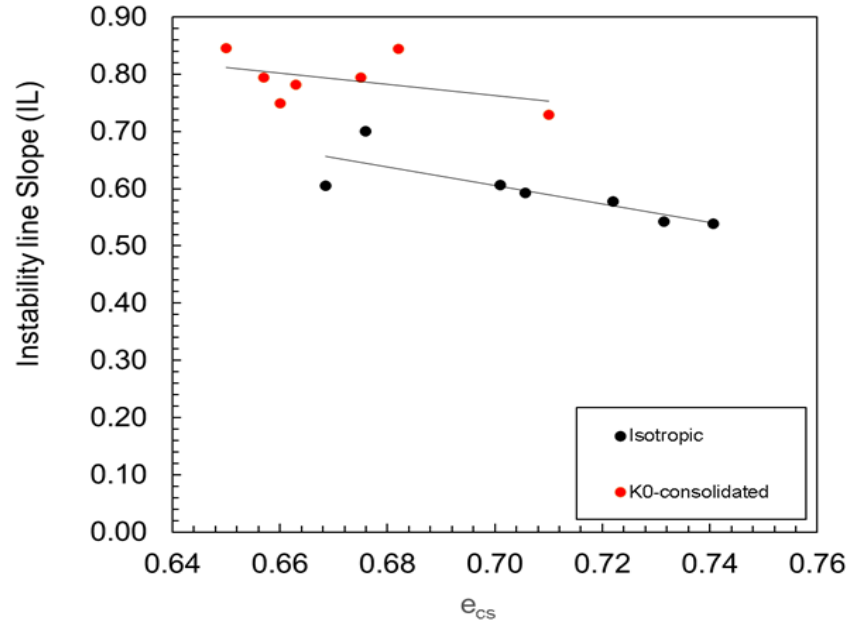


Figure 2.21: Variation of instability line slope with void ratio

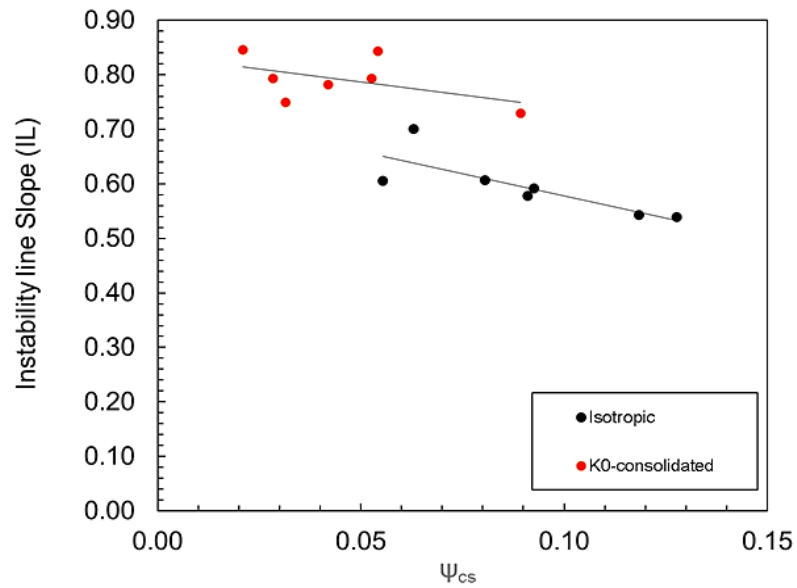


Figure 2.22: Variation of instability line slope with state parameter

2.3.2 K0-consolidated undrained response

A soil element in a natural deposit is subjected to the vertical overburden and radial confining stresses under zero lateral strain condition. In reality, the lateral stresses are smaller than vertical stress. Seven anisotropically consolidated undrained tests were performed to better understand oil sand tailings behavior under a laterally-confined stress condition similar to the in-situ stress state. The K0-consolidation was conducted at a very low strain rate loading to avoid excess pore water pressure generation during the consolidation stage. Following the deviator stress application, the cell pressure was increased to maintain the cross-section area unchanged for the soil specimen during the consolidation. The zero lateral deformation was achieved by cell pressure adjustment.

Figure 2.24 depicts the deviator stress variation with axial strain for the K0-consolidated specimens. The undrained response of the samples commenced with specific deviator stress due to the fact that the sample had been subjected to the K0 consolidation. The deviator stress rapidly increased to its peak stress with the initiation of the undrained shearing stage before reaching the critical state. Also, the pore water pressure generation for K0-consolidated samples was quicker than the isotropically consolidated specimens.

Figure 2.24 shows the effective stress path of the undrained compression test on the K0-consolidated samples. The K0 is the major effective stress ratio during the consolidation stage. Also, the K0 values are provided beside the stress paths. The stress path reaches the yield strength point quickly with the shear loading initiation and eventually moves towards the critical state. The K0 values obtained directly from the experimental test were 0.55 to 0.58 based on different initial states. The critical state friction angle calculated using the equation below for the K0-consolidated samples was $\phi'_{cs} = 36^\circ - 42.4^\circ$ and for the isotropically consolidated samples was $\phi'_{cs} = 31.9^\circ - 40.1^\circ$. Also, the K0 values computed based on the Jaky equation using the critical state friction angle were from 0.59 to 0.67.

$$M_{cs} = \frac{6 \sin \varphi'_{cs}}{3 - \sin \varphi'_{cs}} \quad (2-3)$$

$$K_0 = 1 - \sin \varphi' \quad (2-4)$$

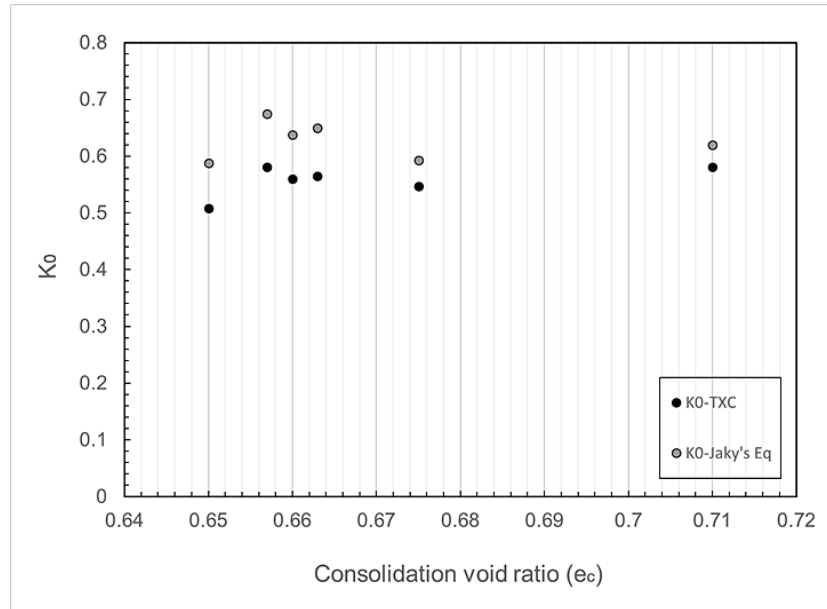
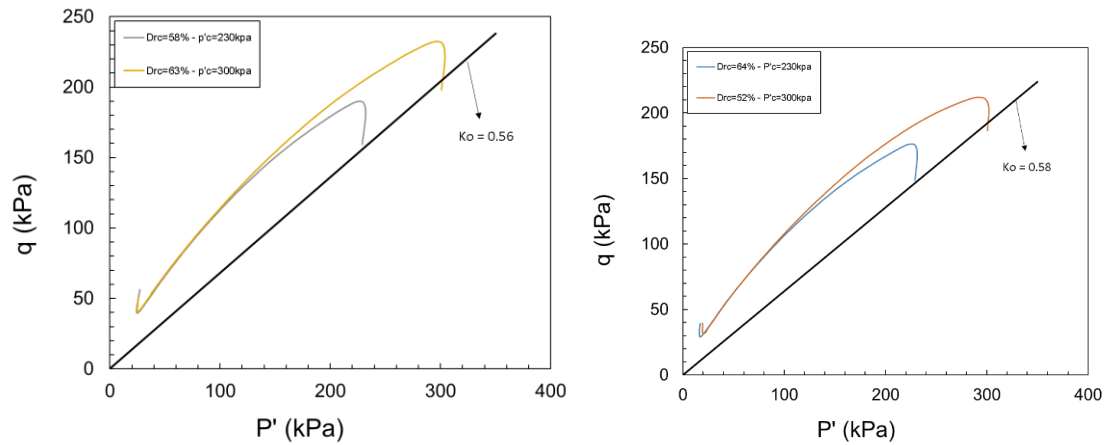


Figure 2.23: Comparison of the K0 values from triaxial tests and Jaky's Eq.



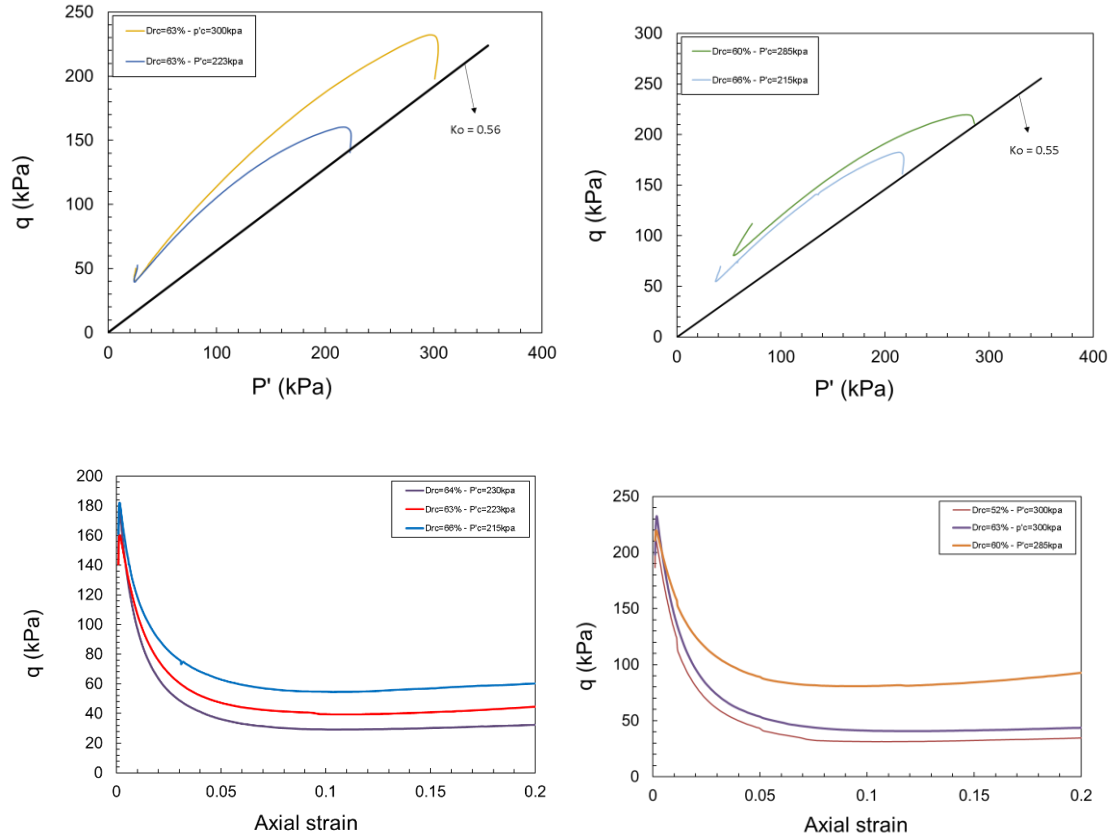


Figure 2.24: Stress paths and stress-strain responses of the K_0 -consolidated triaxial tests under undrained loading condition

2.3.3 Drained shear response

In order to have a precise critical state line parameter, eight triaxial tests with different initial states and under drained shearing condition were performed. The results of the triaxial drained tests are presented in Figure 2.25. The consolidation relative density of the specimens is between 51% to 83%. Also, the specimens are consolidated to the mean effective stress of either 100 kPa or 400kPa. As illustrated in Figure 2.25, lower deviator stresses are mobilized in the looser sample at constant consolidation stress. The stress

path of all specimens with start from a stress ratio (q/p') of $\eta = 3$ and reach the same failure line at a stress ratio of $\eta_f = 1.488$ without exhibiting an unstable behavior. Figure 2.25 and Figure 2.26 compares the volumetric strains (ε_v versus ε_a) and deviator stresses (q versus ε_a) of these tests. Volumetric contraction and dilation behavior are demonstrated by loose and dense specimens, respectively. All loose specimens show a reduction in the volume, followed by a constant volume condition at the critical state. The volumetric strain of the medium-dense samples shows a reversal trend at the minimum strain of $\varepsilon_v = -0.006$ corresponding to $\varepsilon_a = 3.9\%$.

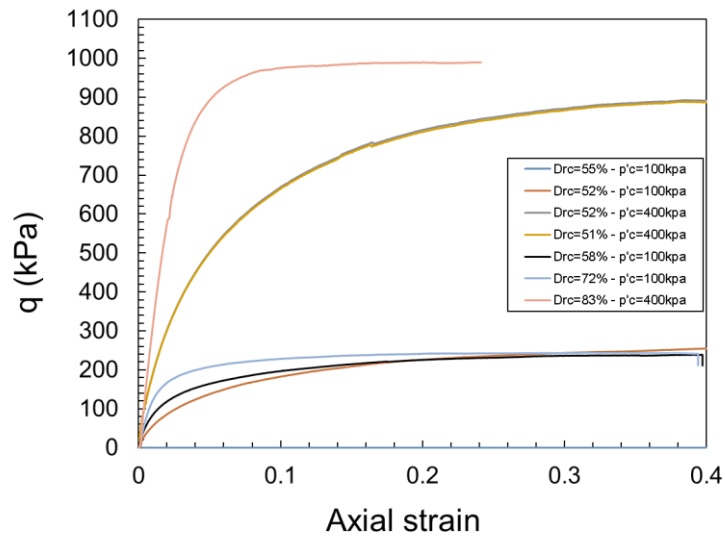


Figure 2.25: Stress-strain response of the oil sand tailings under drained shear condition

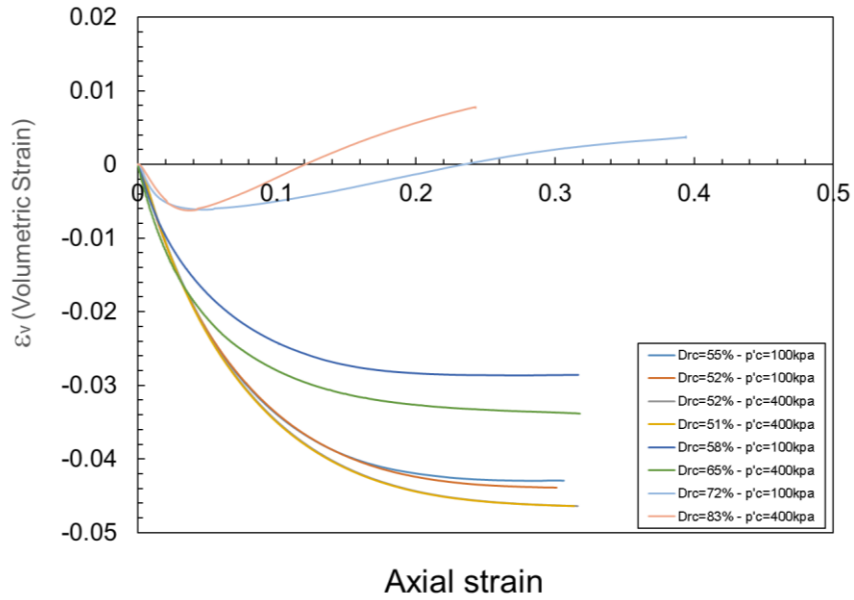


Figure 2.26: Volumetric strain responses of the oil sand tailings in drained tests

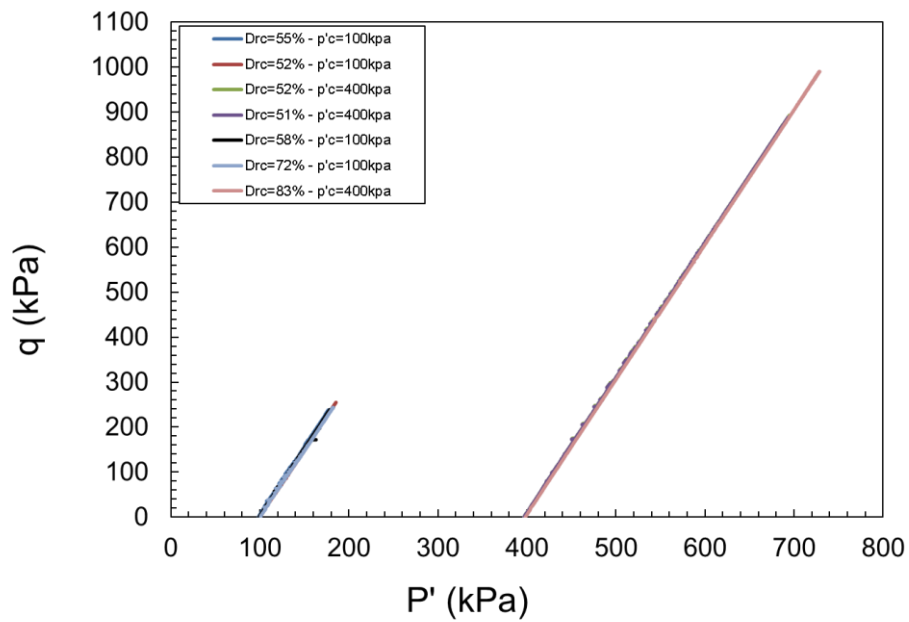


Figure 2.27: Effective stress paths for the isotropically consolidated drained triaxial tests

2.3.4 Critical state line of oil sand tailings

The critical state concept developed by Casagrande (1936) can explain most liquefaction phenomena using the critical void ratio concept (Olson, 2001). Roscoe et al. (1958) defined the critical state as a state in which the soil continuously deforms without change in void ratio and stress under drained condition. To overcome the difficulties of obtaining final states by soil drained shearing response, Castro (1969) and Poulos (1981) suggested undrained shearing condition of contractive soils. Poulos (1981) defined the steady-state of deformation as a state in which soil particles continuously deform at constant volume, constant normal effective stress, constant shear stress, and constant velocity. There is no evidence to distinct the critical state from the steady-state (Been and Jefferies 1985; Been et al. 1991). Been et al. (1991) stated that the critical state had been commonly measured by drained tests on contractive soil specimens, while the steady state is concluded from undrained tests on dilative soil specimens. Following many previous researchers (Riemer and Seed 1997; Jang and Frost 2000; Rahman & Lo 2012), critical state and steady-state are considered equivalent. A single term, critical state, is used in this study.

Critical state line information can be used to assess the liquefaction potential of the tailings. The critical state line includes two components: the stress dependency of critical void ratio in the mean effective stress – void ratio (p' - e) plane, and the other is a line in the mean effective stress – deviator stress plane (q - p'). The critical state line in the q - p' plane is a straight line passing through the origin with a constant slope (M_{cs}). The second component in the e - p' plane is a curve which is conventionally represented as a straight semi-logarithmic line in the e - $\log p'$ space as below:

$$e_{cs} = \Gamma_{cs} - \lambda_{cs} \log p'_{cs} \quad (2-5)$$

$$q_{cs} = M_{cs} p'_{cs} \quad (2-6)$$

Where e_{cs} and p'_{cs} are the void ratio and mean effective stress at critical state, Γ_{cs} and λ_{cs} are the intercept and slope of the CSL which are intrinsic soil properties.

Isotropically ($K_0=1$) consolidated undrained, isotropically consolidated drained and anisotropically consolidated undrained tests were performed on the reconstituted specimens at a range of densities and effective confining pressures, as shown in Table 2.4.

For the undrained triaxial tests, the sample volume was not allowed to change, and the specimen void ratio remained constant during shearing, as illustrated in Figure 2.28. Mean effective stresses at the phase transformation point are used to determine the critical state line data points. All specimens prepared for undrained triaxial test show contractive behavior as they are initially located above the critical state line.

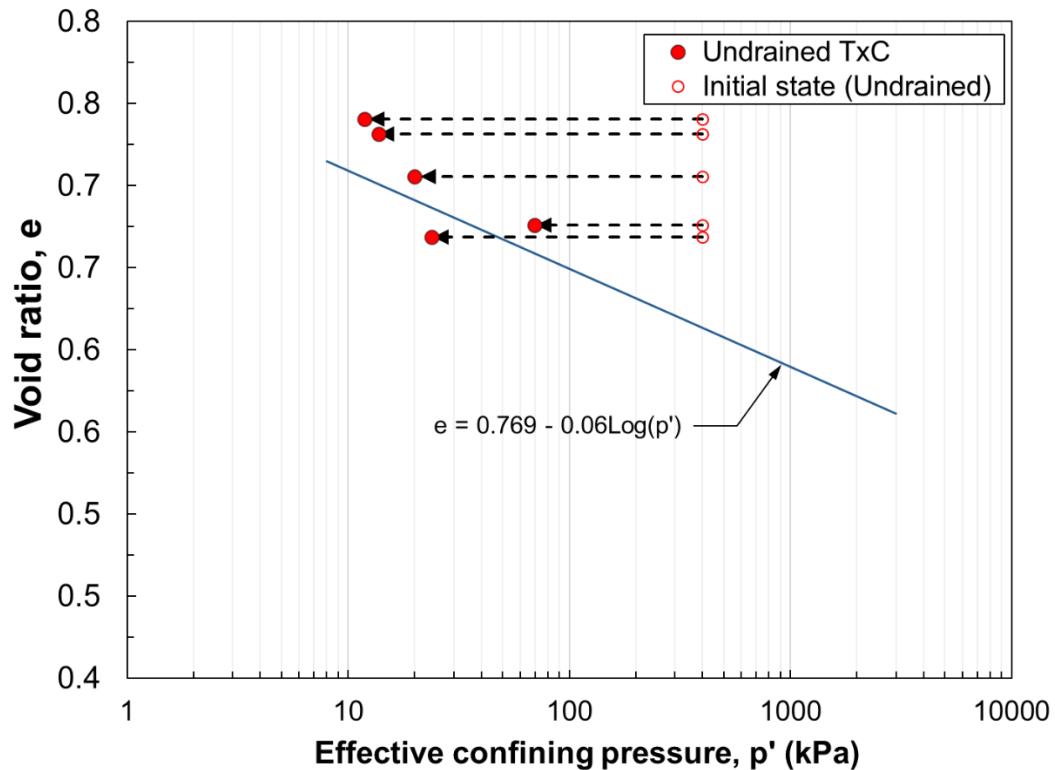


Figure 2.28: Initial and final states of the isotropically consolidated samples under undrained loading condition

Isotropically consolidated drained tests were performed on eight specimens at different densities and confining pressures. Figure 2.29 shows the results of the drained test on the e -log p' plane. At the drained condition, pore water pressure was fully dissipated, and volume change was recorded by the backpressure pump. As discussed before, the stress path of all specimens with different initial states advances toward the critical state. The final void ratio and mean effective stress at the end of the test are used as the data points of the critical state line.

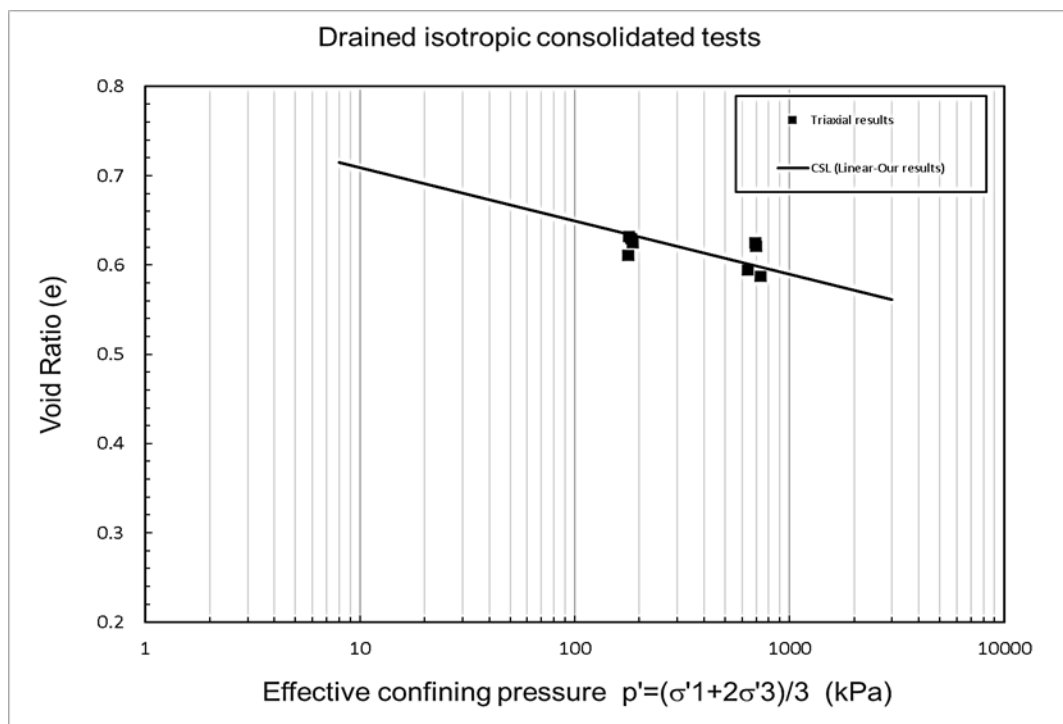


Figure 2.29: Critical state data points obtained from Isotropically-consolidated samples under drained condition

Anisotropically consolidated undrained test results are presented in Figure 2.30. A soil element in a natural deposit is subjected to the vertical overburden and radial confining stresses under zero lateral strain condition. In reality, the lateral pressures are smaller than vertical stress. Seven anisotropically consolidated undrained tests were performed to gain a better insight into oil sand tailings behavior in a natural condition. K0 condition

during the consolidation stage could be achieved by either manually or automated cell pressure and pore pressure adjustments to prevent the cross-sectional area change of soil specimen. For each soil sample, the initial and final states are illustrated in Figure 2.30. Similar to the isotropically consolidated undrained tests, the phase transformation data points determine the critical state parameters.

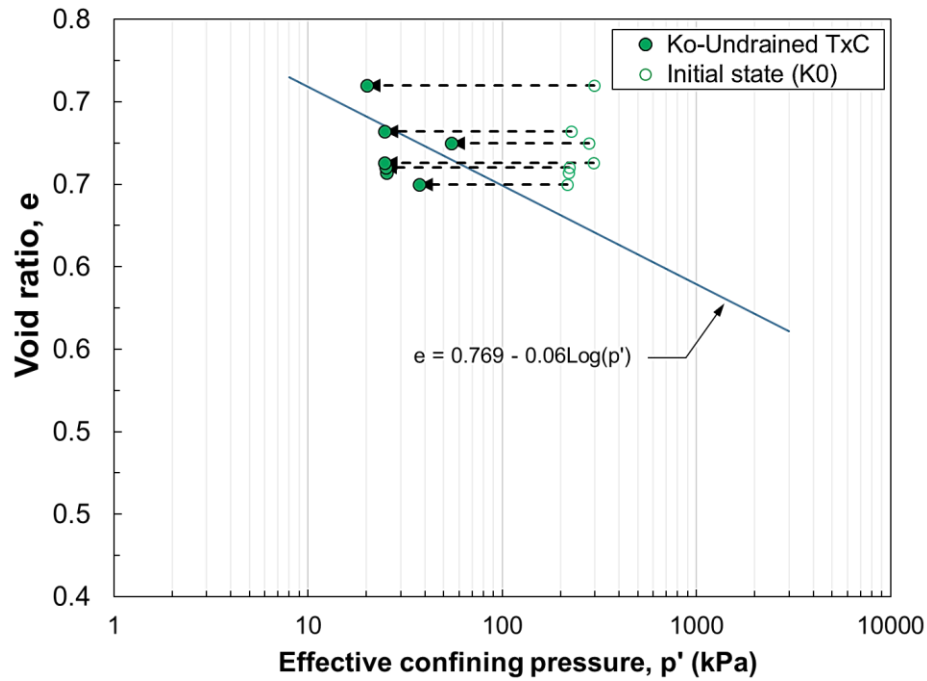


Figure 2.30: Initial and final states of the K0-consolidated samples under undrained loading condition

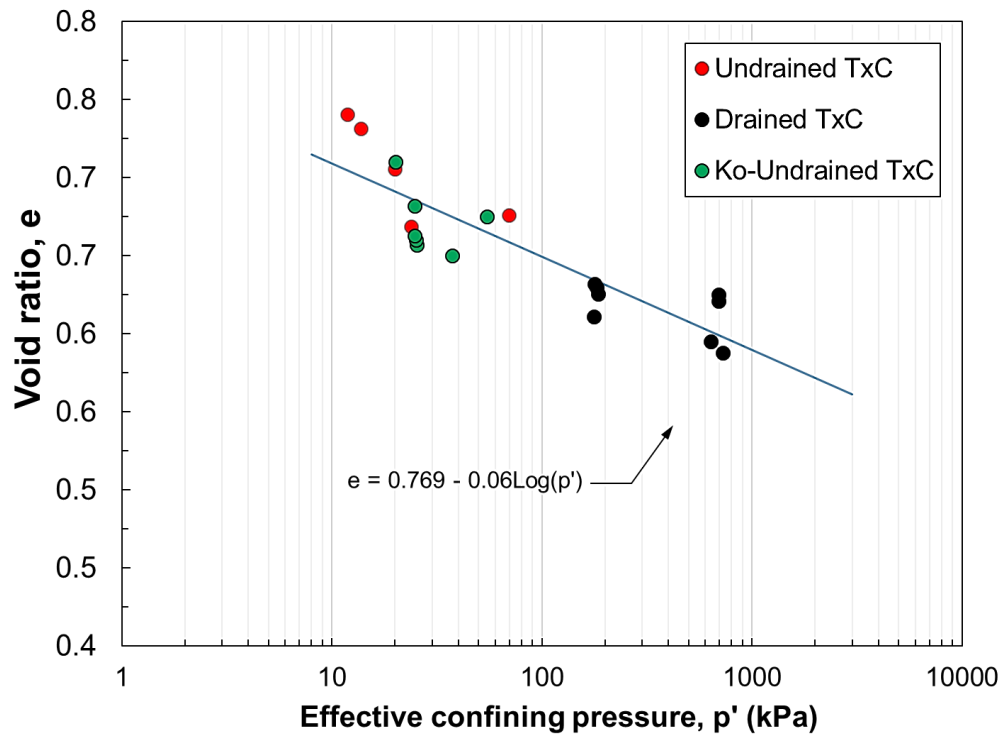
The linear and curved critical state line parameters on the e - $\log p'$ plane obtained from all sets of triaxial tests are presented in Table 2.5.

$$e = \Gamma_{cs} + \lambda_{cs} \log(p') \quad (2-7)$$

$$e = a + b \times \left(\frac{p'}{100(kPa)} \right)^\alpha \quad (2-8)$$

Table 2.5: Linear and curved critical state parameters

	<i>Linear CSL parameters</i>		<i>Curved CSL parameters</i>		
<i>Tag</i>	Γ_{cs}	λ_{cs}	a	b	α
<i>Oil sand tailings</i>	0.769	-0.0598	73.196	-72.547	0.000358

**Figure 2.31: CSL obtained from all triaxial test perform on the oil sand tailing**

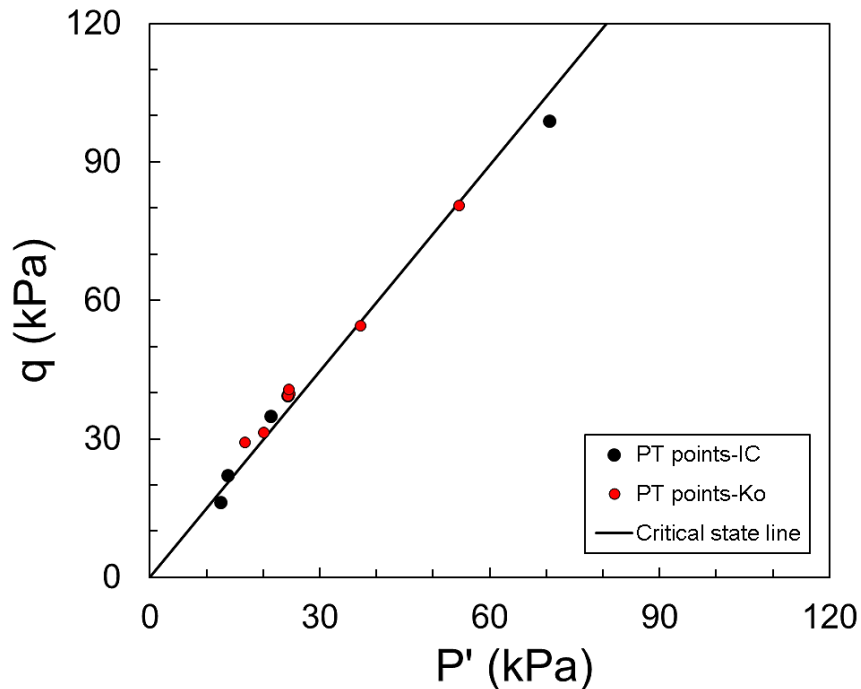


Figure 2.32: Critical state line on the q - p' space obtained from undrained triaxial tests

2.3.5 Effect of void ratio on yield and post-liquefaction strength ratios

Yield and post-liquefaction shear strengths have been normalized by the consolidation stress. Olson and Stark (2003) stated that yield shear strength ratio can be used as an indicator for initiation of the undrained instability and liquefaction. Yield shear strength ratio measured in isotropically consolidated and K0-consolidated triaxial tests were $S_{u(\text{yield})} / \sigma'_v = (0.18 - 0.21)$ and $S_{u(\text{yield})} / \sigma'_v = (0.24 - 0.27)$, respectively for the oil sand tailings in this study. The yield shear strength ratio diminishes with increasing consolidation void ratio, as illustrated in Figure 2.33.

Post-liquefaction shear strength is the constant shear stress at the critical state in which the soil has completely liquefied under constant volume condition. Post-liquefaction shear strength is widely used in the assessment of liquefaction flow failures (Poulos et al.

1988; Seed 1987; Alarcon-Guzman et al. 1988; Seed and Harder 1990; Vaid et al. 1990; Stark and Mesri 1992; Ishihara 1993; Olson and Stark 2002). Post-liquefaction shear strength ratios obtained from undrained triaxial compression tests performed on the isotropically consolidated and K0 consolidated specimens were $S_{u(liq)} / \sigma'_{vc} = (0.016 - 0.04)$ and $S_{u(liq)} / \sigma'_{vc} = (0.03 - 0.07)$ respectively, as illustrated in Figure 2.34. Similar to the yield shear strength ratio, post-liquefaction shear strength ratio decreases with increasing consolidated void ratio. The anisotropically-consolidated specimens also show notably higher $s_u(\text{yield})/\sigma'_{vc}$ values compared to the isotropically-consolidated specimens at a given void ratio.

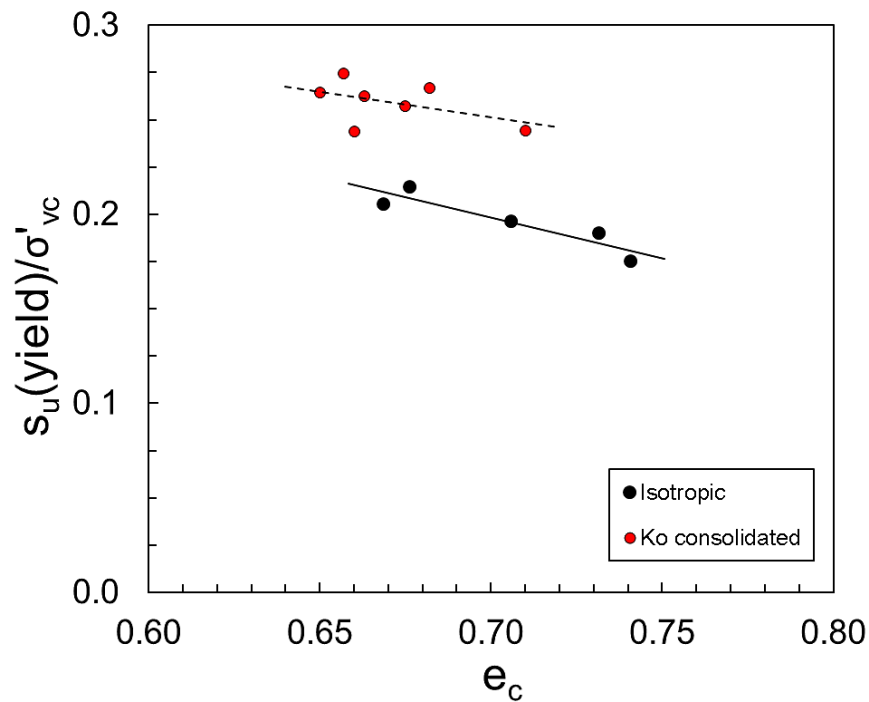


Figure 2.33: Yield shear strength ratio variation with consolidation void ratio for isotropically consolidated and K0-consolidated specimens

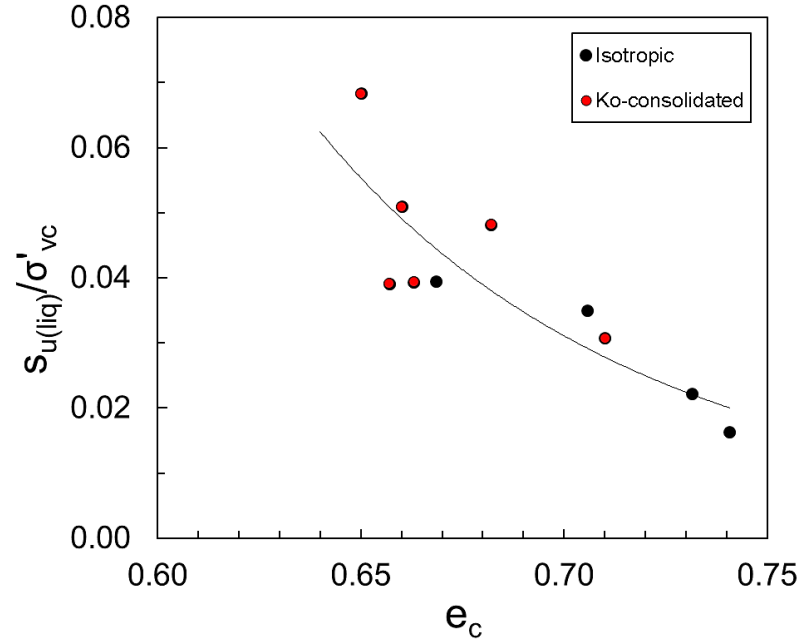


Figure 2.34: Post-liquefaction shear strength ratio variation with consolidation void ratio for isotropically consolidated and K0-consolidated specimens

Friction angle is an essential parameter in evaluating the soil response to shear loading. Several researchers have studied the effect of different factors such as particle shape, initial fabric, fines content, and particle damage on the mobilized friction angle (Chan & Page, 1997; Sukumaran & Ashmawy, 2001; Been et al., 1991; Sladen et al., 1985; Ni et al., 2004; Murthy et al., 2007; Bishop & Green, 1965; Lee & Seed, 1967; Tarantino & Hyde, 2005). The effective stress friction angles mobilized in the oil sand tailings are investigated by undrained triaxial compression tests in this study. The friction angle is mobilized at peak shear strength, and the critical state is termed yield (φ'_{yield}) and post-liquefaction (φ'_{liq}) friction angles. The effective friction angle for triaxial compression tests are defined as:

$$\varphi' = \sin^{-1} \left(\frac{3M}{6+M} \right) \quad (2-9)$$

Where M is the axisymmetric principal stress ratio (q/p'). Figure 2.35 presents the yield friction angles mobilized in the isotropically consolidated and K0-consolidated triaxial

tests. The yield friction angle decreases with increasing consolidation void ratio in conformity with Bishop (1971), Alarcon-Guzman et al. (1988), Yamamuro & Lade (1997).

The effect of the consolidation void ratio on the post-liquefaction friction angle is presented in Figure 2.36. The tests results indicate that post-liquefaction friction angle (ϕ'_{liq}) decreases with consolidation void ratio (e_c).

By comparing the slope of the yield and post-liquefaction friction angle variation, we can understand that the influence of consolidation void ratio on the yield friction angle is greater than the post-liquefaction friction angle. So the effect of the initial fabric gradually decreases with specimen shearing.

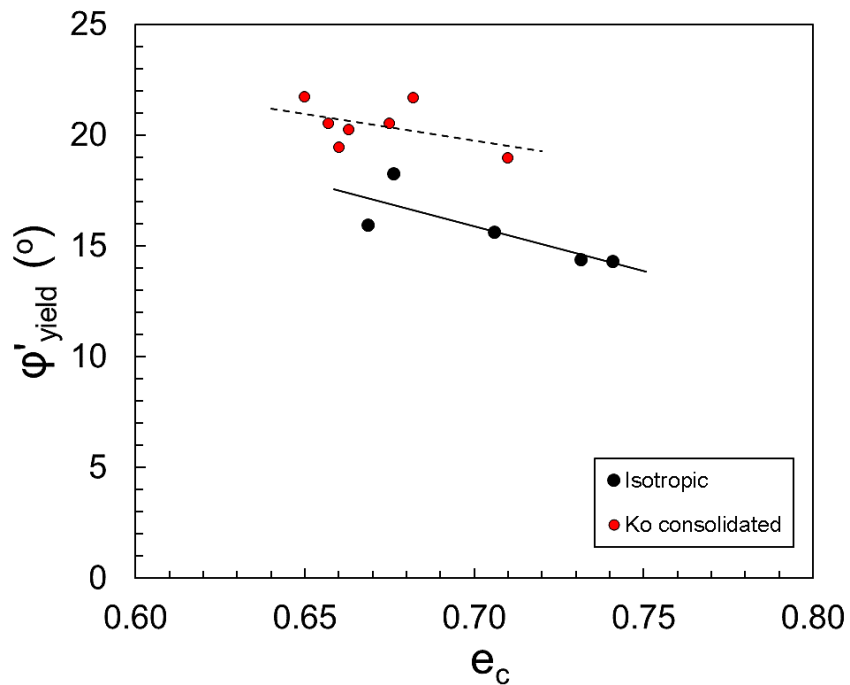


Figure 2.35: Yield friction angle variation with consolidation void ratio

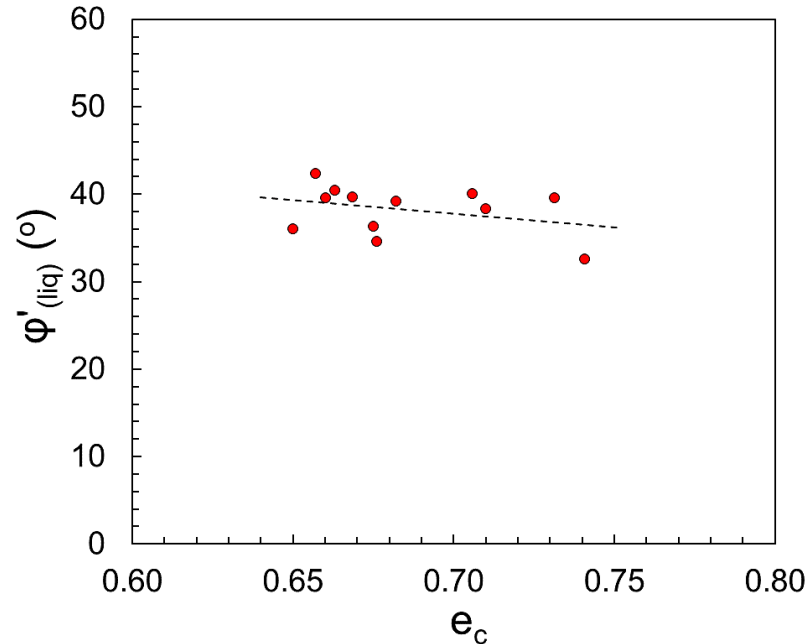


Figure 2.36: Post-liquefaction friction angle variation with consolidation void ratio

2.3.6 Variations of yield and post-liquefaction strength ratios with state parameter

It has been found that soil's initial state, expressed in terms of initial void ratio and effective stress, highly influences the soil shear response. Researchers have proposed several state variables to consider the concurrent effect of density and stress state (Been & Jefferies, 1985; Wang et al., 2002; Thevanayagam & Mohan, 2000; Bobei & Lo, 2001). Among all suggested parameters, state parameter is widely applied, which is defined as the difference between the consolidation void ratio (e_c) and the void ratio corresponding to the same consolidation effective stress on the CSL (e_{cs}):

$$\psi = e_c - e_{cs} \quad (2-10)$$

The state parameter can determine the contractive or dilative behavior of a soil specimen. A negative value indicates dilative behavior with no liquefaction susceptibility, and positive values show contractive behavior with liquefaction potential (Sladen et al. 1985; Jefferies and Been 1987).

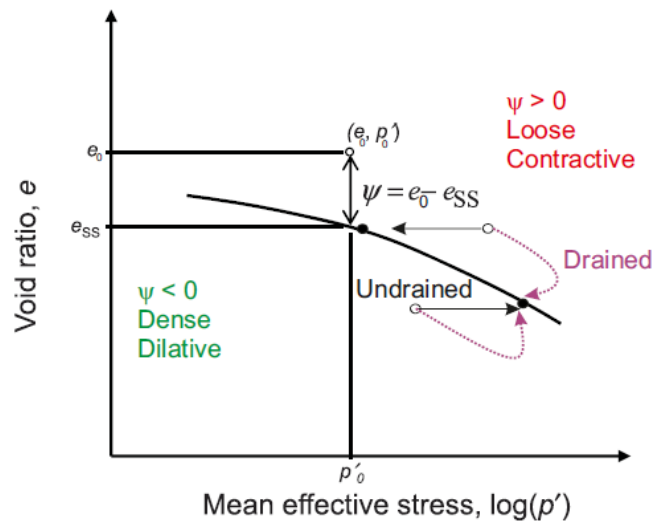


Figure 2.37: Schematic definition of the state parameter (Rahemi, 2018)

Figure 2.38 presents yield strength ratio ($S_{u(\text{yield})} / \sigma'_{vc}$) variation with the state parameter (ψ) for contractive soil specimens. The yield strength ratio decreases with increasing state parameter. Also, the yield strength ratios for the K0-consolidated specimens are higher than the isotropically consolidated samples at similar state parameters. Post-liquefaction strength ratios show a similar behavior as the yield strength ratio, as illustrated in Figure 2.39.

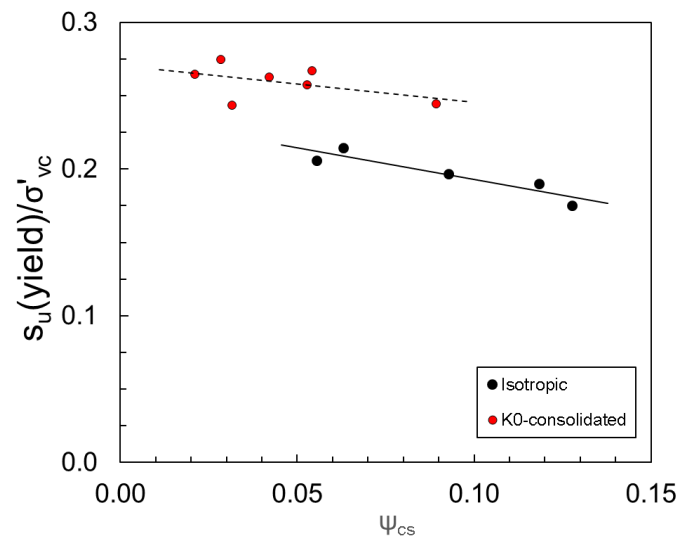


Figure 2.38: Yield shear strength variation with state parameter

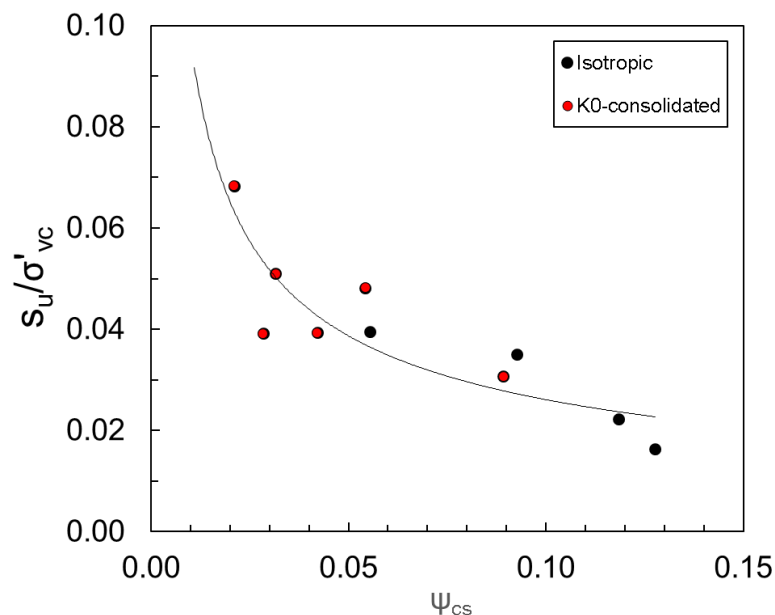


Figure 2.39: Post-liquefaction shear strength variation with state parameter

2.4 Summary and Conclusions

This chapter presents the shearing behavior of oil sand tailings using the triaxial compression test under monotonic loading condition. Three sets of triaxial tests were carried out, including: (1) Isotropically consolidated undrained tests (IU-TXC), (2) K0-consolidated undrained tests (K0U-TXC), and (3) Isotropically consolidated drained test (ID-TXC). Undrained triaxial tests are often used to evaluate the liquefaction susceptibility of the soil sample due to the pore water pressure generation mechanism. One of the major sources of errors that could significantly affect the triaxial test results is sample volume changes during the saturation stage. The sample volume change can highly influence the position of the critical state line. The sample freezing method is used as the main method to measure the void ratio change during the backpressure saturation stage. And two others methods: (1) inflow/outflow method, (2) Cell volume ratio are also assessed for measuring the void volume change. It was demonstrated that the

inflow/outflow method leads to close results to the freezing method and can be used as an alternative method for estimating the void ratio changes in backpressure stage.

Evaluation of the yield and critical state of the oil sand provides a valuable basis for analyzing the failure criteria. Determination and validity of the critical state is of paramount importance.

Based on the undrained triaxial test on the isotropically consolidated sample within consolidation relative density of $D_{rc}=44\%$ to $D_{rc}=61\%$, the instability stress ratio ranges from $\eta=0.54$ to $\eta=0.7$. It was found that The axial strain (ε_a) corresponding to the peak deviator stress increases with relative density. The yield and post-liquefaction shear strength ratios obtained from undrained triaxial compression tests performed on the isotropically consolidated specimens were $S_{u(yield)} / \sigma'_v = (0.18-0.21)$ and $S_{u(liq)} / \sigma'_v = (0.016-0.04)$, respectively. Similar to the yield shear strength ratio, the post-liquefaction shear strength ratio decreases with increasing consolidated void ratio.

A soil element in a natural deposit is subjected to the vertical overburden and radial confining stresses under zero lateral strain condition. In reality, the lateral stresses are smaller than vertical stress. Seven anisotropically consolidated undrained tests were performed to better understand oil sand tailings behavior in a natural condition. The K_0 values obtained directly from the experimental test were 0.55 to 0.58 based on different initial states. The $S_{u(yield)} / \sigma'_{vc} = (0.24-0.27)$ and $S_{u(liq)} / \sigma'_{vc} = (0.03-0.07)$ agree closely with values from earlier laboratory experiments on loose sands.

To have a precise critical state line parameter, eight triaxial tests with different initial states and under drained shearing condition were performed. The consolidation relative density of the specimens is between 51% to 83%. Also, the specimens are consolidated to the mean effective stress of either $P'_c=100$ kPa or $P'_c=400$ kPa. It was observed that the volumetric strain of the dense samples shows a reversal trend at the minimum strain of $\varepsilon_v = -0.006$ corresponding to $\varepsilon_a = 3.9\%$.

Yield and critical state friction angles of oil sands measured in triaxial tests illustrated that the influence of consolidation void ratio on the yield friction angle is greater than that on the post-liquefaction friction angle.

References

- Alarcon-Guzman, A, GA Leonards, and JL Chameau. "Undrained Monotonic and Cyclic Strength of Sands." *Journal of Geotechnical Engineering* 114, no. 10 (1988): 1089-109.
- Baldi, Gualtiero, and Roberto Nova. "Membrane Penetration Effects in Triaxial Testing." *Journal of Geotechnical Engineering* 110, no. 3 (1984): 403-20.
- Been, K, MG Jefferies, and J Hachey. "The Critical State of Sands." *Geotechnique* 41, no. 3 (1991): 365-81.
- Been, Ken, and Mike G Jefferies. "A State Parameter for Sands." *Geotechnique* 35, no. 2 (1985): 99-112.
- Bishop, AW. "The Influence of Progressive Failure on the Choice of the Method of Stability Analysis." *Geotechnique* 21, no. 2 (1971): 168-72.
- Bishop, Alan W, and Gordon E Green. "The Influence of End Restraint on the Compression Strength of a Cohesionless Soil." *Geotechnique* 15, no. 3 (1965): 243-66.
- Bishop, Alan Wilfred, and David John Henkel. "The Measurement of Soil Properties in the Triaxial Test." (1962).
- Black, David K, and Kenneth L Lee. "Saturating Laboratory Samples by Back Pressure." *Journal of the soil mechanics and foundations division* 99, no. 1 (1973): 75-93.
- Bobei, DC, and SR Lo. Static Liquefaction of Sydney Sand Mixed with Both Plastic and Non-Plastic Fines. *Proceedings of the 14th Southeast Asian Geotechnical Conference, Hong Kong, 2001.*
- Casagrande, Arthur. "Characteristics of Cohesionless Soils Affecting the Stability of Slopes and Earth Fills." *J. Boston Society of Civil Engineers* 23, no. 1 (1936): 13-32.

- Casagrande, A. "Liquefaction and Cyclic Deformation in Sands: A Critical Review: Proceeding of the Fifth Pan American Conference in Soil Mechanics and Foundation Engineering." Buenos Aires, Argentina (1975).
- Castro, Gonzalo. "Liquefaction of Sands." ph. D. Thesis, Harvard Soil Mech. (1969).
- Castro, G, JL Enos, JW France, and SJ Poulos. Liquefaction Induced by Cyclic Loading. Report to National Science Foundation, Washington, Dc, No. NSF/CEE-82018, 1982.
- Castro, Gonzalo, and Steve J Poulos. "Factors Affecting Liquefaction and Cyclic Mobility." Journal of the Geotechnical Engineering Division 103, no. 6 (1977): 501-16.
- Finno, Richard J, Wendell W Harris, Michael A Mooney, and Gioacchino Viggiani. "Strain Localization and Undrained Steady State of Sand." Journal of Geotechnical Engineering 122, no. 6 (1996): 462-73.
- Fourie, AB, and G Papageorgiou. "Defining an Appropriate Steady State Line for Merriespruit Gold Tailings." Canadian geotechnical journal 38, no. 4 (2001): 695-706.
- Goudarzy, Meisam. "Micro and Macro Mechanical Assessment of Small and Intermediate Strain Properties of Granular Material." (2016).
- Hanzawa, Hideo. "Undrained Strength and Stability Analysis for a Quick Sand." Soils and foundations 20, no. 2 (1980): 17-29.
- Hazen, Allen. "A Study of the Slip in the Calaveras Dam." Engineering News Record 81, no. 26 (1918): 1158-64.
- Ishihara, Kenji. "Liquefaction and Flow Failure During Earthquakes." Geotechnique 43, no. 3 (1993): 351-451.
- Ishihara, Kenji, Fumio Tatsuoka, and Susumu Yasuda. "Undrained Deformation and Liquefaction of Sand under Cyclic Stresses." Soils and foundations 15, no. 1 (1975): 29-44.
- Jang, Deh-Jeng, and J David Frost. "Use of Image Analysis to Study the Microstructure of a Failed Sand Specimen." Canadian geotechnical journal 37, no. 5 (2000): 1141-49.

Kramer, Steven Lawrence. Geotechnical Earthquake Engineering: Pearson Education India, 1996.

Kramer, Steven L, and Nadarajah Sivanesar. "A Nondestructive, Specimen-Specific Method for Measurement of Membrane Penetration in the Triaxial Test." Geotechnical Testing Journal 12, no. 1 (1989): 50-59.

Krumbein, WC, and LL Sloss. "Stratigraphy and Sedimentation: Wh Freeman Co." San Francisco (1963).

Ladd, RS. "Preparing Test Specimens Using Undercompaction." Geotechnical Testing Journal 1, no. 1 (1978): 16-23.

Lade, Poul V. "Initiation of Static Instability in the Submarine Nerlerk Berm." Canadian geotechnical journal 30, no. 6 (1993): 895-904.

Lambe, T William. Soil Testing for Engineers. Vol. 72, vol. 5: LWW, 1951

Lee, Kenneth L, and H Bolton Seed. "Drained Strength Characteristics of Sands." Journal of the soil mechanics and foundations division 93, no. 6 (1967): 117-41

Mitchell, James Kenneth, and Kenichi Soga. Fundamentals of Soil Behavior. Vol. 3: John Wiley & Sons New York, 2005

Muhammad, Kashif. Case History-Based Analysis of Liquefaction in Sloping Ground: University of Illinois at Urbana-Champaign, 2012.

Mulilis, JP, FC Townsend, and RC Horz. "Triaxial Testing Techniques and Sand Liquefaction." In Dynamic Geotechnical Testing: ASTM International, 1978.

Olson, Scott M. "Liquefaction Analysis of Duncan Dam Using Strength Ratios." Canadian geotechnical journal 43, no. 5 (2006): 484-99.

Olson, Scott Michael. Liquefaction Analysis of Level and Sloping Ground Using Field Case Histories and Penetration Resistance: University of Illinois at Urbana-Champaign, 2001.

Olson, Scott M, and Timothy D Stark. "Liquefied Strength Ratio from Liquefaction Flow Failure Case Histories." Canadian geotechnical journal 39, no. 3 (2002): 629-47.

Olson, Scott M, and Timothy D Stark. "Yield Strength Ratio and Liquefaction Analysis of Slopes and Embankments." *Journal of geotechnical and geoenvironmental engineering* 129, no. 8 (2003): 727-37.

Poulos, Steve J. "The Steady State of Deformation." *Journal of the Geotechnical Engineering Division* 107, no. 5 (1981): 553-62.

Rahman, Md Mizanur. *Modelling the Influence of Fines on Liquefaction Behaviour*: University of New South Wales, Australian Defence Force Academy, School of ..., 2009.

Riemer, Michael F, and Raymond B Seed. "Factors Affecting Apparent Position of Steady-State Line." *Journal of geotechnical and geoenvironmental engineering* 123, no. 3 (1997): 281-88.

Sadrekarami, Abouzar. *Development of a New Ring Shear Apparatus for Investigating the Critical State of Sands*: University of Illinois at Urbana-Champaign, 2009.

Sadrekarami, Abouzar, and Scott M Olson. "Effect of Sample-Preparation Method on Critical-State Behavior of Sands." *Geotechnical Testing Journal* 35, no. 4 (2012): 548-62.

Seed, H Bolton. "Design Problems in Soil Liquefaction." *Journal of Geotechnical Engineering* 113, no. 8 (1987): 827-45.

Sladen, JA, RD D'hollander, and J Krahn. "The Liquefaction of Sands, a Collapse Surface Approach." *Canadian geotechnical journal* 22, no. 4 (1985): 564-78.

Sladen, JA, RD D'hollander, J Krahn, and DE Mitchell. "Back Analysis of the Nerlerk Berm Liquefaction Slides." *Canadian geotechnical journal* 22, no. 4 (1985): 579-88.

Sladen, JA, and JM Oswell. "The Behaviour of Very Loose Sand in the Triaxial Compression Test." *Canadian geotechnical journal* 26, no. 1 (1989): 103-13.

Stark, Timothy D, and Gholamreza Mesri. "Undrained Shear Strength of Liquefied Sands for Stability Analysis." *Journal of Geotechnical Engineering* 118, no. 11 (1992): 1727-47.

Sukumaran, B, and AK Ashmawy. "Quantitative Characterisation of the Geometry of Discret Particles." *Geotechnique* 51, no. 7 (2001): 619-27.

Sze, HY, and J Yang. "Failure Modes of Sand in Undrained Cyclic Loading: Impact of Sample Preparation." *Journal of geotechnical and geoenvironmental engineering* 140, no. 1 (2014): 152-69.

Wang, Zhi-Liang, Yannis F Dafalias, Xiang-Song Li, and Faiz I Makdisi. "State Pressure Index for Modeling Sand Behavior." *Journal of geotechnical and geoenvironmental engineering* 128, no. 6 (2002): 511-19.

Wei, LM, and J Yang. "On the Role of Grain Shape in Static Liquefaction of Sand–Fines Mixtures." *Geotechnique* 64, no. 9 (2014): 740-45.

Yamamuro, Jerry A, and Poul V Lade. "Static Liquefaction of Very Loose Sands." *Canadian geotechnical journal* 34, no. 6 (1997): 905-17.

Zhang, H. *Steady State Behavior of Sands and Limitations of the Triaxial Tests.* University of Ottawa, Ottawa, Canada, Vol. PhD, 1997.

Zhu, JH, and SA Anderson. "Corrections for Triaxial Tests on Undisturbed Soils." *Journal of testing and evaluation* 26, no. 3 (1998): 277-84.

Chapter 3

3 Effect of Fines on Instability of Oil Sand Tailings

3.1 Introduction

Liquefaction is a phenomenon in which the shear strength of saturated sand or silty sand reduces by monotonic, cyclic, or dynamic loading (Castro 1969; Poulos 1981; Terzaghi et al. 1996). Excess pore water generation and effective stress reduction lead to strength loss and rapid deformation during liquefaction. Landslides, lateral movement, dam failure, settling and tilting of buildings, and failure of waterfront retaining structures are examples of liquefaction triggered by static or cyclic loading mechanisms. Undrained triaxial tests are widely used to measure the shear strength in constant volume condition. Several studies have been done on evaluating the liquefaction susceptibility of clean sands. However, most natural soil contains some fines, and flow failure commonly occurs in silty sands, based on the liquefaction failure case histories. Obviously, the presence of fine in soil mass significantly affects the stress-strain behavior (Lade & Yamamuro 1997; Thevanayagam 1998; Georgiannou 2006; Rahman 2009; Baki 2011). Some studies demonstrated that with increasing in fines content, the liquefaction resistance increases (Robertson PK et al., 1994; Seed HB, 1987; Georgiannou, 2006).

On the other hand, some researchers have arrived at a contrary conclusion and demonstrated that the liquefaction resistance decreases with increasing fines content up to a threshold value $FC_{th} \approx 30\%$ (Ishihara and Verdugo 1997; Lade and Yamamuro 1997; Wang and Sassa 2000; Baziar et al., 2004; Das and Sitharam 2011). So the fines can have a significant effect on the soil fabric and stress-strain response. In this chapter, the impact of fines content on the strain-softening behavior of the loose, saturated sand sample is investigated using critical state parameters obtained from undrained triaxial compression tests.

A decrease in the effective stress following excess pore water pressure generation results in a strain-softening behavior in a constant volume shearing condition. At small axial strains, from the initiation of undrained shearing for the contractive specimens, the deviator stress and the effective stress path reach peak shear strength ($S_{u(yield)}$). Yield strength point is associated with the onset of the flow liquefaction and the lower bound of all possible unstable conditions. The line crossing the origin of the q-p' plane, and the peak point of the stress path is known as the instability line. The instability stress ratio ($\eta_{IL} = q_{peak} / p'_{corresponding-to-q(peak)}$) variation with void ratio for sandy silts and silty sands is investigated by many researchers. Chu & Leong (2002) performed undrained triaxial tests on a silty sand with FC=2% - 10%. The moist tamping was used to prepare the specimens. They used the global and intergranular void ratios as the density parameters to evaluate the effect of density on the instability stress ratio. They reported that the η_{IL} decreases with increasing density, as illustrated in Figure 3.1. Murthy et al. (2007) demonstrated the relationship between the instability stress ratio and void ratio for specimens with FC = 0 - 15%. Slurry deposition and moist tamping methods were used to prepare samples. They concluded that the instability stress ratio increased with decreasing void ratio.

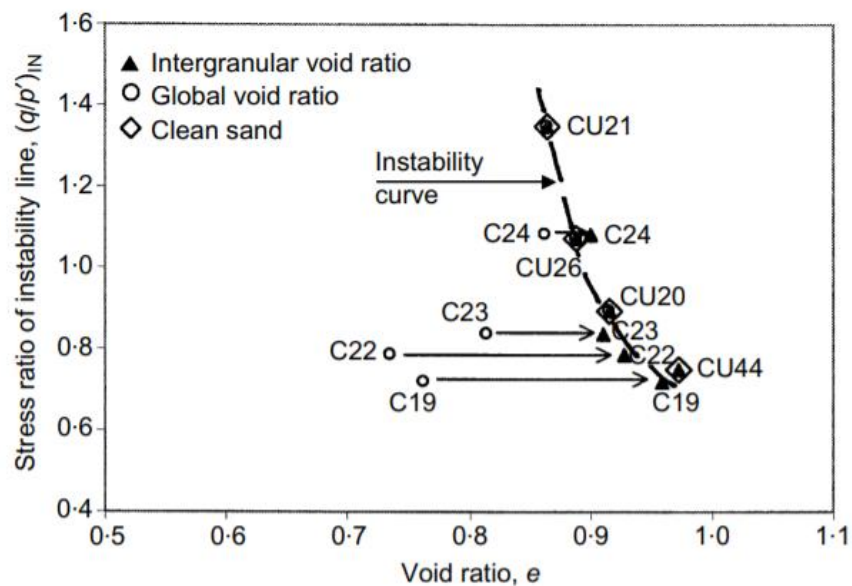


Figure 3.1: Instability stress ratio variation with void ratio (Chu and Leong, 2002)

Abedi and Yasrobi (2010) carried out series of undrained triaxial tests on silty sand specimens with FC = 0 – 30%. They prepared samples in two different densities (1.45 g/cm^3 , 1.5 g/cm^3) and two different confining pressures (100, 400kPa). They observed that the peak shear strength decreased with increasing fines content as illustrated in Figure 3.2.

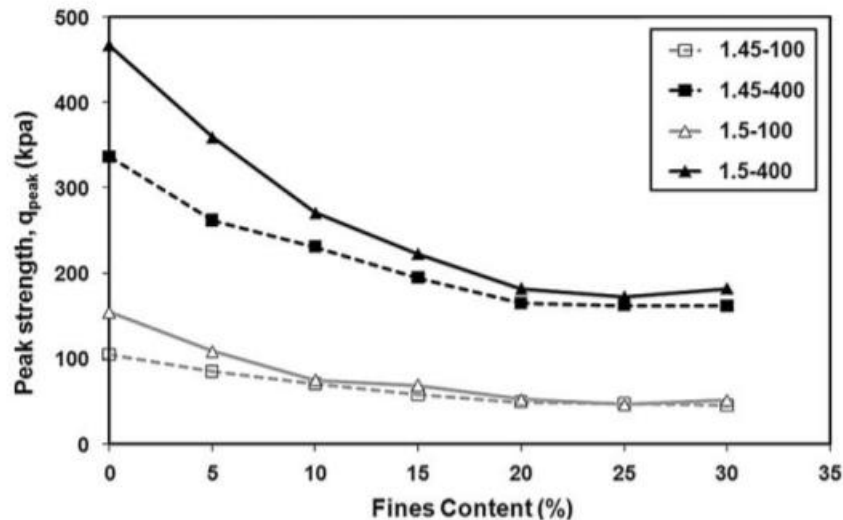


Figure 3.2: Effect of the fines content on the peak shear strength (Abedi and Yasrobi, 2010)

With advancing the strain-softening behavior following the initiation of the flow failure at the yield point, any possible breakage and reorientation occur among soil particles until the critical state. When a soil mass is at a critical state, it deforms continuously at constant shear stress, constant volume, and constant effective stress (Ishihara 1993, Jefferies and Been 2006, Sadrekarimi and Olson 2009). The post-liquefaction shear strength at the critical state is the minimum shear strength mobilized after liquefaction and is termed the post-liquefaction shear strength ($Su_{(liq)}$) by Olson and Stark (2002). Many researchers recommended critical shear strength as a conservative estimate of undrained shear strength, a useful parameter in post liquefaction analysis in practice (Poulos et al. 1985, Seed and Harder 1990, Ishihara 1993, Olson 2006).

3.2 Methodology

3.2.1 Oil sand tailings properties with different fines content

In this chapter, an experimental study was undertaken to clarify the liquefaction susceptibility of the sand-silt mixtures using the critical state framework. Three series of tests were performed on the same sand by adding different percentages of fines. Oil sand tailings from a particular mine site in Alberta are adopted as host soil, and the effect of fluid fine tailings (FFT) on the undrained behavior of tailings is investigated. The amount of the bitumen for the oil sands and fluid fine tailings (FFT) was determined as 1.26% and 7%, respectively, using the ignition method. The physical properties of the sand-silt mixtures are presented in the following section. The particle size distribution was determined by sieve and hydrometer analysis and presented in Figure 3.5. The oil sands grain size ranges from 0.003 mm to 2 mm. Based on the unified soil classification system, the clean sand and sand-silt mixtures are classified as SP and gap-graded, respectively, as per the ASTM D2487 standard procedure. Figure 3.3 and Figure 3.4 presents the scanning electron microscope images for the oil sand and fluid fine tailings. The chart by Krumbein and Sloss (1963) was used for assessment of sphericity and roundness. For the sand particles, sphericity is overall relatively high and elongated particles are rare. The roundness varies widely, from angular to well-rounded with sub-rounded shapes being the most common.

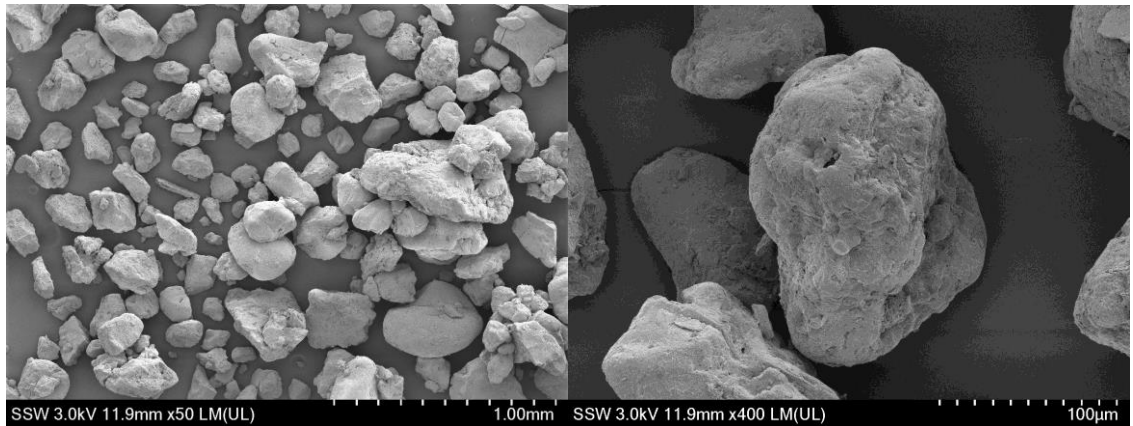


Figure 3.3: Shape of oil sand particles (SEM images)

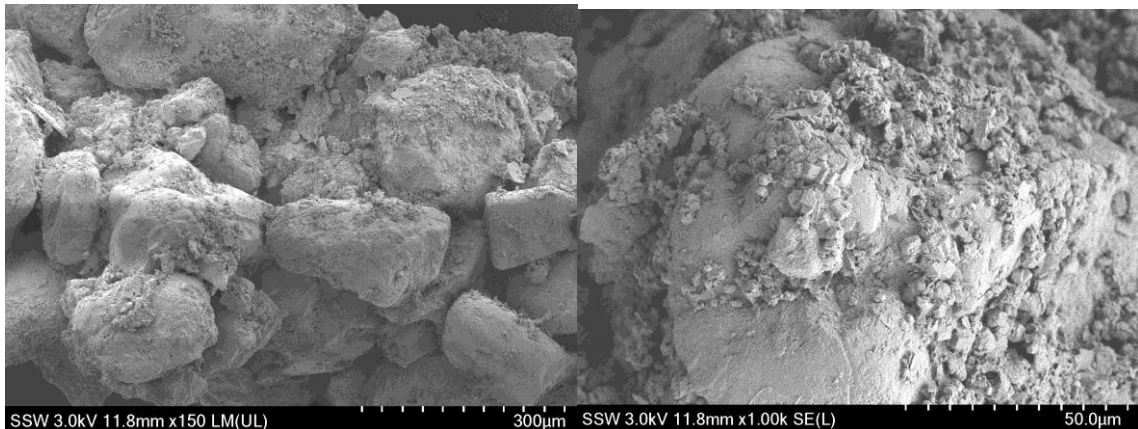


Figure 3.4: Shape of fluid fine tailings (SEM images)

Standard index tests were carried out, and Table 3.1 summarizes index properties for the sand-silt mixtures. The Values of maximum and minimum void ratios were determined using minimum and maximum densities, respectively, according to ASTM D4253. The specific gravity of the soil particles was determined based on the ASTM-D854 standard procedure.

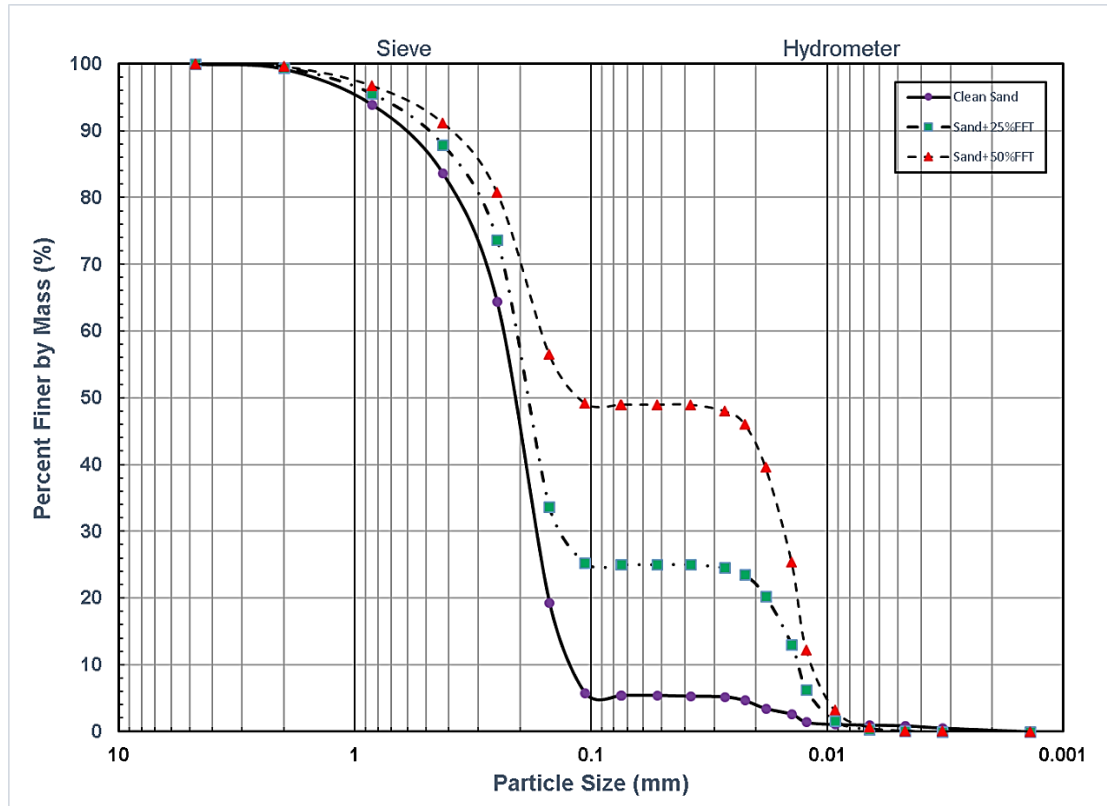


Figure 3.5: Soil particle size distribution for oil sand with 0%, 25%, and 50% FFT

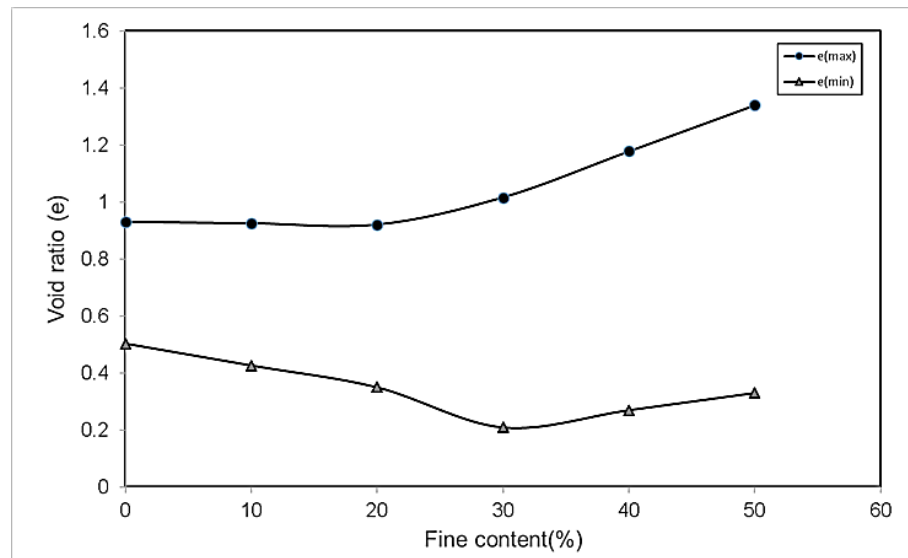


Figure 3.6: Variation of maximum and minimum void ratio with fines content

Table 3.1: Parameters of the oil sand tailings with fines

<i>Soil</i>	D_{50}	G_s	e_{max}	e_{min}
<i>Oil sand tailings</i>	0.218	2.624	0.93	0.503
<i>Sand+25%FFT</i>	0.19	2.628	0.968	0.279
<i>Sand+50%FFT</i>	0.12	2.632	1.339	0.33

3.2.2 Triaxial test apparatus

The triaxial test system used for measuring the intermediate and large strain properties in this research was an automated stress path triaxial system (SIGMA-1TM 5K model) manufactured by GeoTac Company. The loading frame, including an external load cell, is used to apply and measure the axial load in displacement control condition at a rate of 5% per hour. Cell and pore pressure pumps control the pressure and volume of the specimen's pore water and cell fluid. Also, an external pore pressure transducer with a maximum capacity of 1400 kPa is connected to the bottom of the specimen to measure the pore water pressure while the pore pump drainage valves are closed.

3.2.3 Sample preparation and uniformity

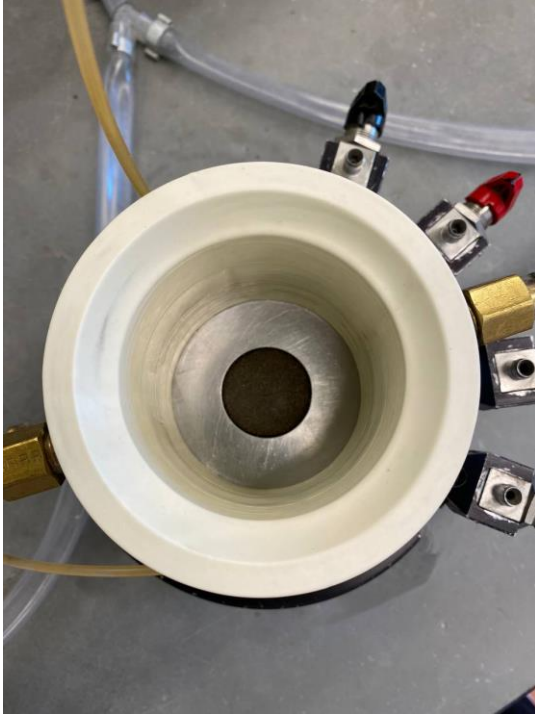
Sample preparation methods affect the engineering characteristics of the soil specimen due to the different soil fabrics (Goudarzy, 2015). The chosen sample preparation method (moist tamping, air pluviation, slurry deposition) must meet the following criteria (Kuerbis, 1985): 1) Uniformity of the void ratio along the sample, 2) Fully saturation of the sample, 3) Homogeneity of the sample, 4) The method must cover the range of density as expected within in-situ soil deposition

The traditional method of moist tamping results in non-uniform void ratio distribution along with the sample since compaction of overlying layers increases the density of underlying layers slightly (Sadrekarimi and Olson 2012). Ladd (1978) suggested the under-compaction method to account for this issue. In the under-compaction method, the preparation density of the underlying layers is lower than the global density, and the density of the overlying layers is higher than the global density of the sample, leading to a uniform soil specimen. The difference in density of the successive layers is called the “under-compaction ratio” (Ladd 1978).

In this study, the under-compaction method was used to prepare specimens with 70 mm diameter and with height to diameter ratio of one. To confirm the uniformity of the specimens, a plug sample test was carried out. In this regard, three aluminum cups were placed through the height of the sample at a certain spacing from each other. Once the sample preparation had been completed, the aluminum cups were gently removed from the sample. The weight of the dried soil inside the cups was measured. Also, the volume of each cup was measured by filling them with water and measuring the weight of water. Then the void ratio for each plug sample was calculated.

The step by step procedure used to prepare the specimen are described briefly in the following:

- 1- Porous stone is boiled for 15 minutes to eliminate all the entrapped air inside the porous stone voids.
- 2- Top and bottom acrylic platens were greased to prevent any water leakage inside the sample.
- 3- The latex membrane was installed around the bottom platen and secured with three O-rings to seal it properly.
- 4- The split mold was installed around the bottom platen and rubber membrane. A specific amount of suction applied through the mold to eliminate all the air between the membrane and the mold. A disk-shape membrane impregnated with oil is placed on the bottom platen to reduce the friction between the soil particles and the platen surface (enlarged platens).
- 5- A predetermined amount of soil using under-compaction method was mixed with water. The prepared mixture poured into the mold and tamped in 4 layers. Each layer being 1.75 cm thickness.
- 6- Another disk-shape membrane impregnated to oil similar to the one used for the bottom of the specimen, was placed on the top of the soil prior to the placement of the upper platen.
- 7- The latex membrane was folded around the upper platen and sealed with three O-rings.
- 8- Once the specimen is prepared, a small amount of suction was applied by pore pressure pump inside the sample to maintain the stability of the sample during taking apart the mold.
- 9- the cylindrical triaxial cell was assembled and placed in the load frame, filled with de-aired water, and the vacuum pressure was replaced by an external cell pressure of 10 kPa.



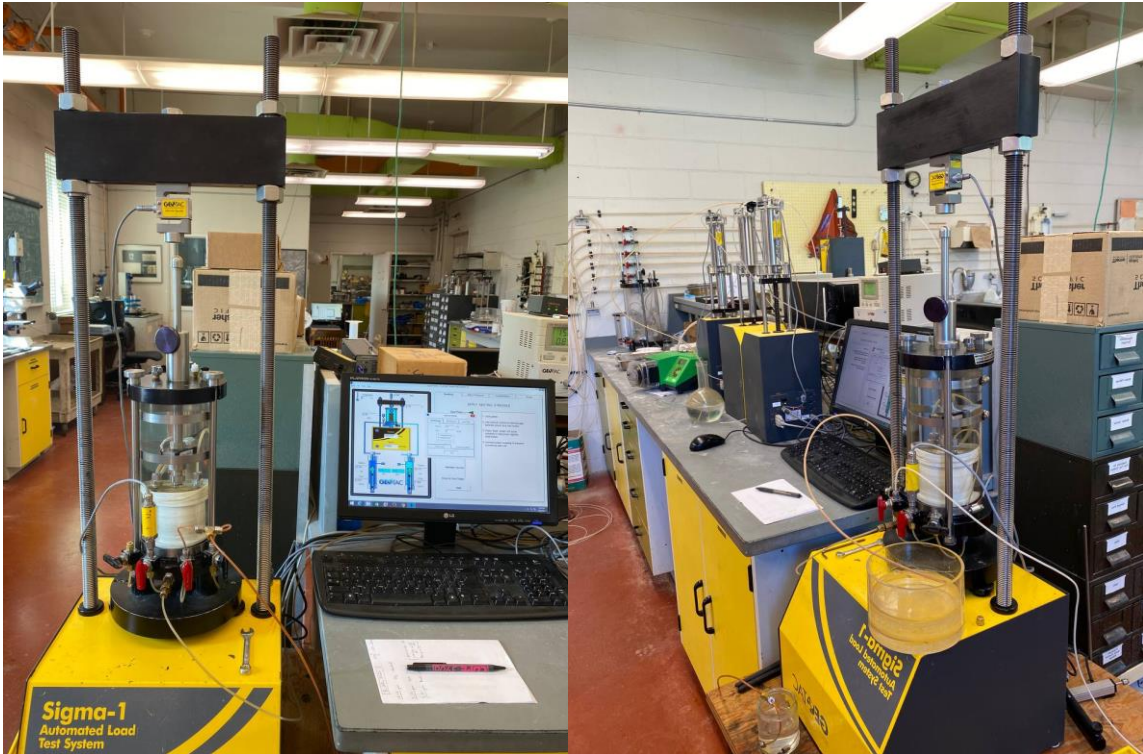


Figure 3.7: Sample preparation procedure at Western university laboratory

3.2.4 Sample saturation

The saturation of the samples was carried out as a three-step process: (1) Carbon dioxide percolation, (2) Water flushing, (3) Back-pressure saturation. After applying 10 kPa cell pressure in 15 minutes, as seating pressure to maintain the specimen fabric, the saturation stage begins with carbon dioxide percolation. Carbon dioxide's higher solubility in water than air allows us to reach a fully saturated level in specimen with reduced time and pressure (Mulilis et al. 1978). The CO₂ percolation through the sample from bottom to top drain lines takes about 60 minutes. And the flow rate was kept to three bubbles in a second to ensure minimal disturbance to the specimen.

The second step of the specimen saturation is de-aired water flushing from the bottom of the sample to the drainage line connected to the top of the sample. In this step, measuring the amount of water that remains inside the sample is of paramount importance to calculate the void volume changes of the sample during saturation. In this regard, the

inflow and outflow water volume was calculated by measuring the weight of the input and output containers connected to the bottom and top drainage lines, respectively, during saturation. The water flow rate is adjusted by the height of the input container from the bottom of the specimen, which should be kept low to prevent fine particles from washing out during water percolation.

The third step of the saturation procedure is backpressure saturation, as Black and Lee (1973) recommended. In this phase, 200kPa – 400kPa backpressure was applied via pore pump to dissolve the remaining carbon dioxide into water. This was done by applying a specific increment of cell pressure while simultaneously maintaining effective stress of 10kPa. To measure the specimen level of saturation, Skempton's pore water pressure was used. The Skempton's pore water pressure B was calculated as the rise in the specimen's pore water pressure divided by the increased cell pressure in each increment. All the saturated specimens in this chapter have a B -value higher than 0.98.

3.2.5 Consolidation Undrained shearing

All the specimens are consolidated under isotropic stress state condition subsequent to the completion of sample saturation. Isotropic consolidating the soil samples consists of maintaining a constant cell pressure while gradually decreasing the pore pressure to a target value. During the consolidation phase, the drainage valves were open. Specimens were allowed to consolidate for about one hour until the pore water volume remains unchanged.

The specimen void volume change during consolidation is very important, as it was used to indicate the density state of a soil specimen. The pore pump can determine the void ratio change in this phase, which records any water volume change inside the sample during consolidation. Figure 3.8 presents the normal compression line (NCL) of specimens with 0% and 25% fines content at different initial states. Normal compression line (NCL) is formulated as:

$$e_c = N - C_c \log(p') \quad (3-1)$$

Where the C_c is the NCL slope and N is soil void ratio at 1(kPa) mean effective stress. The slope of the normal compression line for specimens with 25% fines content is higher than the sand specimens. Fine particles increase sand's compressibility by allowing the sand particles to slide easily and filling the voids between the sand particles.

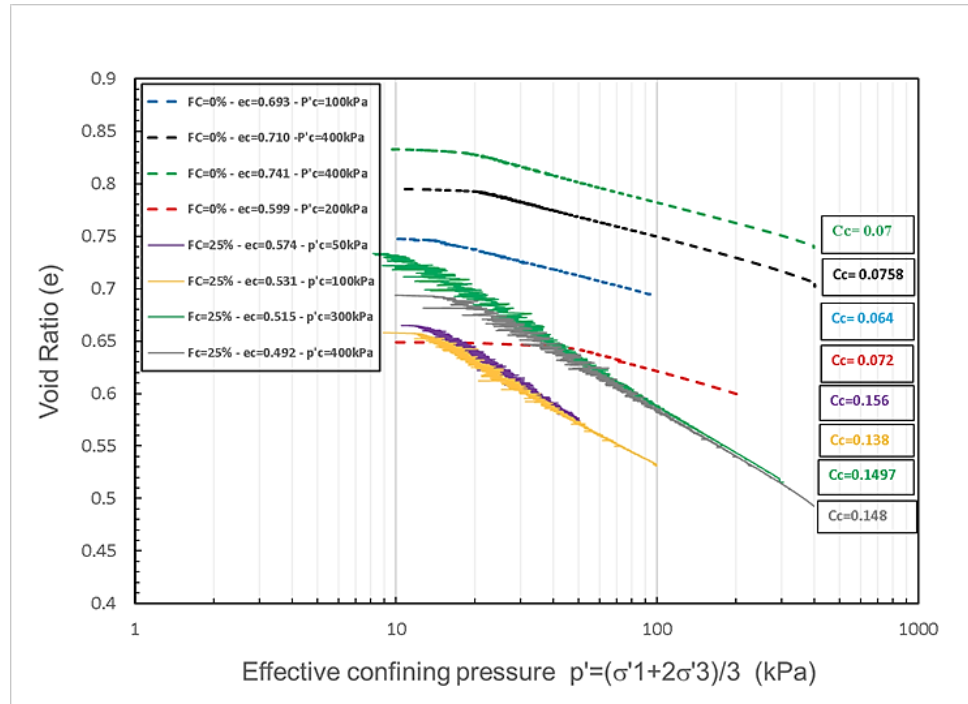


Figure 3.8: Normal compression line for sand with 0% and 25%FFT

3.3 Results and Discussions

The results of the static triaxial tests carried out on oil sand tailings with FC = 0%, 25%, and 50% fines content are presented in Table 3.2. The effect of fines content on the undrained response of the sand is discussed in this chapter. These results include the stress-strain behavior of the sand-silt mixtures with different relative densities (void ratio) and confining pressures.

Table 3.2: Triaxial testing program on the oil sand tailing with fluid fine tailings

<i>Test ID</i>	<i>Fine content</i>	<i>Consolidation relative density</i>	<i>Consolidation void ratio</i>	<i>Critical state void ratio</i>	<i>Consolidation mean effective stress</i>	<i>Behavior</i>
<i>Test type</i>	<i>FC(%)</i>	<i>Drc (%)</i>	<i>e_c</i>	<i>e_{cs}</i>	<i>P'c</i>	<i>Contractive or Dilative</i>
<i>IU-TXC</i>	0%	44.33	0.7407	0.7407	400	Contractive
<i>IU-TXC</i>	0%	59.48	0.676	0.676	400	Contractive
<i>IU-TXC</i>	0%	61.24	0.6685	0.6685	400	Contractive
<i>IU-TXC</i>	0%	52.53	0.7057	0.7057	400	Contractive
<i>IU-TXC</i>	0%	46.51	0.7314	0.7314	400	Contractive
<i>IU-TXC</i>	25%	69.05	0.4925	0.4925	400	Contractive
<i>IU-TXC</i>	25%	70	0.488	0.488	400	Contractive
<i>IU-TXC</i>	25%	62.16	0.54	0.54	400	Contractive
<i>IU-TXC</i>	25%	65.73	0.5154	0.5154	300	Contractive
<i>IU-TXC</i>	25%	50.55	0.574	0.574	50	Contractive
<i>IU-TXC</i>	25%	84.47	0.531	0.531	100	Contractive
<i>ID-TXC</i>	25%	68.76	0.495	0.437	200	-
<i>ID-TXC</i>	25%	59.46	0.559	0.442	300	-
<i>IU-TXC</i>	50%	59.7	0.35	0.35	400	Dilative
<i>IU-TXC</i>	50%	60.5	0.44	0.44	400	Dilative
<i>IU-TXC</i>	50%	72	0.613	0.613	400	Dilative

3.3.1 Changes of stress paths and stress-strain behaviors with fines content

Several researchers have studied the effect of consolidation stress on the undrained response of sand-silt mixtures. In this study, the effect of the consolidation stress and the fines content were investigated by evaluating the effective stress paths, the position of the critical state line, and the yield and post-liquefaction shear strengths. Figure 3.9 presents the effective stress paths of oil sand mixture with 25% fluid fine tailings (FFT) that are consolidated to 50kPa, 100kPa, 300kPa, and 400kPa. This plot clearly reveals that for oil sand tailing with 25% fine, increasing the effective consolidation stress causes a more contractive response. Strain-softening behavior occurs when the applied shear stress crosses the instability line (Lade 1992). The instability line is obtained by connecting the yield shear strengths of the stress paths with a similar consolidation void ratio to the origin, as illustrated in Figure 3.9. With advancing the strain-softening behavior following the initiation of the flow failure at the yield point, any possible breakage and reorientation occur among soil particles until the critical state. When a soil mass is at the critical state, it deforms continuously at constant shear stress, constant volume, and constant effective stress (Ishihara 1993, Jefferies and Been 2006, Sadrekarimi and Olson 2009). Steady-state, ultimate state, and residual state are the terms used in literature to describe the same phenomena as the critical state (Jefferies and Been 2006; Verdugo and Ishihara 1996).

At the critical state, the undrained shear strength ($S_{u(liq)}$) is the minimum shear strength mobilized in liquefaction flow failure. Many researchers recommended post-liquefaction shear strength as a conservative estimate of undrained shear strength. The effect of increasing consolidation stress on the shear response of oil sand tailing with 25% fine are as expected and are summarized below:

- Increase in yield and critical state strengths
- More pronounced strain-softening response

Figure 3.10 depicts the effective stress paths of the oil sand tailings for three different fines contents (FC) at almost equal consolidation void ratios. It was observed that static liquefaction occurred for the oil sand mixtures with FC = 0% and 25%. On the other hand, all specimens with FC = 50% show strain hardening (non-liquefiable) and dilative behavior. The comparison of the effective stress path curves reveals that increasing the fines content results in more dilative behavior. The shear strength of the sand mixture increases with fines content, as illustrated in Figure 3.11. Note that at 50% fines content, the deviator stress continues to climb until the critical state, where it reaches a plateau. In the oil sand mixture with FFT (fluid fine tailings), the fine particles adjust to the pore spaces between the coarse grains during the densification and consolidation, resulting in more contact area and higher shear strength. Therefore, soil particle gradation and FC play an essential role in shearing behavior of oil sand tailings.

Also, the effect of fines content on oil sand tailings at two different consolidation stress (100, 400kPa) is investigated. As illustrated in Figure 3.12, the yield and post-liquefaction shear strengths for both consolidation stresses for oil sand mixture with 25% fines content is higher than the clean sand. The increased shear strengths and more dilative behavior are partly associated with the higher densities of specimens with higher FC.

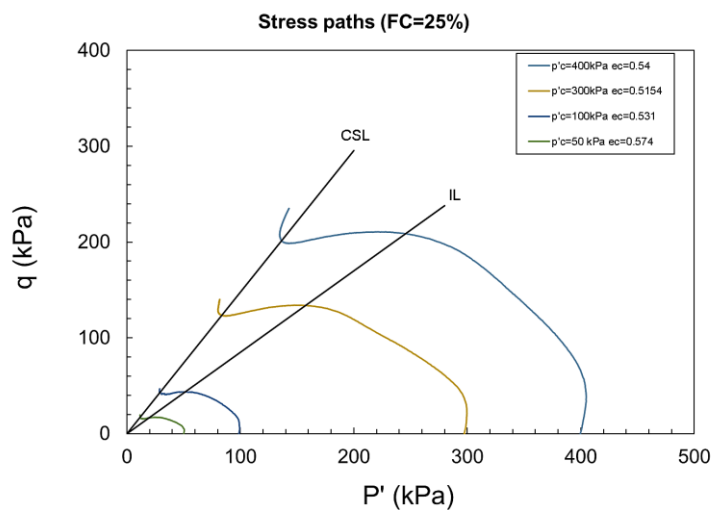


Figure 3.9: Effective stress paths for sand+25%fluid fine tailings at different consolidation stresses

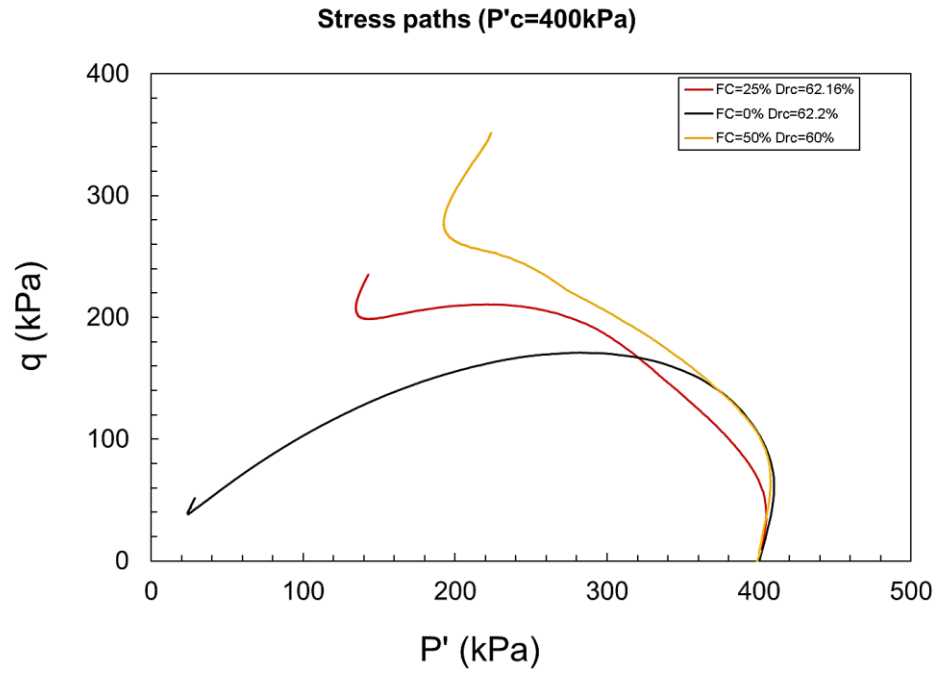


Figure 3.10: Comparison of effective stress paths with different fines content

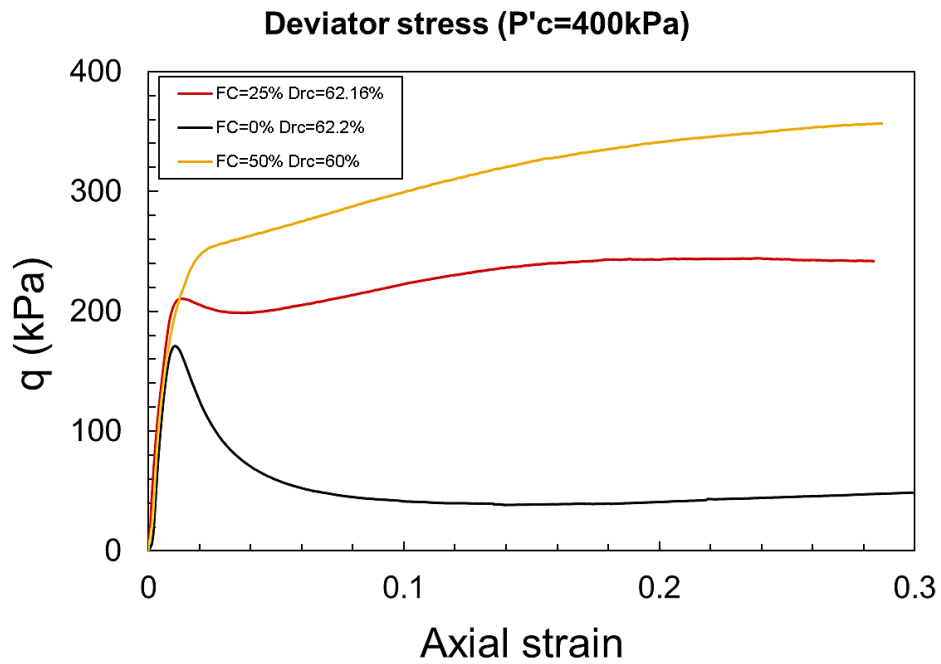


Figure 3.11: Comparison of the stress-strain behavior with different fines content

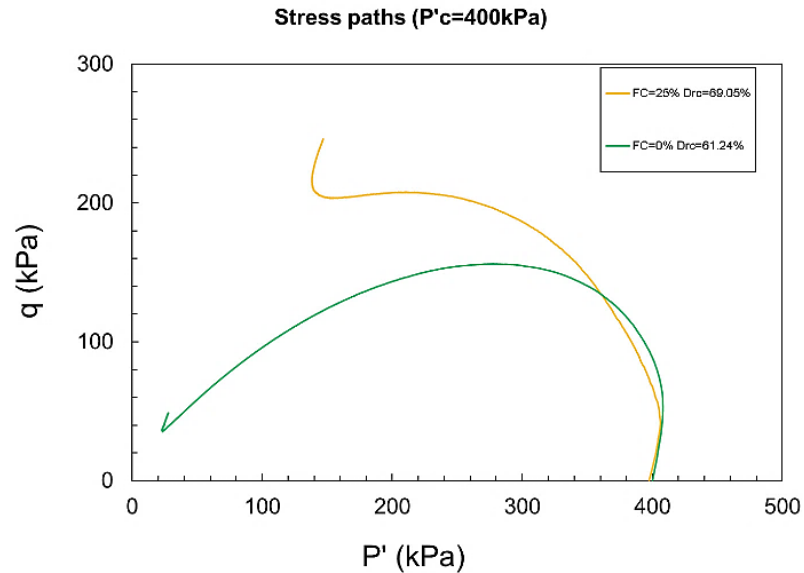


Figure 3.12: Effect of fines content on effective stress paths at two different consolidation stresses

Pitman et al. (1994) performed undrained triaxial tests on loose sand samples with varying percentages of plastic and non-plastic fines. They used the moist tamping method for sample preparation. Samples were isotropically consolidated and subjected to monotonic compression loading. The stress path and deviator stress variation with axial strain reported for the sand with different percentages of silica fines is presented in **Figure 3.13** and **Figure 3.14**. They concluded a clear trend of decreasing strain-softening response with increasing fines content. Carraro et al. (2003) and Yang (2004) also reported a similar conclusion regarding fines' effect on the sand-silt undrained behavior.

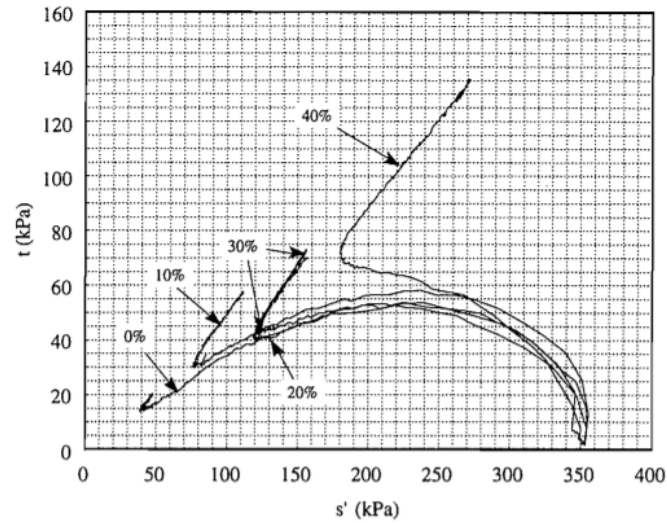


Figure 3.13: Effect of fines content on the effective stress path (Pitman et al, 1994)

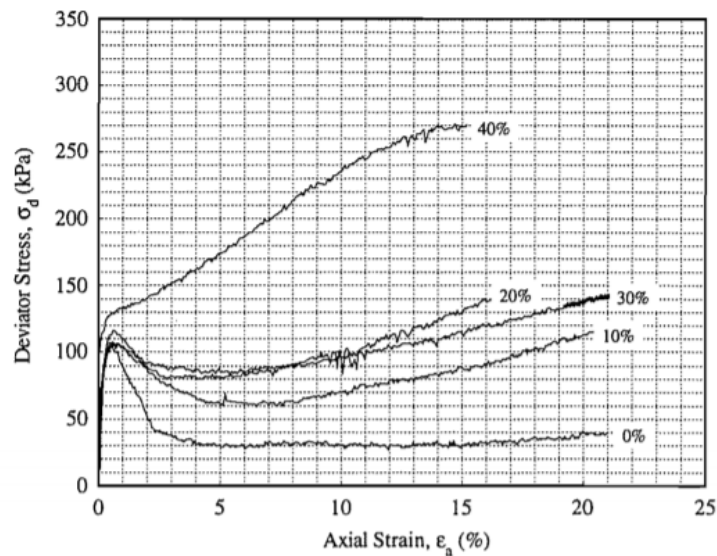


Figure 3.14: Effect of fine on stress-strain response (Robertson and Segoo (1994)

The mobilized friction angles variation with axial strain for two sets of triaxial tests on the oil sand tailings with FC = 0% and 25% are compared at almost similar consolidation void ratios. The consolidation stress for all the specimens was $P'_c = 400\text{kPa}$. As illustrated in Figure 3.15, at the yield point, which corresponds to the initiation of the static

liquefaction and flow failure, the friction angle φ'_{yield} of the sand+25% fines content is higher than that for the clean sand. However, with advancing the strain-softening behavior, the influence of the fines on the mobilized friction angles disappears. Therefore, the void ratio of the tailings mixture appears to have a significant effect on the friction angle in the early stages of shearing.

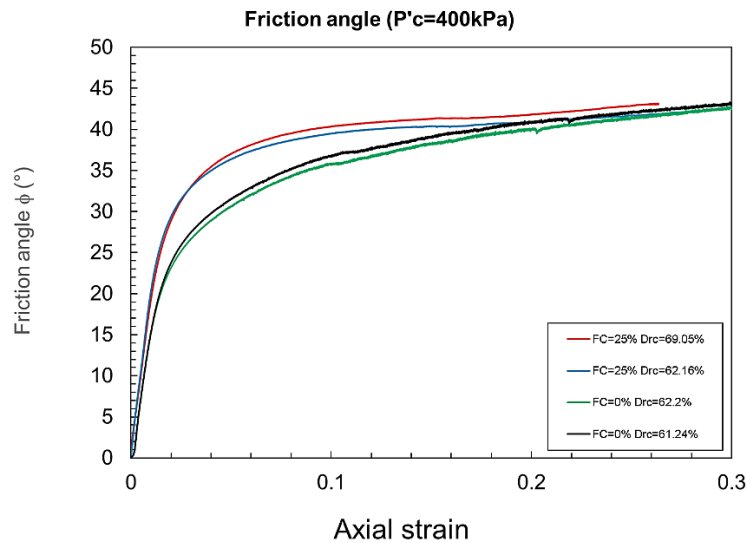


Figure 3.15: Effect of fines content on the friction angle

3.3.2 Effect of FC on critical state line of oil sand tailings

In the current study, the undrained shear behavior of the oil sand tailings mixture is evaluated based on the critical state framework. Poulos (1981) defined the critical state deformation as a state in which any soil particles continuously deform at constant volume, constant normal effective stress, constant shear stress, and constant velocity. In order to understand the influence of fines content on the liquefaction susceptibility of the tailings mixture, the variation of the critical state line with fines content needs to be characterized. The change of the shape and position of the critical state line with increasing fines content can be evaluated by considering the soil characteristics, including

soil particle size distribution, particle shape, and mineralogy. Many researchers reported that adding fines up to threshold value would essentially result in a downward movement of the CSL (decreasing Γ_{cs}) in the e-log p' plane, while the further increase of fines content will move the CSL upward (Pitman et al. 1994; Zlatovic & Ishihara 1997; Thevanayagam & Mohan 2000; Thevanayagam et al. 2002; Yang et al. 2006b; Murthy et al. 2007; Papadopoulou & Tika 2008; Rahman et al. 2008; Bobei et al. 2009; Carrera et al. 2011; Wei & Yang 2014).

Yang et al. (2006) performed drained and undrained triaxial tests on the Hokksund sand with varying percentages of the Chengbei non-plastic silt. Both sand and silt were made of similar minerals with similar shapes. They observed that the void ratio intercept of CSL decreased as the fines content increases up to a threshold value ($FC_{th} = 30\%$) without significant changes in the slope of the CSL (λ_{cs}). Numerous studies have investigated the effect of fines content on the slope of the CSL. Been and Jefferies (1985); Fear and Robertson (1995) reported that increasing fines content up to a specific percentage increases λ_{cs} in e-log p' space, as illustrated in Figure 3.16.

Bouckovalas et al. (2003) reported a clockwise rotation of the CSL around a pivot point with increasing fines content (see Figure 3.17). Olson (2001) indicated that soil particles' angularity and gradation affect the position of the CSL more significantly than the fines content.

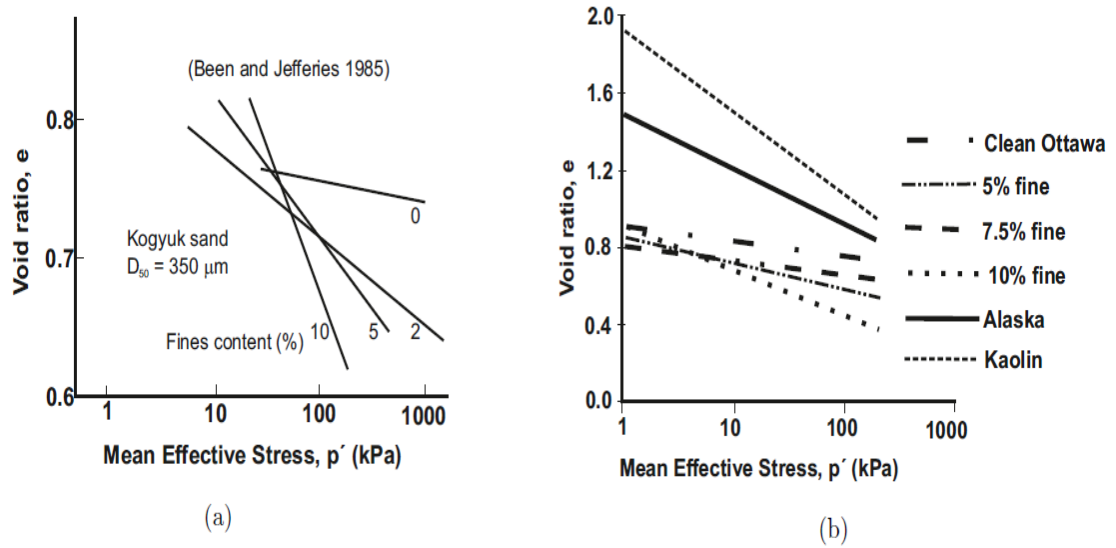


Figure 3.16: Critical state lines of sand-silt mixtures (a) Been and Jefferies (1985); (b) Fear and Robertson (1995)

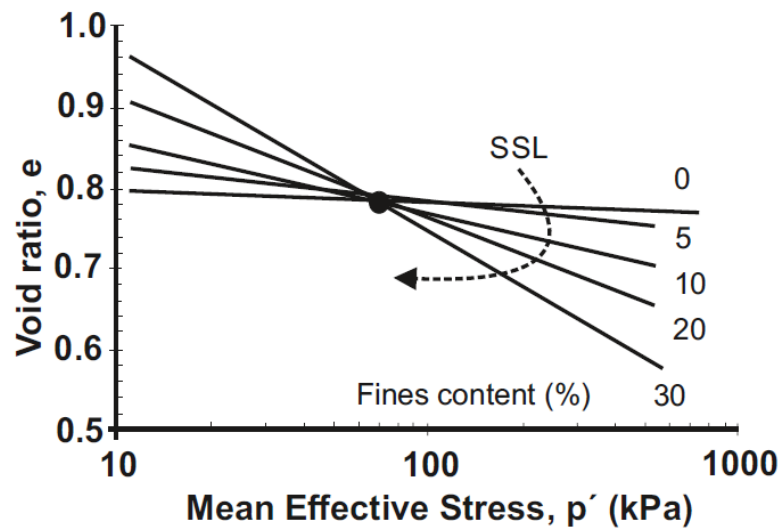


Figure 3.17: Effect of fines content on the critical state line (Bouckovalas et al, 2003)

In this study, the critical state line for the oil sand tailings with 25% fines content is compared with that of the clean sand. Figure 3.19 shows the critical state lines obtained for tailings specimens with FC = 0% and 25% in the e - $\log(p')$ space. The slope of the critical state line (λ_{cs}) for the clean sand is slightly steeper than that of the higher FC specimens. The void ratio intercepts of CSL (Γ_{cs}) for 0% and 25% FFT (fluid fine tailings) are 0.769 and 0.663, respectively. Therefore, the CSL has moved to denser void ratios (downward movement) with increasing FC to 25%. The slope of the critical state lines (λ_{cs}) measured for the oil sand with 0% and 25% fluid fine tailings are -0.0598 and -0.0784, respectively. Adding fluid fine tailings to the oil sand tailings results in a clockwise rotation of the critical state line in e - $\log p'$ space.

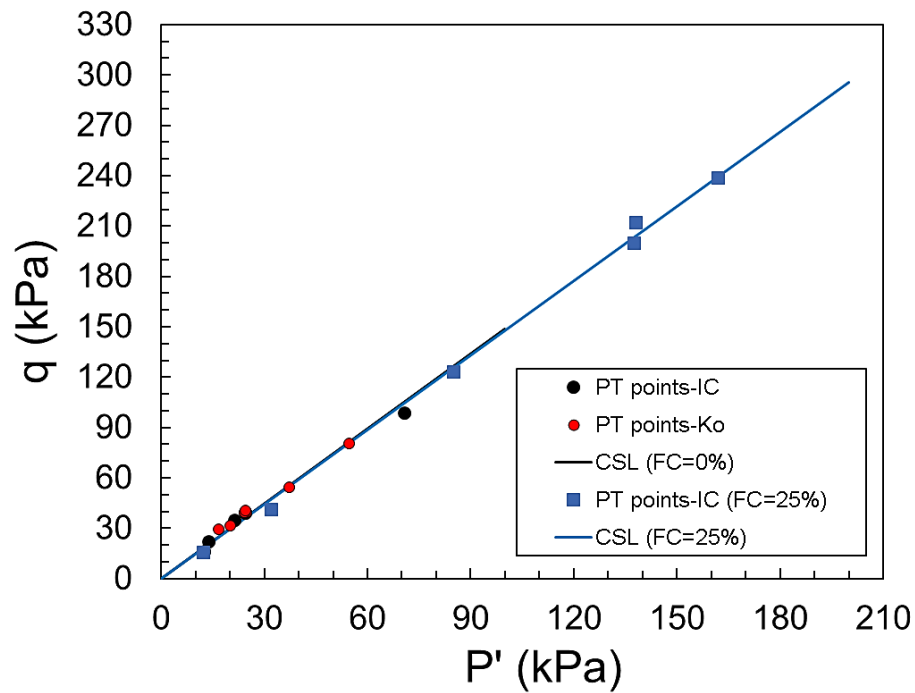


Figure 3.18: Critical state line on q - p' space for oil sand with 0% and 25% fines content

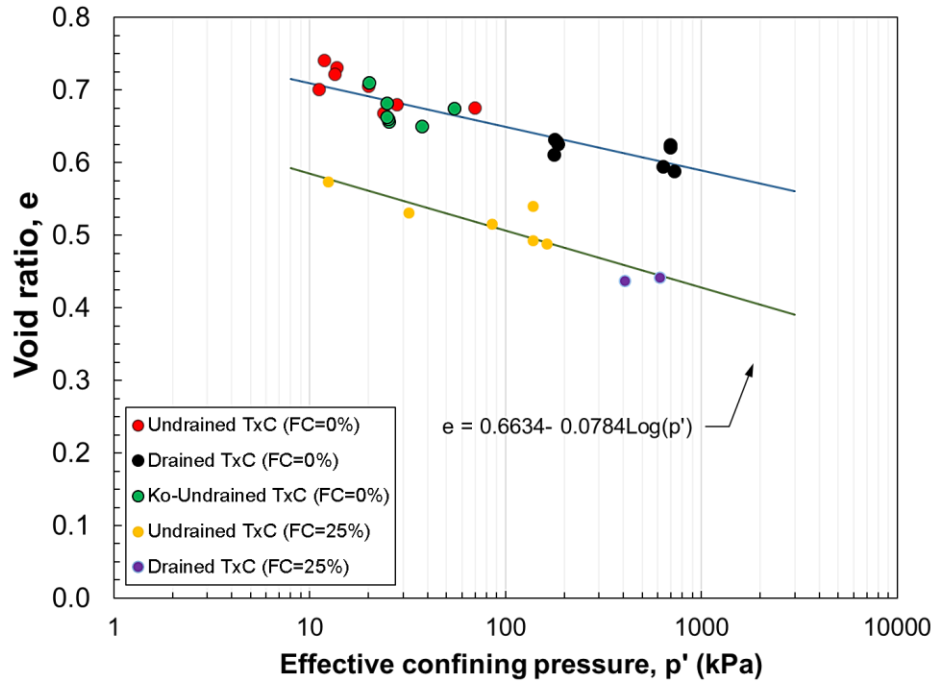


Figure 3.19: Critical state lines on e -log p' space for oil sand with 0% and 25% fines content

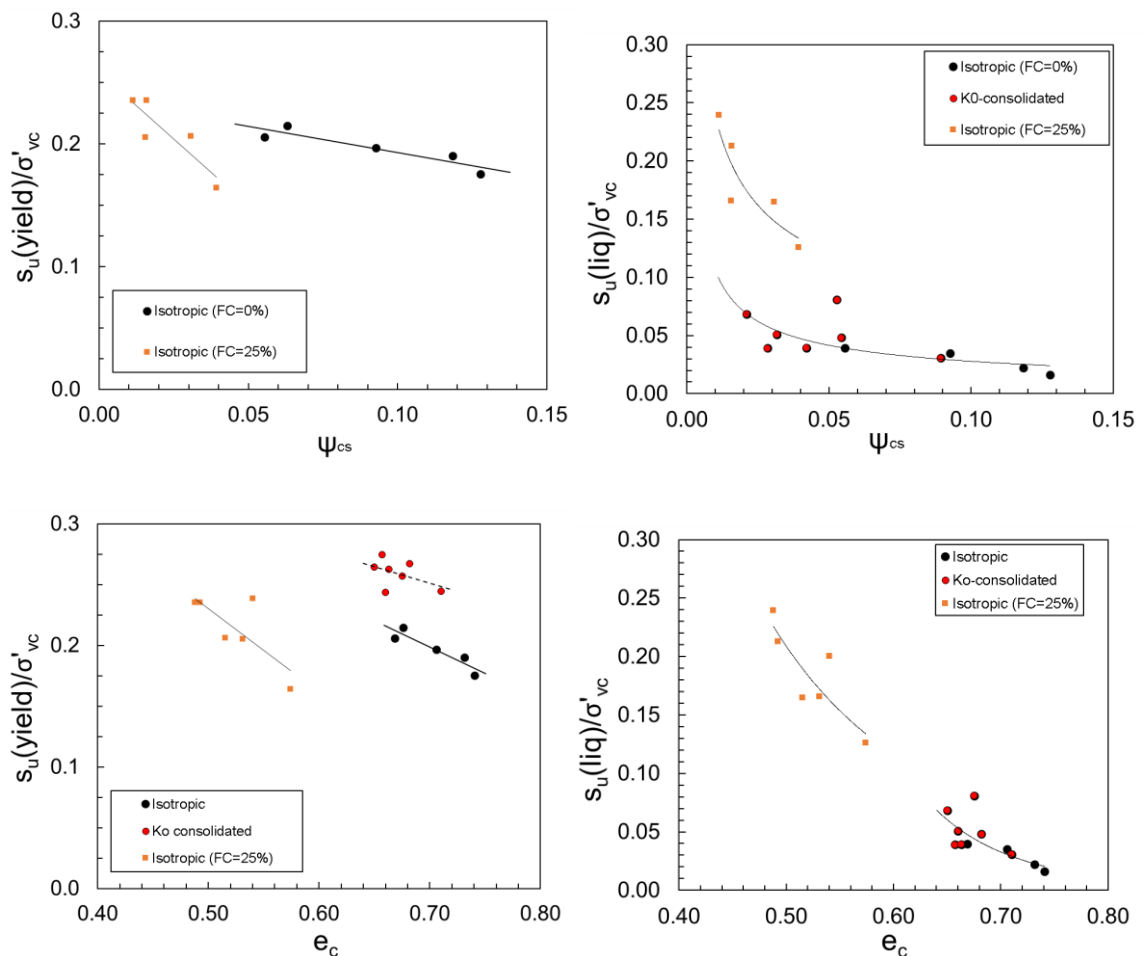
3.3.3 Effect of FC on yield and post-liquefaction strength ratios

Yield and post-liquefaction shear strengths have been normalized by the consolidation stress to account for the soil shear strength variation with overburden pressure and throughout soil depth. The effect of the fines content on the yield and critical shear strength ratios are evaluated below.

Figure 3.20 illustrates the yield and critical shear strength ratios variations with consolidation void ratio. Post-liquefaction shear strength ratio ranges for the oil sand with 0% and 25% fines content are $S_{u(liq)} / \sigma'_{vc} = (0.016 - 0.081)$ and $S_{u(liq)} / \sigma'_{vc} = (0.126 - 0.24)$, respectively. And the yield shear strength ratios for the oil sand tailings with 0% and 25% fines content are $S_{u(yield)} / \sigma'_{vc} = (0.18 - 0.21)$ and

$S_{u(\text{yield})} / \sigma'_{vc} = (0.16 - 0.24)$, respectively. Figure 3.20 clearly demonstrates that both $S_{u(\text{yield})} / \sigma'_{vc}$ and $S_{u(\text{liq})} / \sigma'_{vc}$ decrease with increasing consolidation void ratio. However, the effect of fines content on the shear strength ratios is not clear enough since the covered range of the consolidation void ratio is not the same. Therefore, the state parameter is used to see the effect of fines content. The state parameter is defined as the difference between the consolidation void ratio and the critical state void ratio corresponding to the same consolidation effective stress on the CSL. The state parameter considers the concurrent effect of density and stress state (Been & Jefferies, 1985; Wang et al., 2002; Thevanayagam & Mohan, 2000; Bobei & Lo, 2001).

Figure 3.20 depicts the shear strength ratios variation with state parameter for oil sand tailings with FC = 0% and 25%. Similar to figure 3.2, $S_{u(\text{liq})} / \sigma'_{vc}$ decreases with increasing state parameter.



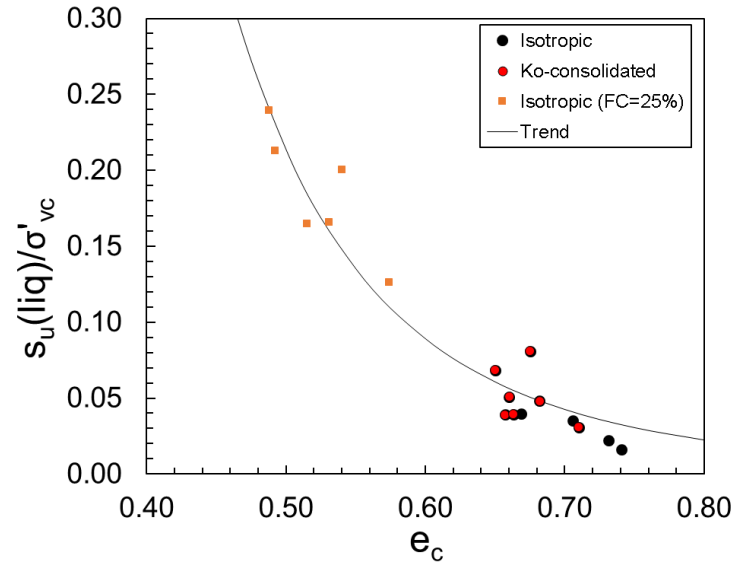


Figure 3.20: Effect of the fines content on shear strength ratios in terms of the void ratio and state parameter

3.4 Conclusions

This chapter presented the influence of the fines content (fluid fine tailings) on undrained shear behavior of the oil sand tailings. The critical state framework was used to interpret the triaxial compression test results. The findings of this chapter can be summarized as follows:

- The effect of increasing consolidation effective stress on the shear response of oil sand tailing with FC = 25% was investigated. Increases in yield and post-liquefaction strengths and more pronounced strain-softening response were the results of the increasing consolidation effective stress.
- It was observed that static liquefaction occurred for the oil sand tailings with FC = 0% and 25%. On the other hand, all specimens with FC = 50% exhibited strain hardening behavior.

- The stress-strain analyses of oil sand tailings with different percentages of fines showed that the shear strength ratios of tailings mixtures increased with increasing fines content at a given void ratio.
- The yield friction angle ϕ'_{yield} of the tailings with 25% FFT (fluid fine tailings) was higher than that for the clean tailings (FC = 0%). However, the influence of fines on the mobilized friction angle disappeared at large strains. Therefore, the initial void ratios of tailings mixtures appeared to have a significant effect on the friction angle in the early stages of shearing.
- The slope of the critical state line (λ_{cs}) for the clean tailings was slightly higher than that of tailings with FC = 25%. The void ratio intercept of CSL (Γ_{cs}) for FC = 0% and 25% were 0.769 and 0.663, respectively. Therefore, the CSL moves to the denser void ratios (downward movement) as the fines content increased to 25%. The slope of the critical state lines (λ_{cs}) measured for the oil sand with 0% and 25% fines content were -0.0598 and -0.0784, respectively. Adding fines to the oil sand tailings resulted in a clockwise rotation of the critical state line in e-log p' space.
- Post-liquefaction shear strength ratio ranges for the oil sand tailings with FC = 0% and 25% were $S_{u(liq)} / \sigma'_{vc} = (0.016 - 0.081)$ and $S_{u(liq)} / \sigma'_{vc} = (0.126 - 0.24)$, respectively. The yield shear strength ratios for the oil sand tailings with FC = 0% and 25% were $S_{u(yield)} / \sigma'_{vc} = (0.18 - 0.21)$ and $S_{u(yield)} / \sigma'_{vc} = (0.16 - 0.24)$, respectively. Figure 3.20 clearly demonstrates that both $S_{u(yield)} / \sigma'_{vc}$ and $S_{u(liq)} / \sigma'_{vc}$ decrease with increasing consolidation void ratio and state parameter.

References

- Abedi, Mehdi, and S Shahaboddin Yasrobi. "Effects of Plastic Fines on the Instability of Sand." *Soil Dynamics and Earthquake Engineering* 30, no. 3 (2010): 61-67.
- Alarcon-Guzman, A, GA Leonards, and JL Chameau. "Undrained Monotonic and Cyclic Strength of Sands." *Journal of Geotechnical Engineering* 114, no. 10 (1988): 1089-109.
- Baki, AL. "Cyclic Liquefaction Behaviour of Granular Materials with Fines." Ph. D., University of New South Wales at Australian Defence Force Academy, 2011.
- Baldi, Gualtiero, and Roberto Nova. "Membrane Penetration Effects in Triaxial Testing." *Journal of Geotechnical Engineering* 110, no. 3 (1984): 403-20.
- Been, K, MG Jefferies, and J Hachey. "The Critical State of Sands." *Geotechnique* 41, no. 3 (1991): 365-81.
- Been, Ken, and Mike G Jefferies. "A State Parameter for Sands." *Geotechnique* 35, no. 2 (1985): 99-112.
- Belkhatir, Mostefa, Ahmed Arab, Nouredine Della, Hanifi Missoum, and Tom Schanz. "Liquefaction Resistance of Chlef River Silty Sand: Effect of Low Plastic Fines and Other Parameters." *Acta Polytechnica Hungarica* 7, no. 2 (2010): 119-37.
- Bishop, AW. "The Influence of Progressive Failure on the Choice of the Method of Stability Analysis." *Geotechnique* 21, no. 2 (1971): 168-72.
- Bishop, Alan W, and Gordon E Green. "The Influence of End Restraint on the Compression

Strength of a Cohesionless Soil." *Geotechnique* 15, no. 3 (1965): 243-66.

Bishop, Alan Wilfred, and David John Henkel. "The Measurement of Soil Properties in the Triaxial Test." (1962).

Black, David K, and Kenneth L Lee. "Saturating Laboratory Samples by Back Pressure." *Journal of the soil mechanics and foundations division* 99, no. 1 (1973): 75-93.

Bobei, DC, and SR Lo. *Static Liquefaction of Sydney Sand Mixed with Both Plastic and Non-Plastic Fines*. Proceedings of the 14th Southeast Asian Geotechnical Conference, Hong Kong, 2001.

Bouckovalas, George D, Konstantinos I Andrianopoulos, and Achilleas G Papadimitriou. "A Critical State Interpretation for the Cyclic Liquefaction Resistance of Silty Sands." *Soil Dynamics and Earthquake Engineering* 23, no. 2 (2003): 115-25.

Carraro, JAH, P Bandini, and R Salgado. "Liquefaction Resistance of Clean and Nonplastic Silty Sands Based on Cone Penetration Resistance." *Journal of geotechnical and geoenvironmental engineering* 129, no. 11 (2003): 965-76.

Casagrande, Arthur. "Characteristics of Cohesionless Soils Affecting the Stability of Slopes and Earth Fills." *J. Boston Society of Civil Engineers* 23, no. 1 (1936): 13-32.

Casagrande, A. "Liquefaction and Cyclic Deformation in Sands: A Critical Review: Proceeding of the Fifth Pan American Conference in Soil Mechanics and Foundation Engineering." *Buenos Aires, Argentina* (1975).

Castro, G, JL Enos, JW France, and SJ Poulos. *Liquefaction Induced by Cyclic Loading. Report to National Science Foundation, Washington, Dc, No. NSF/CEE-82018*, 1982.

Castro, Gonzalo, and Steve J Poulos. "Factors Affecting Liquefaction and Cyclic Mobility." *Journal of the Geotechnical Engineering Division* 103, no. 6 (1977): 501-16.

Chan, Leonard CY, and Neil W Page. "Particle Fractal and Load Effects on Internal Friction in Powders." *Powder Technology* 90, no. 3 (1997): 259-66.

Chu, J, and WK Leong. "Effect of Fines on Instability Behaviour of Loose Sand." *Geotechnique* 52,

no. 10 (2002): 751-55.

Cubrinovski, Misko, and Kenji Ishihara. "Flow Potential of Sandy Soils with Different Grain Compositions." *Soils and foundations* 40, no. 4 (2000): 103-19.

Dash, HK, and TG Sitharam. "Undrained Monotonic Response of Sand–Silt Mixtures: Effect of Nonplastic Fines." *Geomechanics and Geoengineering: An International Journal* 6, no. 1 (2011): 47-58.

Georgiannou, VN. "The Undrained Response of Sands with Additions of Particles of Various Shapes and Sizes." *Geotechnique* 56, no. 9 (2006): 639-49.

Goudarzy, Meisam. "Micro and Macro Mechanical Assessment of Small and Intermediate Strain Properties of Granular Material." (2016).

Hazen, Allen. "A Study of the Slip in the Calaveras Dam." *Engineering News Record* 81, no. 26 (1918): 1158-64.

Jang, Deh-Jeng, and J David Frost. "Use of Image Analysis to Study the Microstructure of a Failed Sand Specimen." *Canadian geotechnical journal* 37, no. 5 (2000): 1141-49.

Kuerbis, Ralph H. "The Effect of Gradation and Fines Content on the Undrained Loading Response of Sand." University of British Columbia, 1989.

Ladd, RS. "Preparing Test Specimens Using Undercompaction." *Geotechnical Testing Journal* 1, no. 1 (1978): 16-23.

Lade, Poul V, and Jerry A Yamamuro. "Evaluation of Static Liquefaction Potential of Silty Sand Slopes." *Canadian geotechnical journal* 48, no. 2 (2011): 247-64.

Md. Mizanur, Rahman, and SR Lo. "Predicting the Onset of Static Liquefaction of Loose Sand with Fines." *Journal of geotechnical and geoenvironmental engineering* 138, no. 8 (2012): 1037-41.

Mulilis, JP, FC Townsend, and RC Horz. "Triaxial Testing Techniques and Sand Liquefaction." In *Dynamic Geotechnical Testing*: ASTM International, 1978.

- Murthy, TG, D Loukidis, JAH Carraro, M Prezzi, and R Salgado. "Undrained Monotonic Response of Clean and Silty Sands." *Geotechnique* 57, no. 3 (2007): 273-88.
- Naeini, SA, and MH Baziar. "Effect of Fines Content on Steady-State Strength of Mixed and Layered Samples of a Sand." *Soil Dynamics and Earthquake Engineering* 24, no. 3 (2004): 181-87.
- Ni, QTST, TS Tan, GR Dasari, and DW Hight. "Contribution of Fines to the Compressive Strength of Mixed Soils." *Geotechnique* 54, no. 9 (2004): 561-69.
- Olson, Scott M. "Liquefaction Analysis of Duncan Dam Using Strength Ratios." *Canadian geotechnical journal* 43, no. 5 (2006): 484-99.
- Olson, Scott Michael. *Liquefaction Analysis of Level and Sloping Ground Using Field Case Histories and Penetration Resistance*: University of Illinois at Urbana-Champaign, 2001.
- Olson, Scott M, and Timothy D Stark. "Yield Strength Ratio and Liquefaction Analysis of Slopes and Embankments." *Journal of geotechnical and geoenvironmental engineering* 129, no. 8 (2003): 727-37.
- Papadopoulou, Anthi, and Theodora Tika. "The Effect of Fines on Critical State and Liquefaction Resistance Characteristics of Non-Plastic Silty Sands." *Soils and foundations* 48, no. 5 (2008): 713-25.
- Pitman, TD, PK Robertson, and DC Segro. "Influence of Fines on the Collapse of Loose Sands." *Canadian geotechnical journal* 31, no. 5 (1994): 728-39.
- Riemer, Michael F, and Raymond B Seed. "Factors Affecting Apparent Position of Steady-State Line." *Journal of geotechnical and geoenvironmental engineering* 123, no. 3 (1997): 281-88.
- Sladen, JA, RD D'hollander, and J Krahn. "The Liquefaction of Sands, a Collapse Surface Approach." *Canadian geotechnical journal* 22, no. 4 (1985): 564-78.
- Sladen, JA, RD D'hollander, J Krahn, and DE Mitchell. "Back Analysis of the Nerlerk Berm Liquefaction Slides." *Canadian geotechnical journal* 22, no. 4 (1985): 579-88.

- Sladen, JA, and JM Oswell. "The Behaviour of Very Loose Sand in the Triaxial Compression Test." *Canadian geotechnical journal* 26, no. 1 (1989): 103-13.
- Stark, Timothy D, and Gholamreza Mesri. "Undrained Shear Strength of Liquefied Sands for Stability Analysis." *Journal of Geotechnical Engineering* 118, no. 11 (1992): 1727-47.
- Sukumaran, B, and AK Ashmawy. "Quantitative Characterisation of the Geometry of Discret Particles." *Geotechnique* 51, no. 7 (2001): 619-27.
- Sze, HY, and J Yang. "Failure Modes of Sand in Undrained Cyclic Loading: Impact of Sample Preparation." *Journal of geotechnical and geoenvironmental engineering* 140, no. 1 (2014): 152-69.
- Tarantino, Alessandro, and Adrian FL Hyde. "An Experimental Investigation of Work Dissipation in Crushable Materials." *Geotechnique* 55, no. 8 (2005): 575-84.
- Thevanayagam, S. "Effect of Fines and Confining Stress on Undrained Shear Strength of Silty Sands." *Journal of geotechnical and geoenvironmental engineering* 124, no. 6 (1998): 479-91.
- Thevanayagam, S, and S Mohan. "Intergranular State Variables and Stress–Strain Behaviour of Silty Sands." *Geotechnique* 50, no. 1 (2000): 1-23.
- Wang, Zhi-Liang, Yannis F Dafalias, Xiang-Song Li, and Faiz I Makdisi. "State Pressure Index for Modeling Sand Behavior." *Journal of geotechnical and geoenvironmental engineering* 128, no. 6 (2002): 511-19.
- Wei, LM, and J Yang. "On the Role of Grain Shape in Static Liquefaction of Sand–Fines Mixtures." *Geotechnique* 64, no. 9 (2014): 740-45.
- Yamamuro, Jerry A, and Poul V Lade. "Static Liquefaction of Very Loose Sands." *Canadian geotechnical journal* 34, no. 6 (1997): 905-17.
- Yang, Shaoli. *Characterization of the Properties of Sand-Silt Mixtures*: Norwegian University of Science and Technology, Faculty of Engineering ..., 2004.
- Yang, SL, R Sandven, and L Grande. "Instability of Sand–Silt Mixtures." *Soil Dynamics and Earthquake Engineering* 26, no. 2-4 (2006): 183-90.
- Yang, SL, R Sandven, and L Grande. "Steady-State Lines of Sand–Silt Mixtures." *Canadian geotechnical journal* 43, no. 11 (2006): 1213-19.

Zlatovic, Sonja, and Kenji Ishihara. "Normalized Behavior of Very Loose Non-Plastic Soils: Effects of Fabric." *Soils and foundations* 37, no. 4 (1997): 47-56.

Chapter 4

4 « Effect of Saturation on Instability of Oil sand tailings »

4.1 Introduction

Static liquefaction is one of the devastating structural failures in both the mining and geotechnical industry, which results in dramatic instability and large shear deformation in a relatively short duration due to loss of shearing resistance. There have been numerous tailings dam failures resulting from monotonically increasing loads worldwide, which lead to high costs, environmental cleanup, and loss of life. Mount Polley and Fundao are examples of recent tailings dam failures, which have brought attention to static liquefaction and strength loss caused by undrained failure.

Static liquefaction occurrence can be determined by evaluating the flow potential of the soil sample. Over the past decades, intensive efforts have been made by the geotechnical research community to understand the mechanism of mine tailings liquefaction based on laboratory work, physical modeling as well as on numerical analysis. However, the behavior of sand can be significantly influenced not only by the initial state but also by the saturation parameter.

Examination of the undisturbed samples of frozen tailings sand indicates that the specimens were not fully saturated (Fourier et al., 2001). A few meters above the phreatic surface, the air bubbles were determined by compression wave velocity measurement, which indicates the partially saturated condition (Ishihara et al., 2001; Nakazawa et al., 2004). Mathiroban and Grozic (2004) asserted that the pore pressure response and liquefaction potential of the oil sands and their corresponding tailings ponds had been altered on account of the presence of gas.

Partial saturation:

The soil conditions based on the degree of saturation are often categorized as fully saturated, partially saturated, or unsaturated. Fredlund and Rahardjo (1993) illustrated the transformation from fully saturated to unsaturated conditions, as shown in Figure 4.1.

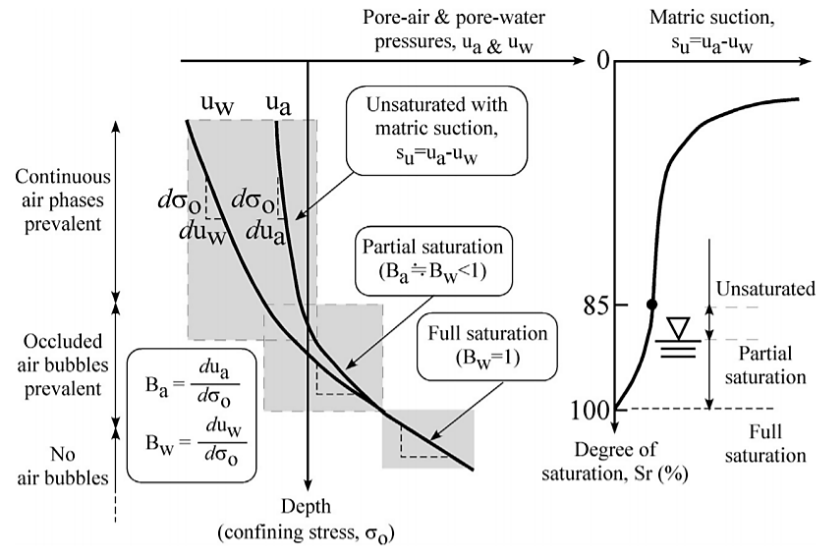


Figure 4.1: Schematic interpretation of fully, partially, and unsaturated soil deposits (Tsukamoto et al. 2014).

For an unsaturated soil (at layers above the groundwater table) with some continuous air phases, large matric suction comes into effect due to surface tension. The mobilization of shear strength is affected by surface tension that tends to interact with the soil structure.

With increasing depth and therefore increasing confining pressure, the pore water and pore air pressures increase too. However, the pore water pressure tends to grow faster than pore air pressure. Therefore, the matric suction, defined as the differences between pore water and pore air pressure, gradually decreases with depth. As a result, when the air entry value of the soil is met, the occluded air bubbles will substitute the continuous air phase of the soil, which would not interact with the soil structure. However, these

occluded air bubbles would increase the compressibility of the pore fluid. There would be some point that matric suction would become negligible, leading to the condition in which two pore pressure coefficients would become equal and lower than the unity. This zone is categorized as a “partially saturated” zone.

Soils that contain a large amount of dissolved gas are termed gassy soils (Sobkowcz, 1984). Gassy soil is in the same category as partially-saturated soils in which gas in its free form or solution in the pore water is found. Świdziński and Mierczyński (2017) performed some triaxial monotonic tests on cohesiveless partially-saturated samples. The degree of saturation was controlled during the triaxial compression test through Skempton’s pore pressure coefficient. In order to obtain samples with various degrees of saturation, the time of passage of the carbon dioxide and deaerated water were varied. They concluded that liquefaction susceptibility decreased with a reduction in saturation degree. They also found that the instability line was strongly curved and was not a straight line in the stress path space.

Many liquefaction flow failures have been reported in underwater and submarine slopes containing gas bubbles within the soil voids, such as in the Fraser River Delta, British Columbia (Chillarige et al. 1997), Mississippi River Delta, California (Whelan et al. 1977), and Klamath River Delta, California (Field 1991).

Whelan et al. (1977) examined the effect of gas on the behavior of Mississippi River soft delta clay deposits. These investigations revealed that the failure of marine sediments and reduced shear strength were due to the presence of gas.

Wheeler (1988) examined the behavior of sea marine deposits. The results show that the undrained shear strength of gassy clays could be higher or lower than that of similar but saturated clays. He Jia (2013) indicated that the occluded gas bubbles in the sand could either strengthen or weaken the liquefaction susceptibility under monotonic loading. Sobkowcz (1984) showed that gas exsolution in the unloading path results in a drastic drop in the mean effective stress.

The compressibility of the gas-water mixture is affected by the presence of pore gas based on Boyle's law and Henry's law (Dessault 1979; Schuurman 1992). The fluid pore pressure for a gassy soil can be determined using the following equation proposed by Sobkowicz (1982):

$$A \Delta u^2 + B \Delta u + C = 0$$

(4-1)

$$\begin{cases} A = nS \beta_w \\ B = n(p_0 S \beta_L + 1 - S + SH) - \beta_T \Delta \sigma' \\ C = -p_0 \Delta \sigma' \beta_T \end{cases}$$

Gas bubbles affect the stability of a slope in different ways, such as increasing pore fluid compressibility, partial drainage due to the occluded bubbles during undrained loading, and generation of excess pore pressure due to evolving gas bubbles and making the soil underconsolidated (Mathiroban et al. 2004).

Atigh et al. (2003) proposed an elastoplastic model to predict the undrained behavior of gassy soil as equivalent to saturated soil behavior under partially drained loading. They examined the behavior of submarine slopes in the Fraser River delta during tidal variations. These investigations demonstrated that a small amount of expansive volumetric strain due to gas compressibility could lead to different pore pressure generations with depth. The reduced pore-pressure response at lower depths resulted in a reduction in effective stresses during low tides.

Vaid and Eliadorani (1998) performed an experimental investigation of static liquefaction of saturated Fraser River sand under undrained and partially-drained conditions. They concluded that small expansive volumetric strains in a partially-drained condition could transform a stable undrained behavior into an unstable condition. Rad et al. (1994) carried out a comprehensive experimental investigation on the effect of gas type, the amount of gas, and the pore pressure level on the undrained static and cyclic strength of sands with higher density and lower consolidation pressure to see the gas effect more

pronounced due to the maximum dilation (Rad and Vianna 1989). They postulate that the higher solubility of the gas or higher amount of the gas or lower pore pressure results in the weaker specimen under undrained shearing.

Ishihara et al. (2004) carried out a multiple series of undrained monotonic and cyclic tests on nearly saturated sand specimens with a relative density range from 5 to 70%. They used Skempton's B parameter instead of the degree of saturation to quantify the saturation state. They demonstrated that the behavior of a sample under undrained condition changed from contractive to dilative response with decreasing B from 0.95 to 0.1, which was almost analogous to that under drained condition (Tsukamoto et al., 2002). Also, these investigations revealed that for loose to medium-dense sands, the shear strength increased and sands behavior became moremore dilative with decreasing the degree of saturation. The reduced pore pressure and increased effective stress were due to the increased overall compressibility of the soil due to the presence of air in the pore water. However, this trend was reversed in dense sands in which the shear strength reduced at a lower degree of saturation. This resulted from the inability of air-containing pore water to develop sufficient suction to maintain a constant volume condition. In a dense sand, the undrained deformation characteristic resemble that of a drained condition. It is worth mentioning that the discussed behavior for the dense sand can hold true in a range of large axial strains. The shear stress required for a particular small strain in dense sand increases with decreasing the degree of saturation.

Based on Chaney (1978) and Yoshimi et al. (1989) studies, when the degree of saturation drops to 90%, the liquefaction resistance increases roughly two times as much as that of fully saturated samples.

Grozic et al. (1999) examine the effect of saturation on the stress-strain behavior of loose sand under undrained loading conditions. They illustrated that the threshold value of the degree of saturation which can change soil behavior from strain-softening to strain-hardening is around 90%. Lade and Pradel (1990) demonstrated that the generation of the pore pressure was mitigated, and the unstable condition was prevented when the degree of saturation was low enough due to the presence of compressible gas.

HE JIA (2013) carried out undrained triaxial compression and extension test on the medium dense sand to evaluate the effect of degree of saturation on the undrained resistance of desaturated samples using the microbial method. He demonstrated that the undrained resistance at small shear strain increased by reducing the degree of saturation. However, at large shear strains, the trend was reversed, and the shear resistance decrease.

4.2 Methodology

4.2.1 Oil sand tailings properties

Oil sand tailings are the material left over after bitumen extraction, including water, sand, fine particles, residual bitumen, or other hydrocarbons. The amount of the bitumen for the oil sands and fluid fine tailings (FFT) was determined as 1.26% and 7%, respectively, using the ignition method. The physical properties of these sands are presented in the following section. The particle size distribution was determined by sieve and hydrometer analysis and presented in Figure 4.3. The grain size range from 0.003 mm to 2 mm. Distribution of the soil particles shows a poorly graded material with most particles in the fine-sand size range and 5.45% of particles passing No. 200 sieve (< 0.075 mm). The sand is classified as an SP sand based on the unified soil classification system as per the ASTM D2487 standard procedure. The sphericity and roundness of the oil sand particles were estimated by Krumbein and Sloss's (1963) chart. For the sand particles, sphericity is overall relatively high, and elongated particles are rare. The roundness varies widely, from angular to well-rounded, with subangular shapes being the most common.

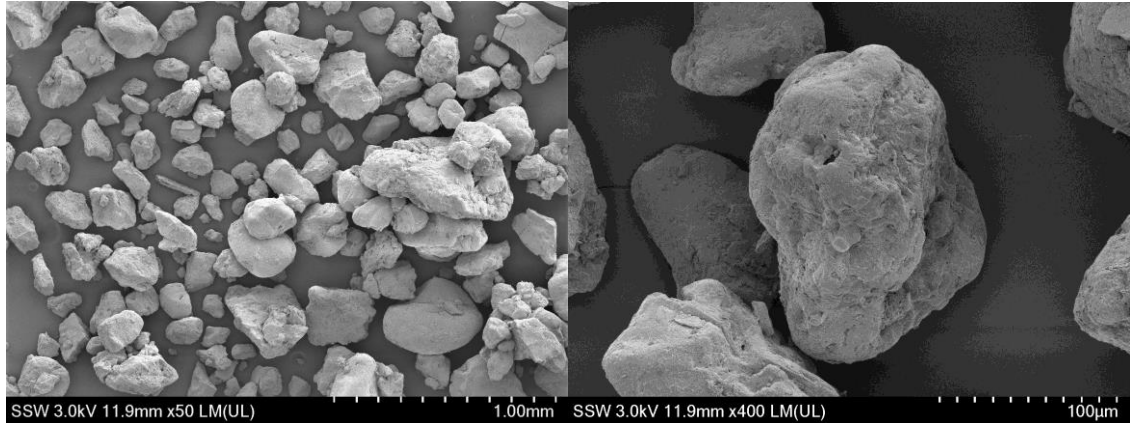


Figure 4.2 Shape of oil sand particles (SEM images)

Standard index tests were carried out, and Table 4.1 presents a summary of index properties for the samples. The median grain size (D_{50}) was determined as 0.218mm, and the measured coefficient of uniformity (C_u) and the coefficient of curvature (C_c) are 2.01 and 1.05, respectively. The Values of maximum and minimum void ratios were determined using minimum and maximum densities, respectively, according to ASTM D4253. The specific gravity of the sand particles was about 2.624, following the ASTM-D854 standard procedure.

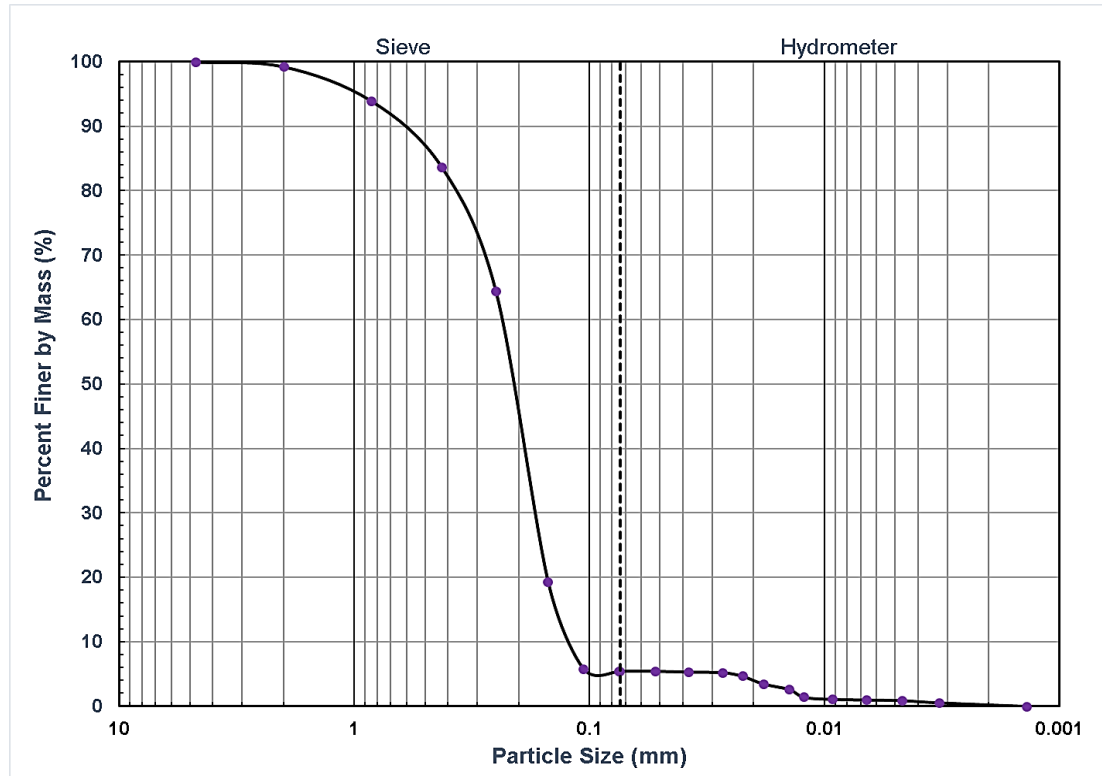


Figure 4.3: Particle size distribution of the oil sand tailings

Table 4.1: Parameters of the oil sand tailings

D_{50} (mm)	G_s	e_{max}	e_{min}	C_u	C_c
0.218	2.624	0.93	0.503	2.01	1.05

4.2.2 Sample preparation at different saturation ratios

In this study, the under-compaction method was employed to prepare specimens of 50 mm in diameter and a height to diameter ratio of one. In the under-compaction method, the preparation density of the underlying layers is lower than the global density, and the density of the overlying layers is higher than the global density of the sample, leading to

a uniform soil specimen. The step-by-step procedure used to prepare the specimens are described briefly in the following paragraphs:

- 1- Porous stone is boiled for 15 minutes to eliminate all the entrapped air inside the porous stone voids.
- 2- Top and bottom acrylic platens were greased to prevent any water leakage inside the sample.
- 3- The latex membrane was installed around the bottom platen and secured with three O-rings to seal it properly.
- 4- The split mold was installed around the bottom platen and rubber membrane. A specific amount of suction was applied through the mold to eliminate all the air between the membrane and the mold. A disk-shaped membrane impregnated with oil is placed on the bottom platen to reduce the friction between the soil particles and the platen surface (enlarged platens).
- 5- A predetermined amount of soil using the under-compaction method was calculated and mixed with 5% water content. The prepared mixture was poured into the mold and tamped in 2 layers.
- 6- Another disk-shaped membrane impregnated with oil similar to the one used for the bottom of the specimen was placed on the top of the soil before placing the upper platen.
- 7- The latex membrane was folded around the upper platen and sealed with three O-rings.
- 8- Once the specimen is prepared, a small amount of suction was applied by the pore pressure pump inside the sample to maintain the stability of the sample while taking apart the mold.
- 9- The cylindrical triaxial cell was assembled and placed in the load frame, filled with de-aired water, and the vacuum pressure was replaced by an external cell pressure of 10 kPa.

4.2.3 Sample partial saturation

It is generally difficult to precisely measure the degree of saturation, particularly when the soil element is partly saturated near the state of complete saturation. The B-value changes quite widely in the range of $S_r = 80$ to 100%. The pore pressure parameter B is therefore found to serve as a useful index to compare the state of saturation for a partially saturated soil. There are different methods to achieve different levels of saturation, including:

- No carbon dioxide flushing
- Reducing back pressure
- Using aeriated water

The saturation of the sample in this study consisted of two steps: (1) Water percolation, (2) Backpressure saturation.

The first step of the specimen saturation included non-deaired water which was flushed from the bottom of the sample to the drainage line connected to the top of the sample. The water flushing duration was adjusted according to the required level of saturation.

The second step of the saturation procedure included backpressure saturation, as recommended by Black and Lee (1973). In this stage, the sample saturation level was controlled by checking Skempton's B parameter. This was done by applying a specific increment of cell pressure while maintaining an effective stress of 10kPa. The Skempton's pore water pressure B was calculated as the rise in the specimen's pore water pressure divided by the increased cell pressure in each increment. In the backpressure saturation, by applying an increment of the cell pressure to measure the corresponding

change in pore pressure, the Skempton's B would increase at each increment due to air dissolution into water. The back pressure saturation continues until the required B -value is reached.

4.2.4 Consolidation

All the specimens were consolidated under isotropic stress condition. Isotropic consolidating the soil samples consisted of maintaining a constant cell pressure while gradually decreasing the pore pressure to a target value. During the consolidation phase, the drainage valves were open. Specimens were allowed to consolidate for about one hour until the pore water volume change became negligible. Figure 4.4 presents the normal compression line (NCL) of oil sand with an initial void ratio of 0.753. The specimen was consolidated to $p'_c = 400$ kPa, at which the consolidation void ratio was $e_c = 0.668$. Normal compression line (NCL) is formulated as:

$$e_c = N - C_c \log(p')$$
(4-2)

Where the C_c is the NCL slope and N is soil void ratio at 1 kPa mean effective stress.

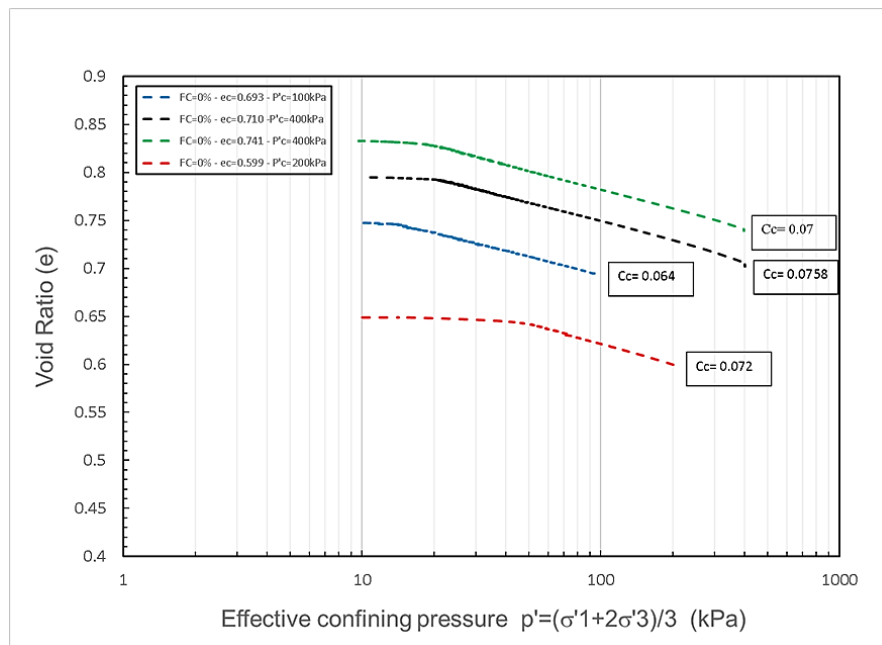


Figure 4.4: Normal compression line for oil sand tailings

4.2.5 Undrained shearing

Once the sample was completely consolidated, and the pore pump volume stabilized, the specimen was sheared. The axial load was applied in a strain-controlled mode. The cell pressure was kept constant, and pore pressure was measured with a pressure transducer in the undrained tests, while the backpressure pump recorded volume change during drained shearing. The applied axial deformation rate was chosen based on the ASTM guideline for the undrained shearing condition:

$$\dot{\varepsilon} = \frac{4\%}{10t_{50}} \Rightarrow CIU \quad (4-3)$$

Where t_{50} is the times corresponding to the 50% level of consolidation. The axial deformation rate was chosen to ensure the complete equalization of pore water pressure in the undrained triaxial test. The target axial deformation to reach the critical state was 30% axial strain.

4.2.6 Measurement of saturation ratio

In this study, the compression waves velocity (V_p) is used as an indicator for determining the saturation level of oil sand specimens. While Skempton's B is easy to use in laboratory soil testing and has been widely used in triaxial testing to evaluate specimens' saturation level, it is not applicable in soil deposits in the field condition.

On the other hand, measurements of the shear wave velocity and compression wave velocity in the field have commonly been carried out using the cross-hole and down-hole techniques in the routine investigation.

For this purpose, the triaxial setup was developed with a set of ultrasonic transducer platens with 200 kHz compression crystals and bender elements for P and S velocity measurements. Figure 4.5 presents the details of the new bender element caps installed on the triaxial platens.

Yang (2002) introduced a theoretical relationship between the B-value as an index of saturation level and the velocity of P-wave:

$$V_p = \left(\frac{\frac{4G}{3} + \frac{K_b}{1-B}}{\rho} \right)^{0.5} \quad (4-4)$$

Where G is the shear modulus and ρ is the total density and K_b is the bulk modulus of the soil skeleton.

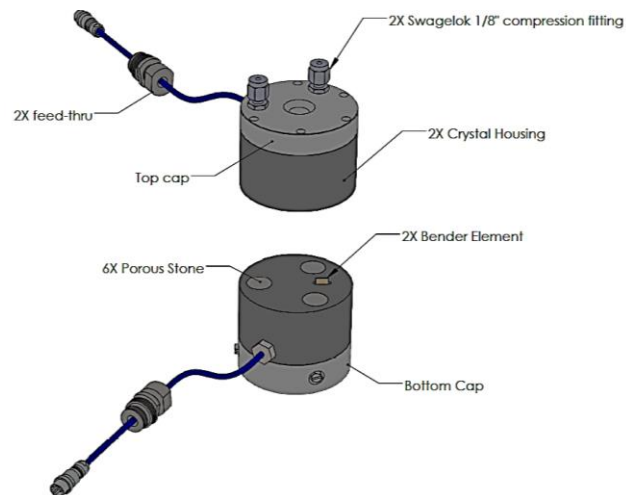


Figure 4.5: Compression crystals and bender elements installed on triaxial platen

Based on the conception above, compression wave velocity (V_p) and B-value are measured at each level of saturation obtained by a stepwise increase of backpressure.

In order to understand the degree of saturation corresponding to the measured B-value and compression wave velocity, theoretical relationship between the B-value and degree of saturation (S_r) is used.

The compressibility C_1 of a partially saturated sand can be derived by separately considering the influence of pore-air and pore-water phases, and therefore neglecting the effects of surface tension (Fredlund, D.G. and Rahardjo, H. 1993), as follows,

$$C_1 = C_a(1 - S_r)B_a + C_w S_r B_w \quad (4-5)$$

where C_a and C_w are the compressibility of air and water phases. B_a and B_w are the rate of pore air and pore water pressure variation with a change in confining stress. Herein, the assumption of $B_a = B_w (=B)$ would be reasonable for sands within the zone of partial saturation as discussed above. The following relation was separately derived by assuming the theory of wave propagation through a poro-elastic medium (Tsukamoto et al. 2002):

$$B = \frac{\Delta u}{\Delta \sigma} = \frac{1}{1 + \frac{nC_1}{C_b}} \quad (4-6)$$

or

$$B = \frac{1}{1 + n \frac{k_{sf}}{k_f}} \quad (4-7)$$

where n is the porosity, k_{sf} is the bulk modulus of soil skeleton, k_f is the bulk modulus of the pore fluid, and C_b is the compressibility of soil skeleton and given as follows,

$$C_b = \frac{1}{K_b} \quad (4-8)$$

$$K_b = \frac{2G_0(1+\nu_b)}{3(1-2\nu_b)} \quad (4-9)$$

Herein, G_0 is the maximum shear modulus and ν_b is the soil skeleton Poisson's ratio. The B-value can be further related to the S_r as:

$$\frac{1}{k_f} = \frac{1}{k_w} + \frac{1-S_r}{p_{af}} \quad (4-10)$$

Where P_{af} is the absolute pore fluid pressure including the atmospheric pressure.

Therefore, the following relation between S_r and B can be obtained (Tasukamoto et al. 2002):

$$S_r = \frac{C_a - \frac{C_b(1-B)}{nB^2}}{C_a - C_w} = \frac{C_a - \frac{3}{2G_0n} \frac{1-2\nu_b}{1+\nu_b} \frac{1-B}{B^2}}{C_a - C_w} \quad (4-11)$$

Or

$$B = \frac{1}{1 + n \frac{k_b}{k_w} + n \frac{k_b}{P_a} (1-S_r)} \quad (4-12)$$

In addition to the wave propagation theory to obtain the saturation ratio, an alternative method is described below for calculating the degree of saturation and the consolidation void ratio at the end of the shearing.

In this approach, sample freezing and the measurement of void volume change during saturation are used to determine S_r . Void ratio changes during saturation can be obtained by the following equation:

$$\Delta e_{saturation} = \frac{V_{v(final)} - V_{v(initial)}}{V_s} \quad (4-13)$$

$$V_{v(final)} = V_{w(final)} + V_{a(final)} = [V_{w(sat)} + V_{w(B.P)} + V_{w(i)} + V_{w(lines)}] + \left[\left(\frac{e_0}{1+e_0} \right) V_0 (1-S_r) \right] \quad (4-14)$$

Where $V_{v(final)}$ is the void volume after saturation and backpressure (before consolidation), $V_{v(initial)}$ is the initial void ratio ($V_0 - V_s$), $V_{w(sat)}$ is the volume of water trap inside the sample during water flushing at saturation stage, and $V_{w(i)}$ is 5% of the soil sample mass.

$$\Delta e_{saturation} = \frac{V_{w(sat)} + V_{w(B.P)} + V_{w(i)} + V_{w(lines)} + \left(\frac{e_0}{1+e_0} \right) V_0 (1-S_r) - (V_0 - V_s)}{V_s} \quad (4-15)$$

$$e_c = \Delta e_{saturation} + \Delta e_{consolidation} + e_0 \quad (4-16)$$

$$e_c = \frac{V_{w(sat)} + V_{w(B.P)} + V_{w(i)} + V_{w(lines)} + \left(\frac{e_0}{1+e_0} \right) V_0 (1-S_r) - (V_0 - V_s)}{V_s} + \Delta e_{consolidation} + e_0 \quad (4-17)$$

In the equation above the variables we need to obtain are S_r and e_c . We know the value of the rest.

On the other hand, we have:

$$\omega \times G_s = S_r \times e_c \quad (4-18)$$

$$e_c = \frac{\omega \times G_s}{S_r} \quad (4-19)$$

We know the water content and specific gravity values of each sample. So we have two equations and two variables to solve.

4.2.7 Determination of SWCC from pressure plate tests

The soil water characteristic curve determines the relationship between the water content in an unsaturated soil and the matric suction. Several methods have been developed to measure the SWCC, including pressure plate extractor, the tempe cell, and the constant flow laboratory system (Sun et al., 2006; Lu et al., 2006). The pressure plate extractor was employed here to obtain the soil water characteristic curve (SWCC) of oil sand tailings. The pressure plate extractor is an efficient, cost-effective, and convenient method to measure the SWCC. Oil sand tailings specimens with 0%, 10%, 25%, 50% fines content (fluid fine tailings) were used in this experiment. Each tailings sample was air-dried and packed to predetermined relative densities in a cutting ring with an inner diameter of 5.33 cm and a height of 1.5 cm as illustrated in Figure 4.6.

The compacted soil samples were placed on saturated ceramic discs and saturated entirely by increasing the water level inside the pressure plate with a filter paper. The samples were allowed to fully saturate for one day to one week according to their fines content. The test was conducted by increasing the air pressure inside the pressure plate to specific values. The soil sample was removed and weighted when the outflow water from the ceramic disc was less than 0.05 grams. The oven-dried weight of the sample was measured to determine the sample water content.

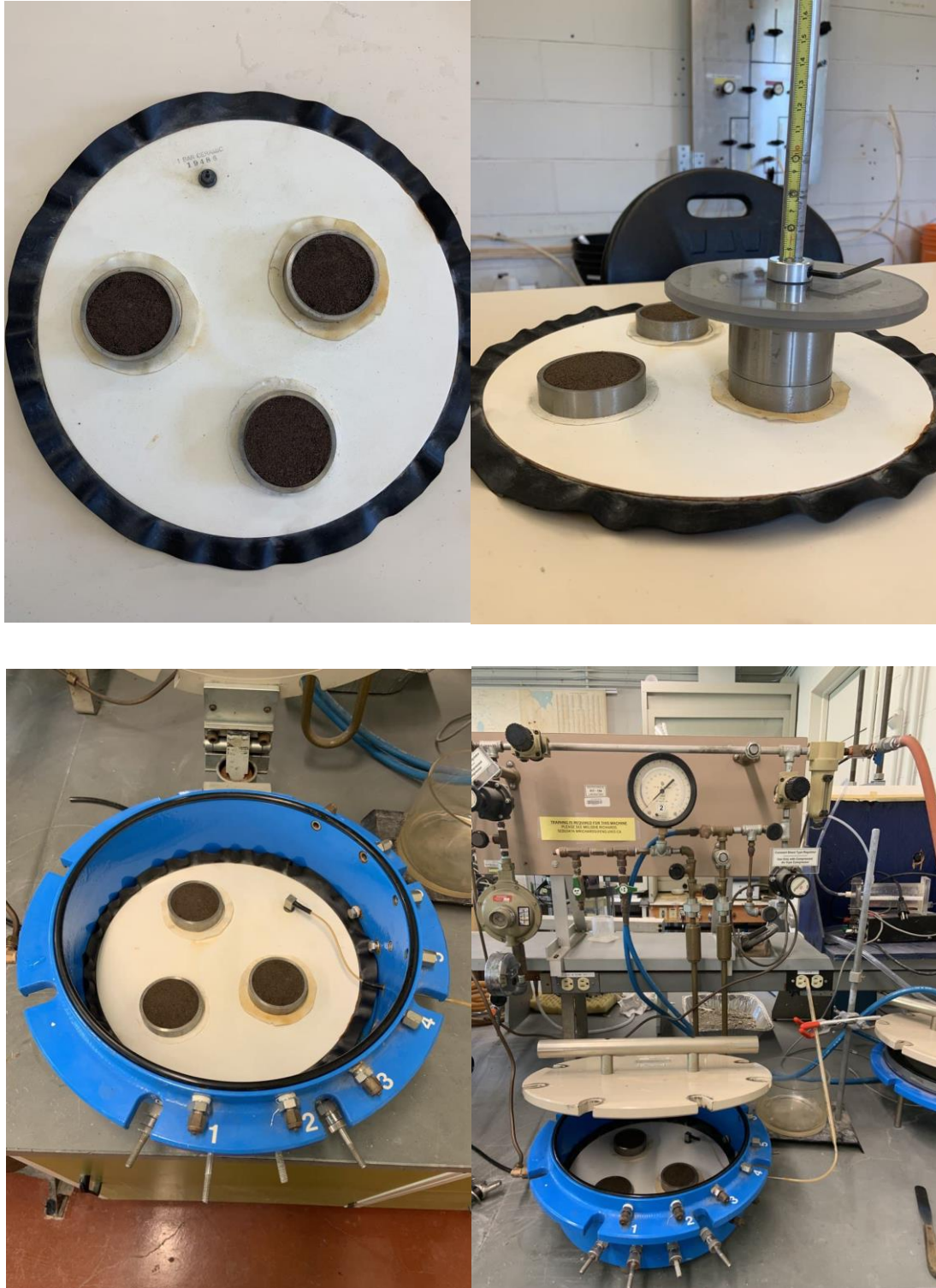


Figure 4.6: Sample preparation and pressure plate extractor apparatus

4.3 Results and Discussions

4.3.1 Soil water characteristic curve for different fines contents

The soil water characteristic curve for the oil sand tailings with different fines content is illustrated in Figure 4.7. It is found that the matric suction corresponding to a specific degree of saturation increases with fines content. The matric suction for the partially saturated oil sand tailings ($S_r > 80\%$) is 4 kPa which is insignificant in evaluating the shear behavior of a partially saturated oil sand tailings.

As illustrated in Figure 4.7, the data points obtained from the pressure plate test are interpolated using the SWCC model proposed by Fredlund and Xing (1994). The model fitting parameters are calculated and compared for different fines contents which are summarized in Table 4.2.

$$\frac{\theta_w}{\theta_s} = \left[1 - \frac{\ln\left(1 + \frac{\psi}{\psi_r}\right)}{\ln\left(1 + \frac{10^6}{\psi_r}\right)} \right] \left[\frac{1}{\left(\ln \left[e + \left(\frac{\psi}{a} \right)^n \right] \right)^m} \right] \quad (4-20)$$

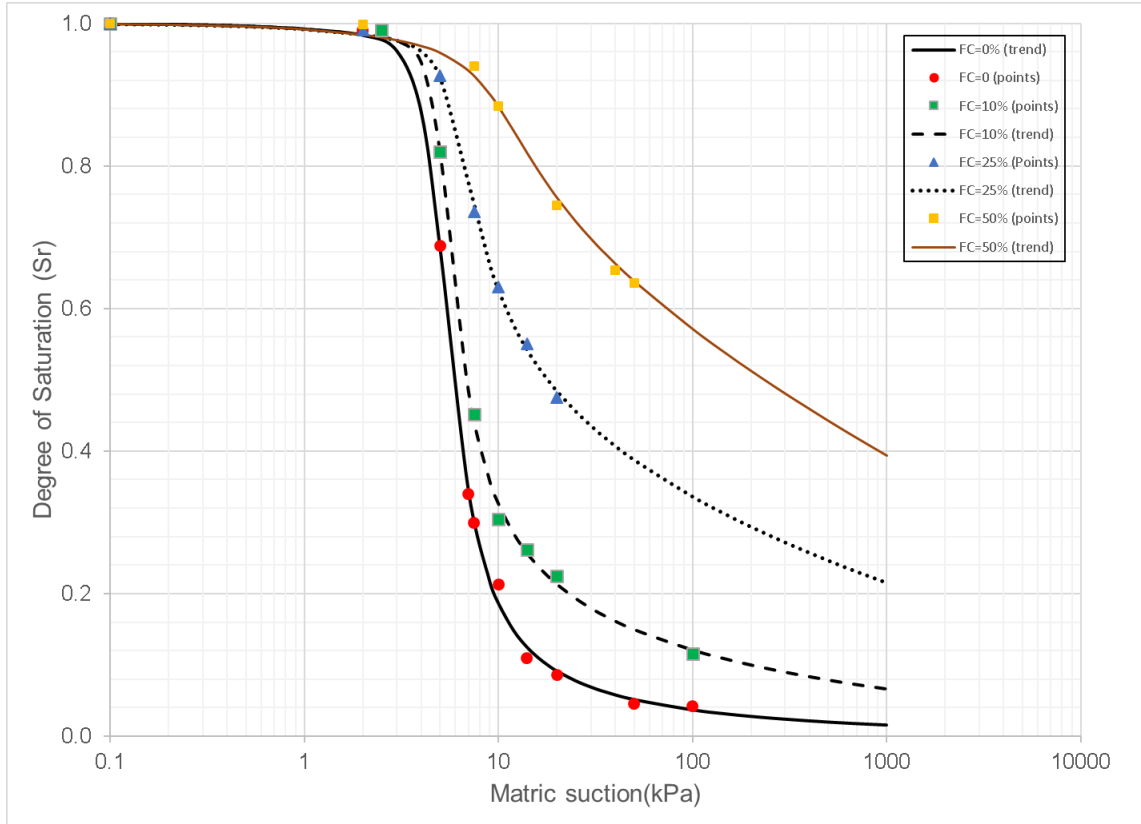


Figure 4.7: Soil water characteristic curve for oil sand tailings with different fines contents

Table 4.2: SWCC fitting parameters for oil sand tailings with different fines content

FC	a	n	m
0	4.795953	6.592323	1.021453
10	4.960871	9.322807	0.562557
25	5.533642	6.99385	0.284796
50	8.3975	3.99385	0.142398

4.3.2 Compression wave velocity at different levels of saturation

Compression wave velocity (V_p) and B-value are measured at each level of saturation obtained by a stepwise increase of backpressure. Figure 4.8 presents the V_p values at different Skempton's B for the oil sand tailings mixture with 0%, 10%, 25% and 50% fines content. Compression wave for all mixtures of oil sand with fines content, travels faster as B-value increases. Also, differences in arrival time of the P-wave become more pronounced at higher B-values. The comparison of the theoretical model introduced by Yang (2002) with the experimental results indicates that the theoretical model provides a reasonable estimation of the P-wave velocity at different saturation levels.

The effect of Poisson's ratio on the P-wave velocity for two saturation ratios of 99% and 100% are investigated. Figure 4.9 presents that the effect of Poisson's ratio in comparison with incomplete saturation is very small.

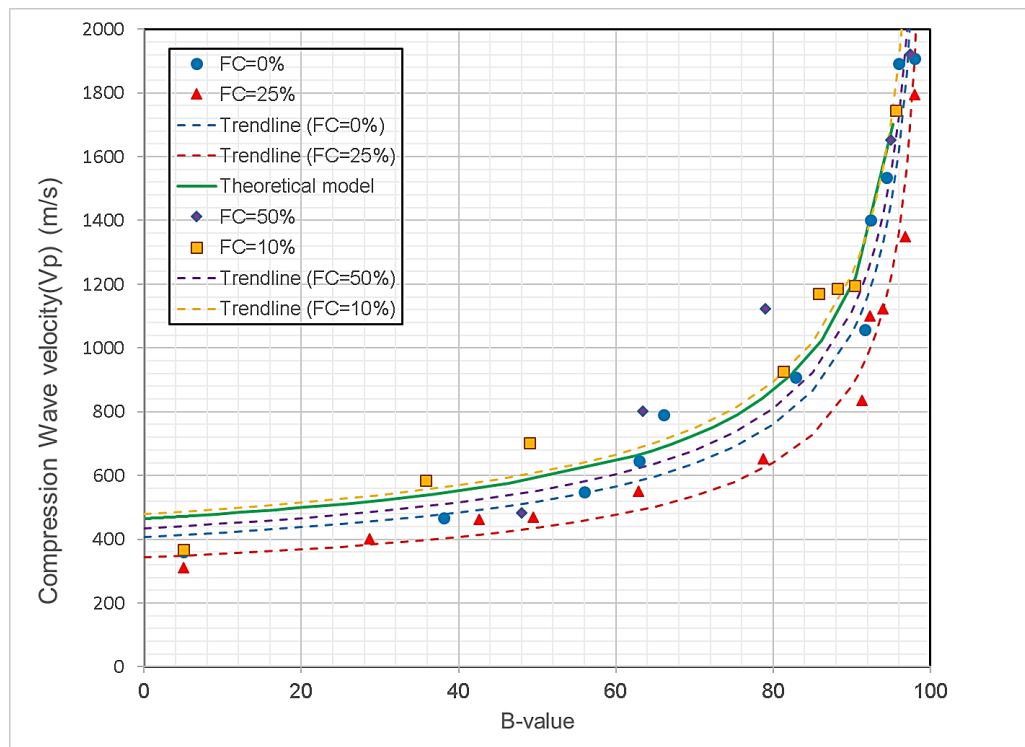


Figure 4.8: Compressional wave velocities for the oil sand tailings mixture with 0, 10, 25, 50% fines content at different B-values.

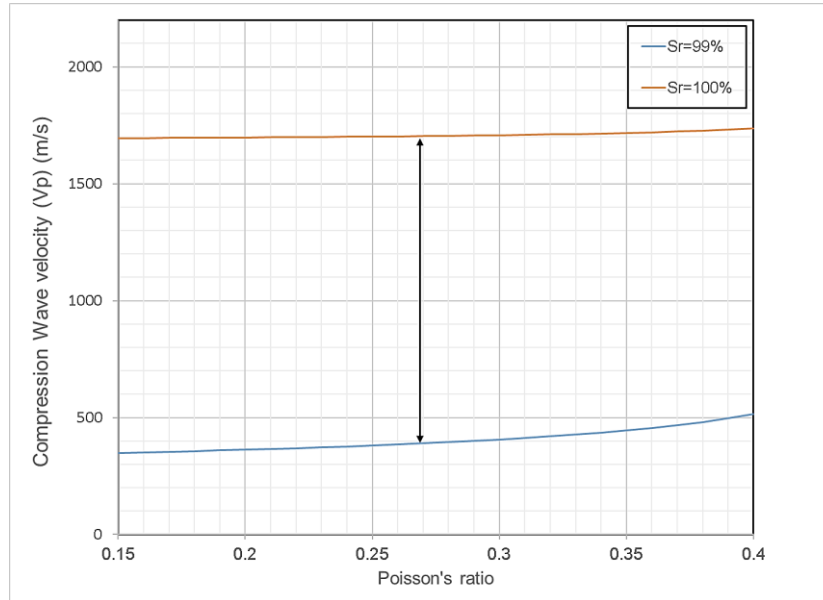


Figure 4.9: Effect of poisson's ratio on P-wave velocity

Variation of the saturation ratio (S_r) with Skempton's B , using the relation derived by the theory of wave propagation through a poroelastic medium, is illustrated in Figure 4.11. The bulk modulus of the soil skeleton is determined by:

$$K_b = \frac{2G(1+\nu)}{3(1-2\nu)} \quad (4-21)$$

Where ν is the Poisson's ratio which is assumed as 0.3. G is the shear modulus which is calculated based on the shear wave velocity (V_s) and total density (ρ) as below:

$$G = \rho V_s^2 \quad (4-22)$$

$$\rho = \rho_d(1+\omega) \quad (4-23)$$

$$\omega = (e \times S_r) / G_s$$

Where ω is the water content, ρ_d is the dry density and G_s is the specific gravity of the soil. Shear wave velocities at different consolidation normal stress are plotted for the oil

sand tailings at loose, medium, and dense states in Figure 4.10. The bulk modulus of water depends on the temperature and pore water pressure. Regarding the testing condition the bulk modulus of water is calculated as 2.216 GPa. Figure 4.11 shows small influence of the consolidation void ratio on the S_r -B curves.

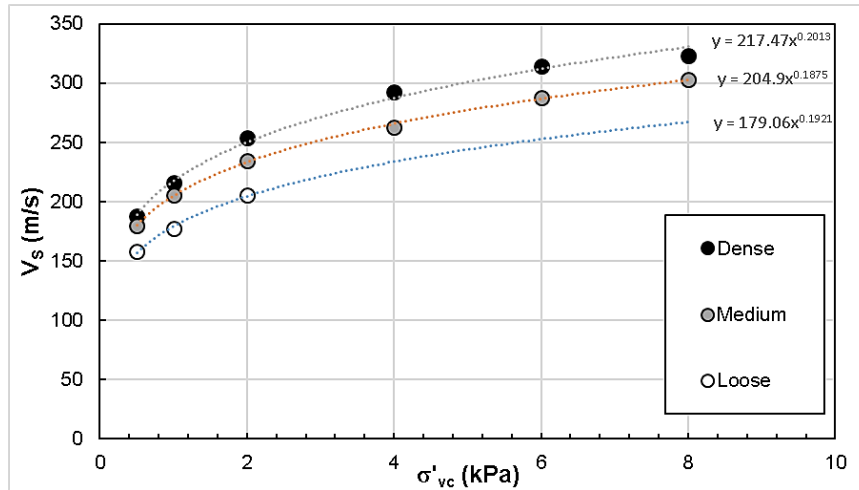


Figure 4.10: Shear wave velocities of the dense, medium, and loose oil sand tailings at different normalized consolidation stresses (Grytan, 2021).

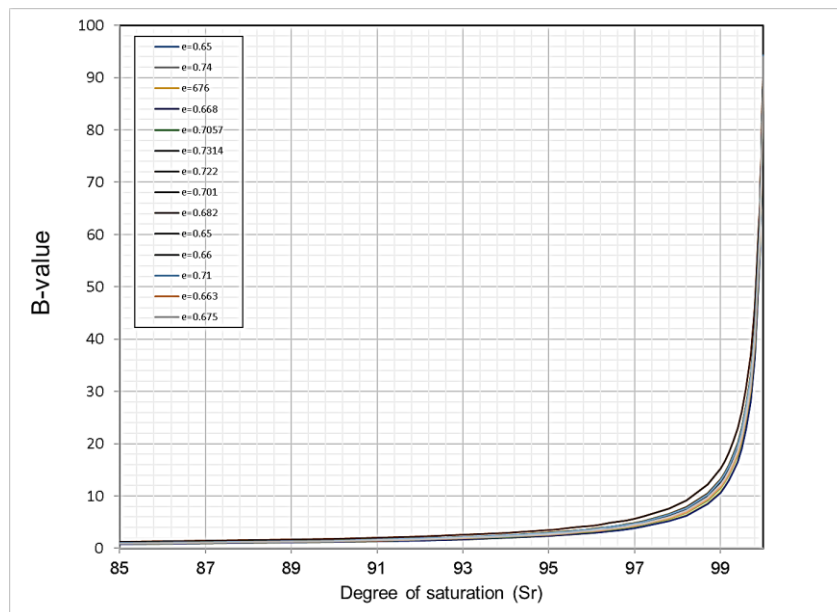


Figure 4.11: Effect of consolidation void ratio on the S_r -B plot

An alternative method for determination of saturation ratio based on the sample freezing and the measurement of void volume change during saturation stage are explained above. the results of the aforementioned method are compared with the prediction model in Figure 4.12.

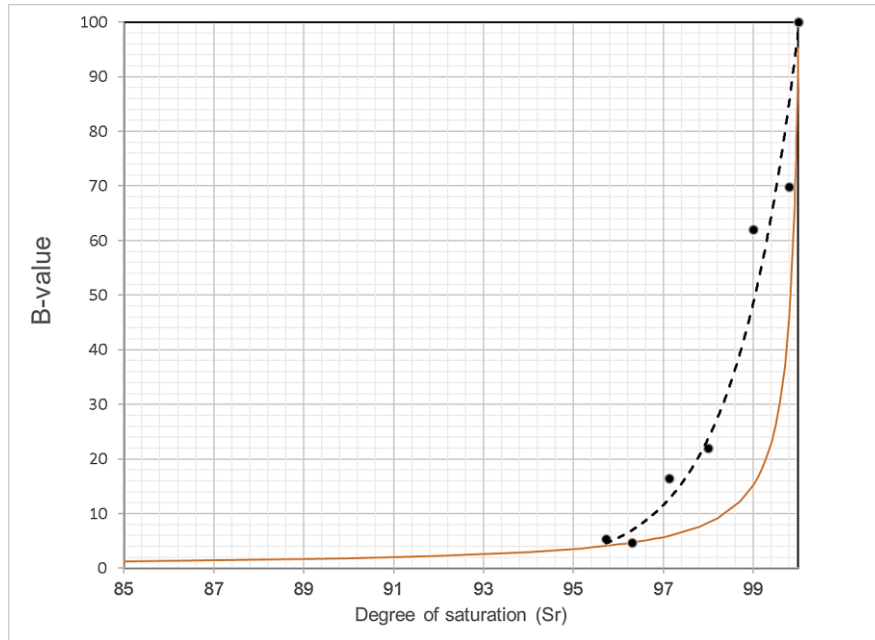


Figure 4.12: Comparison of the predicted S_r with the measured S_r using the proposed alternative method.

4.3.3 Effect of S_r on stress path and stress-strain response of tailings with different FC

Two series of triaxial tests were conducted on reconstituted samples of oil sand tailings with varying saturation levels. The outcome of these tests is presented in the Table 4.3.

Table 4.3: Triaxial testing program on the oil sand tailing with different saturation levels

Test ID	Initial relative density	Consolidation void ratio	Critical state void ratio	Consolidation stress		Skempton $s' B$	CS confining pressure
				$\sigma'1$ (kPa)	$\sigma'3$ (kPa)		
Test type	Dr_i (%)	e_c	$e(cs)$			B-value (%)	$P'(cs)$ (kPa)
IU-TXC	10	0.5996	0.5996	400	400	5.4	Dilative
IU-TXC	10	0.6321	0.6321	400	400	16.4	307.03
IU-TXC	10	0.6008	0.6008	400	400	22.0	258.22
IU-TXC	10	0.6360	0.6360	400	400	69.8	82.20
IU-TXC	10	0.6314	0.6314	400	400	99.0	20.32
IU-TXC	45	0.6741	0.6741	400	400	4.7	Dilative
IU-TXC	45	0.6314	0.6314	400	400	6.4	Dilative
IU-TXC	45	0.6819	0.6819	400	400	32.5	276.81
IU-TXC	45	0.6376	0.6376	400	400	62.0	137.80
IU-TXC	45	0.6951	0.6951	400	400	99.0	25.26

Figure 4.13 and Figure 4.14 present the monotonic undrained response of the oil sand tailings for different B parameters. The Skempton B value was used as to compare the saturation level, which correlates with the degree of saturation as discussed earlier. It is shown that the increase in B value results in a reduction of yield and post-liquefaction shear strengths. The undrained response of all samples reaches an instability line as the soil specimen is sheared. The instability line is defined for stress paths showing flow liquefaction. The instability line crosses the origin of the q-p' plane and the peak point of the stress path. The instability line slope increases with decreasing B value corresponding to reduced saturation.

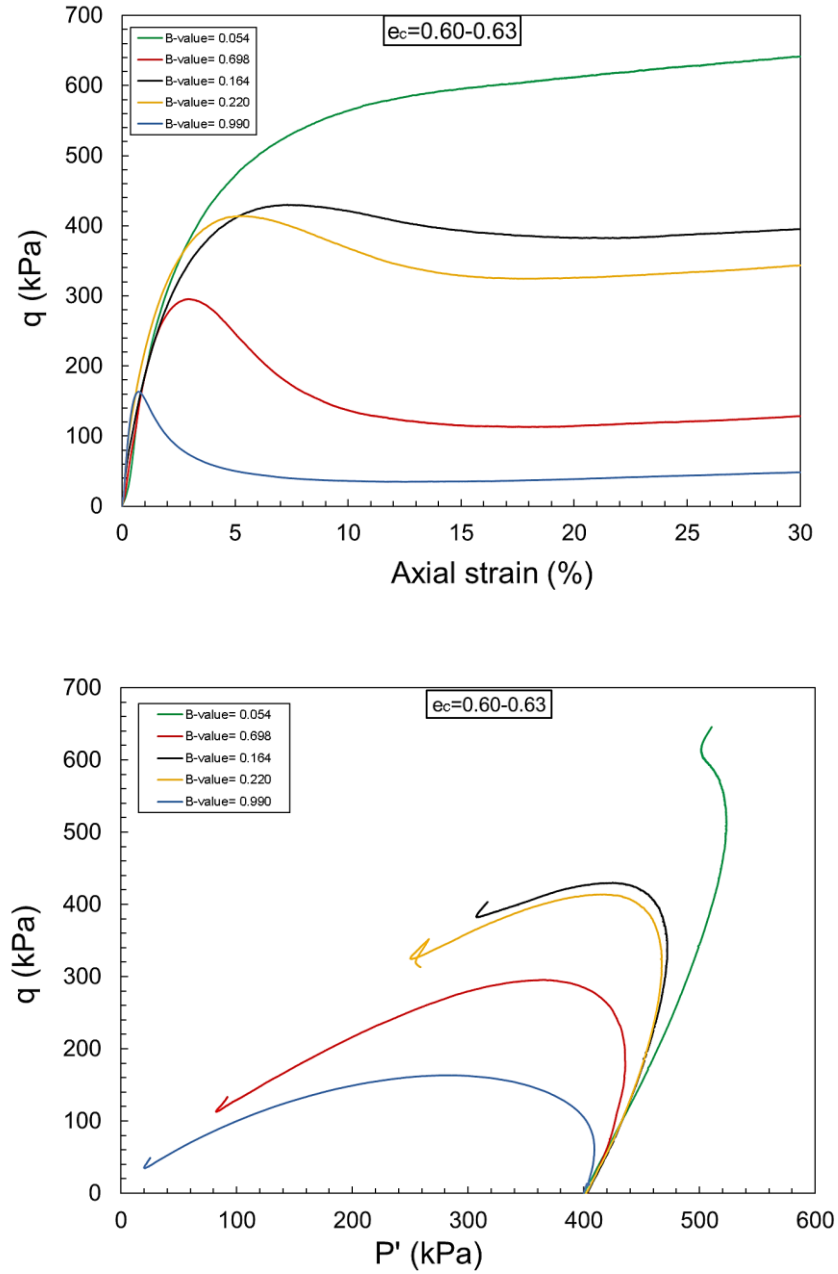


Figure 4.13: Effect of B-value on the stress-strain response and effective stress paths for oil sand with consolidation stress of 400kPa and consolidation void ratio of 0.60 to 0.63

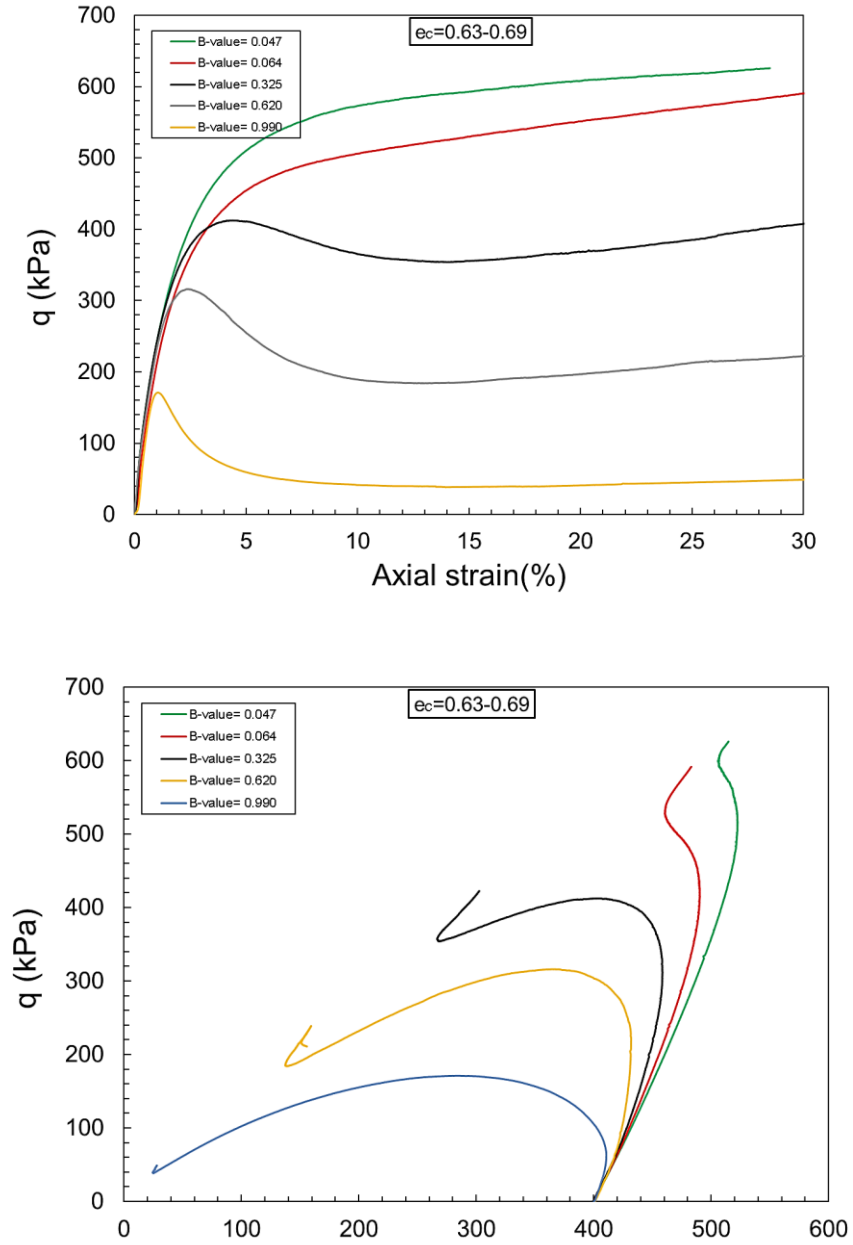


Figure 4.14: Effect of B-value on the stress-strain response and effective stress paths for oil sand with consolidation stress of 400 kPa and consolidation void ratio of 0.63 to 0.69

4.3.4 Comparison of pore pressure generations in saturation and unsaturated samples

Figure 4.15 shows the pore pressure generated during a monotonic undrained shear test. The increase of the B value leads to an increase in the pore water pressure, followed by a reduction in effective confining pressure and, consequently, a decrease in undrained shear strength.

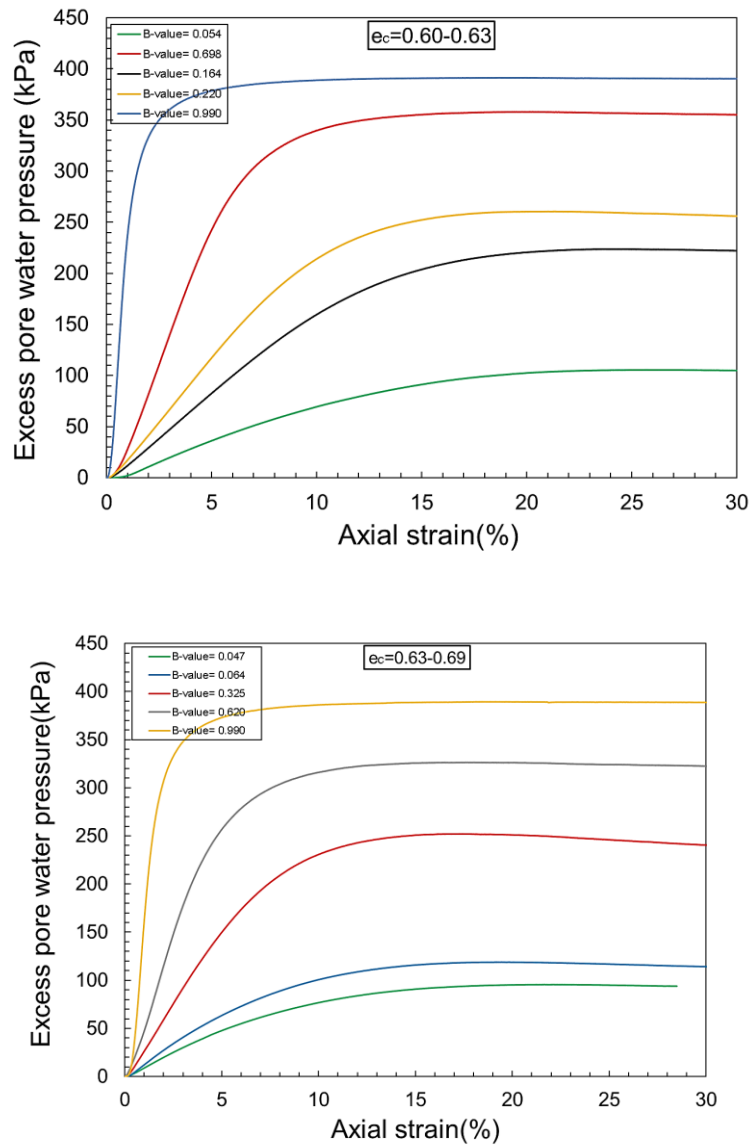


Figure 4.15: Effect of B-value on the developed pore water pressure for oil sand tailings

4.4 Conclusions

In this chapter the liquefaction susceptibility of partially-saturated oil sand tailings was investigated. Degree of saturation (S_r), Skempton B-value, and compression wave velocity are the saturation parameters used in this study to evaluate the effect of saturation on the undrained response of oil sand tailings. The great advantage of using P-wave velocity rather than other parameters such as B-value and saturation ratio is that it can be measured both in the field and in the laboratory. Also, the measured compression wave velocity in the field holds an equal level of credibility to that measured in the laboratory. The triaxial setup was developed with a set of ultrasonic transducer platens with 200 kHz compression crystals and bender elements for P-wave and S-wave velocity measurements. Compression wave velocity (V_p) and B-value are measured at each level of saturation obtained by a stepwise increase of backpressure. For all mixtures of oil sand with fines content, P-wave velocity increases with B-value, which is in agreement with the prediction model introduced by Yang (2002). Also, differences in arrival time of the P-wave become more pronounced at higher B-values. The influence of Poisson's ratio on the P-wave velocity is very small compared to the effect of incomplete saturation. Saturation ratio corresponding to the measured B-value and compression wave velocity is determined by (I) Theoretical relationship between the B-value and degree of saturation (S_r) based on the theory of wave propagation (II) Alternative method based on the sample freezing and the measurement of void volume change during the saturation stage. The results indicate that liquefaction resistance increases with decreasing the degree of saturation. Previous researches had shown similar conclusion for unsaturated ($S_r < 80\%$) soils. They proposed that the generated matric suction as the main reason for decreasing liquefaction susceptibility of the soils with decreasing the degree of saturation. However, SWCC of the partially saturated oil sand tailings shows a negligible amount of the matric suction (< 4 kPa) for the oil sand tailings. This low value of matric suction validates the proposition made in the wave propagation theory for partially saturated oil sand tailings. Therefore, the reduction in liquefaction susceptibility by decreasing the degree of

saturation is due to the increased compressibility of the pore fluid which dampens the generation of excess pore pressure rather than the strengthening effect of soil suction.

References

- Alarcon-Guzman, A, GA Leonards, and JL Chameau. "Undrained Monotonic and Cyclic Strength of Sands." *Journal of Geotechnical Engineering* 114, no. 10 (1988): 1089-109.
- Baldi, Gualtiero, and Roberto Nova. "Membrane Penetration Effects in Triaxial Testing." *Journal of Geotechnical Engineering* 110, no. 3 (1984): 403-20.
- Been, K, MG Jefferies, and J Hachey. "The Critical State of Sands." *Geotechnique* 41, no. 3 (1991): 365-81.
- Been, Ken, and Mike G Jefferies. "A State Parameter for Sands." *Geotechnique* 35, no. 2 (1985): 99-112.
- Bishop, AW. "The Influence of Progressive Failure on the Choice of the Method of Stability Analysis." *Geotechnique* 21, no. 2 (1971): 168-72.
- Bishop, Alan W, and Gordon E Green. "The Influence of End Restraint on the Compression Strength of a Cohesionless Soil." *Geotechnique* 15, no. 3 (1965): 243-66.
- Bishop, Alan Wilfred, and David John Henkel. "The Measurement of Soil Properties in the Triaxial Test." (1962).
- Bjerrum, Laurits. "The Shear Strength of a Fine Sand." *Proc. V ICSMFE* 1 (1961): 29-37.
- Black, David K, and Kenneth L Lee. "Saturating Laboratory Samples by Back Pressure." *Journal of the soil mechanics and foundations division* 99, no. 1 (1973): 75-93.
- Casagrande, Arthur. "Characteristics of Cohesionless Soils Affecting the Stability of Slopes and Earth Fills." *J. Boston Society of Civil Engineers* 23, no. 1 (1936): 13-32.

- Casagrande, A. "Liquefaction and Cyclic Deformation in Sands: A Critical Review: Proceeding of the Fifth Pan American Conference in Soil Mechanics and Foundation Engineering." *Buenos Aires, Argentina* (1975).
- Castro, Gonzalo. "Liquefaction of Sands." *ph. D. Thesis, Harvard Soil Mech.* (1969).
- Castro, G, JL Enos, JW France, and SJ Poulos. *Liquefaction Induced by Cyclic Loading. Report to National Science Foundation, Washington, Dc, No. NSF/CEE-82018, 1982.*
- Castro, Gonzalo, and Steve J Poulos. "Factors Affecting Liquefaction and Cyclic Mobility." *Journal of the Geotechnical Engineering Division* 103, no. 6 (1977): 501-16.
- Eseller-Bayat, Ece, Mishac K Yegian, Akram Alshawabkeh, and Seda Gokyer. "Liquefaction Response of Partially Saturated Sands. I: Experimental Results." *Journal of geotechnical and geoenvironmental engineering* 139, no. 6 (2013): 863-71.
- Fourie, AB, and G Papageorgiou. "Defining an Appropriate Steady State Line for Merriespruit Gold Tailings." *Canadian geotechnical journal* 38, no. 4 (2001): 695-706.
- Hazen, Allen. "A Study of the Slip in the Calaveras Dam." *Engineering News Record* 81, no. 26 (1918): 1158-64.
- Jang, Deh-Jeng, and J David Frost. "Use of Image Analysis to Study the Microstructure of a Failed Sand Specimen." *Canadian geotechnical journal* 37, no. 5 (2000): 1141-49.
- Ladd, RS. "Preparing Test Specimens Using Undercompaction." *Geotechnical Testing Journal* 1, no. 1 (1978): 16-23.
- Lade, Poul V. "Initiation of Static Instability in the Submarine Nerlerk Berm." *Canadian geotechnical journal* 30, no. 6 (1993): 895-904.
- Mitchell, James Kenneth, and Kenichi Soga. *Fundamentals of Soil Behavior*. Vol. 3: John Wiley & Sons New York, 2005

- Mulilis, JP, FC Townsend, and RC Horz. "Triaxial Testing Techniques and Sand Liquefaction." In *Dynamic Geotechnical Testing*: ASTM International, 1978.
- Sadrekarami, Abouzar, and Scott M Olson. "Effect of Sample-Preparation Method on Critical-State Behavior of Sands." *Geotechnical Testing Journal* 35, no. 4 (2012): 548-62.
- Seed, H Bolton. "Design Problems in Soil Liquefaction." *Journal of Geotechnical Engineering* 113, no. 8 (1987): 827-45.
- Sladen, JA, RD D'hollander, and J Krahn. "The Liquefaction of Sands, a Collapse Surface Approach." *Canadian geotechnical journal* 22, no. 4 (1985): 564-78.
- Sladen, JA, RD D'hollander, J Krahn, and DE Mitchell. "Back Analysis of the Nerlerk Berm Liquefaction Slides." *Canadian geotechnical journal* 22, no. 4 (1985): 579-88.
- Sladen, JA, and JM Oswell. "The Behaviour of Very Loose Sand in the Triaxial Compression Test." *Canadian geotechnical journal* 26, no. 1 (1989): 103-13.
- Stark, Timothy D, and Gholamreza Mesri. "Undrained Shear Strength of Liquefied Sands for Stability Analysis." *Journal of Geotechnical Engineering* 118, no. 11 (1992): 1727-47.
- Sukumaran, B, and AK Ashmawy. "Quantitative Characterisation of the Geometry of Discret Particles." *Geotechnique* 51, no. 7 (2001): 619-27.
- Sze, HY, and J Yang. "Failure Modes of Sand in Undrained Cyclic Loading: Impact of Sample Preparation." *Journal of geotechnical and geoenvironmental engineering* 140, no. 1 (2014): 152-69.
- Tsukamoto, Yoshimichi, Shohei Kawabe, Jo Matsumoto, and Shotaro Hagiwara. "Cyclic resistance of two unsaturated silty sands against soil liquefaction." *Soils and Foundations* 54, no. 6 (2014): 1094-1103.
- Vaid, YP, and S Sivathayalan. "Static and Cyclic Liquefaction Potential of Fraser Delta Sand in Simple Shear and Triaxial Tests." *Canadian geotechnical journal* 33, no. 2 (1996): 281-89.
- Vaid, Yoginder Pal, and S Sivathayalan. "Fundamental Factors Affecting Liquefaction Susceptibility of Sands." *Canadian geotechnical journal* 37, no. 3 (2000): 592-606.
- Wang, FW, Kyoji Sassa, and Gonghui Wang. "Mechanism of a Long-Runout Landslide Triggered by the August 1998 Heavy Rainfall in Fukushima Prefecture, Japan." *Engineering Geology* 63, no. 1-2 (2002): 169-85.

Yong, J. "Liquefaction resistance of sand in relation to P-wave velocity." *Geotechnique* 52, no. 4 (2002): 295-298.

Zhang, H. *Steady State Behavior of Sands and Limitations of the Triaxial Tests.* University of Ottawa, Ottawa, Canada, Vol. PhD, 1997.

Zhu, JH, and SA Anderson. "Corrections for Triaxial Tests on Undisturbed Soils." *Journal of testing and evaluation* 26, no. 3 (1998): 277-84.

Chapter 5

5 Conclusion

This chapter summarizes all the studies carried out in the previous chapters and provides concluding remarks on them.

A comprehensive experimental investigation on the effect of fines content and level of saturation on the liquefaction susceptibility of the oil sand tailings was accomplished in current research. This includes, in short, the shearing behavior of saturated oil sand tailings using the triaxial compression test under monotonic loading conditions in chapter 2, the influence of the fines content on undrained shear behavior of the saturated oil sand tailings in chapter 3, and liquefaction susceptibility of the partially saturated oil sand tailings in chapter 4. This chapter provides a more general summary of the accomplished goals and addressed objectives discussed within the first chapter.

Research in chapter 2 sought about the shear behavior of the oil sand tailings based on the critical state concept. Twenty-three triaxial tests were carried out, including: (1) Isotropically consolidated undrained tests (IU-TXC), (2) K₀-consolidated undrained tests (K₀U-TXC), and (3) Isotropically consolidated drained test (ID-TXC). Determination of the soil specimen volume change during the saturation stage is one of the major sources of errors in triaxial testing. The sample freezing method is used as the main method to measure the void volume change during the backpressure saturation stage. And two others methods: (1) inflow/outflow method, (2) Cell volume ratio are also assessed for measuring the void volume change. It was demonstrated that the inflow/outflow method leads to close results to the freezing method and can be used as an alternative method for estimating the void ratio changes in backpressure stage. Undrained triaxial tests are often used to evaluate the liquefaction susceptibility of the soil sample due to the pore water pressure generation mechanism. Evaluation of the yield and post-liquefaction shear strength ratios of the oil sands provides a valuable basis for analyzing the failure criteria. According to the IU-TxC, both yield and post-liquefaction shear strength ratios decreases

with increasing consolidation void ratio, and the range of these parameters measured as $S_{u(\text{yield})} / \sigma'_{vc} = (0.18-0.21)$ and $S_{u(\text{liq})} / \sigma'_{vc} = (0.016-0.04)$, respectively. It was also found that The axial strain corresponding to the peak deviator stress increases with relative density. A soil element in a natural deposit is subjected to the vertical overburden and radial confining stresses under zero lateral strain condition. In reality, the lateral stresses are smaller than vertical stress. Seven K_0 U-TxC tests were performed to better understand oil sand tailings behavior in a natural condition. The K_0 values obtained directly from the experimental test were 0.55 to 0.58 based on different initial states. The $S_{u(\text{yield})} / \sigma'_{vc} = (0.24-0.27)$ and $S_{u(\text{liq})} / \sigma'_{vc} = (0.03-0.07)$ agree closely with values from earlier laboratory experiments on loose sands. Yield and critical state friction angles of oil sands measured in triaxial tests illustrated that the influence of consolidation void ratio on the yield friction angle is greater than that on the post-liquefaction friction angle.

The goal in chapter 3 was to investigate the influence of fines content on the undrained shear behavior of oil sand tailings using the critical state framework. The stress-strain analyses of oil sand tailings with different percentages of fines showed that the shear strength ratios of tailings mixtures increased with increasing fines content at a given void ratio. The yield friction angle of the tailings with 25% fines content was higher than that for the clean tailings (FC = 0%). However, the influence of fines on the mobilized friction angle disappeared at large strains. Therefore, the initial void ratios of tailings mixtures appeared to have a significant effect on the friction angle in the early stages of shearing. The critical state lines for 0% and 25% fines content. The slope of the critical state line for the clean tailings was slightly higher than that of tailings with FC = 25%. The void ratio intercept of CSL for FC = 0% and 25% were 0.769 and 0.663, respectively. Therefore, the CSL moves to the denser void ratios (downward movement) as the fines content increased to 25%. The slope of the critical state lines measured for the oil sand with 0% and 25% fines content were -0.0598 and -0.0784, respectively. Adding fines to the oil sand tailings resulted in a clockwise rotation of the critical state line in e -log p' space. The yield and post-liquefaction shear strength ratios increase with the fines content. At the same time, these two shear strength ratios decrease with increasing state parameter.

Chapter 5 investigates the liquefaction susceptibility of the partially saturated oil sand tailings using undrained triaxial tests. The soil water characteristic curves for the oil sand tailings with different fines content are measured using the pressure plate extractor tests and compared in chapter 5. It is found that the matric suction corresponding to a specific degree of saturation increases with fines content. The matric suction for the partially saturated oil sand tailings ($S_r > 80\%$) is 4 kPa which is insignificant in evaluating the shear behavior of a partially saturated oil sand tailings. The fitting parameters of the SWCC model proposed by Fredlund and Xing (1994) are estimated and compared for different fines content.

Partially saturated specimens for triaxial tests were prepared using different methods including: (I) No carbon dioxide flushing, (II) Reducing back pressure (III) Using aeriated water. Degree of saturation (S_r), Skempton B-value, and compression wave velocity are the saturation parameters used in this study to evaluate the effect of saturation on the undrained response of oil sand tailings. The great advantage of using P-wave velocity rather than other parameters such as B-value and saturation ratio is that it can be measured both in the field and in the laboratory. Also, the measured compression wave velocity in the field holds an equal level of credibility to that measured in the laboratory. The triaxial setup was developed with a set of ultrasonic transducer platens with 200 kHz compression crystals and bender elements for P-wave and S-wave velocity measurements. Compression wave velocity (V_p) and B-value are measured at each level of saturation obtained by a stepwise increase of backpressure. For all mixtures of oil sand with fines content, P-wave velocity increases with B-value, which is in agreement with the prediction model introduced by Yang (2002). Also, differences in arrival time of the P-wave become more pronounced at higher B-values. The influence of Poisson's ratio on the P-wave velocity is very small compared to the effect of incomplete saturation. Saturation ratio corresponding to the measured B-value and compression wave velocity is determined by (I) Theoretical relationship between the B-value and degree of saturation (S_r) based on the theory of wave propagation (II) Alternative method based on the sample freezing and the measurement of void volume change during the saturation stage.

The undrained triaxial test results indicate that liquefaction resistance increases with decreasing the degree of saturation. Previous researches had shown similar conclusion for unsaturated ($S_r < 80\%$) soils. They proposed that the generated matric suction as the main reason for decreasing liquefaction susceptibility of the soils with decreasing the degree of saturation. However, SWCC of the partially saturated oil sand tailings shows a negligible amount of the matric suction (< 4 kPa) for the oil sand tailings. This low value of matric suction validates the proposition made in the wave propagation theory for partially saturated oil sand tailings. Therefore, the reduction in liquefaction susceptibility by decreasing the degree of saturation is due to the increased compressibility of the pore fluid which dampens the generation of excess pore pressure rather than the strengthening effect of soil suction.

Curriculum Vitae

Farshad Zehforoosh

SUMMARY OF QUALIFICATIONS

- Experienced in conducting in-situ and laboratory advanced testing as well as soil sampling and assessment. Able to explain sophisticated calculations and drawings to clients. Strong interpersonal, organizational, decision-making, and team working skills.
- Advanced knowledge of Static and dynamic liquefaction analysis and seismic design.
- Completely familiar with critical state mechanics of soil
- Strong knowledge in using cyclic and monotonic triaxial testing, MCPT testing, Pressure plate extractor testing, shear wave velocity measurement using bender elements, and data analyzing.
- Detailed working knowledge of unsaturated and partially saturated oil sand tailings.
- Solid understanding in effect of fine content and other initial states on monotonic response of oil sand tailings.
- Sound knowledge of Analysis and design of earth-structures
- Proficient computer skills: GeoStudio (SIGMA/W, SEEP/W, SLOPE/W), Plaxis, Flac, DEEPSOIL, NovoTech Softwares (NOvoLIQ, NovoSPT, NovoCPT), CLiq, LiqSVs, ETABS, SAFE, AutoCAD, CAPFOS, Microsoft Office (Word, Excel, Powerpoint), ExcelVBA, MATLAB, Fortran 90

EDUCATION

M.Sc Civil Engineering – Geotechnical Engineering University of Western Ontario, London, ON	Sep. 2019 – Present
M.Sc Civil Engineering – Geotechnical Engineering University of Tehran, Tehran, Iran	Sep. 2014 – Sep. 2017
B.Sc Civil Engineering University of Tabriz, Tabriz, Iran	Sep. 2010 – Jun. 2014

THESIS OBJECTIVES AND ACADEMIC RELEVANT WORKS

- Studied instability and critical state behavior of oil sand tailings (research project funded by Natural Sciences and Engineering Research Council supervised by Dr. Abouzar Sadrekarimi).
- Studied the effect of fine content and degree of saturation on liquefaction susceptibility of oil sand tailings
- Participation in Design and Construction of Dynamic Triaxial Apparatus, Equipped with Bender Elements and Capable of Measuring Wide Range of Strains; University of Tehran; Under Supervision of Dr. Abbas Ghalandarzadeh.
- Studying the influence of non-plastic fine content on Cone Resistance through CPT Tests; University of Tehran; Under Supervision of Dr. Abbas Ghalandarzadeh.
- Evaluation the Liquefaction Resistance of sand-silt mixtures through Cyclic Triaxial Tests; University of Tehran; Under Supervision of Dr. Abbas Ghalandarzadeh.
- Studying and Analyzing Effects of Different Variables on Shear Wave Velocity of Saturated Clean and Mixed Sands; University of Tehran; Under Supervision of Dr. Abbas Ghalandarzadeh.
- Establishing Correlations among Shear Wave Velocity, Cone Resistance and Liquefaction Resistance in term of non-plastic fine content.
- Analyzed the failure of Feijão dam using the novel Norsand model in FLAC2D.

WORK EXPERIENCE

Internship, Baroge Construction Co., Urmia, Iran

June 2014 – March 2015

- Communicated effectively with contractors and labourers, outlining the plans of the earth structures
- Prepared detailed and technical reports on findings, projects and relevant data. Presented the process to clients using Microsoft Powerpoint.
- Maintained general office files; prepared documents for the consultant company such as as-built plans, daily tasks accomplishments and contracts for site engineers and labourers

AWARDS AND GRANTS

- Fully funded MSc Position at Western University
- Ranked 54th in Civil Engineering Master Entrance Exam in Iran, 2014
- Ranked 1st in the first stage of the 19th National Scientific Olympiad in field of Civil Engineering,
- Achieving top two place among all teams participated from Tehran University and 16th place among all participating teams in the second Iran National GeoWall Competition

CERTIFICATES AND LICENSES

Standard First Aid & CPR/AED Level C | Fire Extinguisher | Laboratory Safety and Hazardous Waste Management | Supervisor Health and Safety Awareness | WHMIS | Ontario Driver's G License